MOLECULAR CHARACTERIZATION, PURIFICATION, AND IMMOBILIZATION OF A BACTERIAL CARBONIC ANHYDRASE FOR EFFICIENT CO_2 CONVERSION

Thesis submitted in fulfilment of the requirements for the Degree of

DOCTOR OF PHILOSOPHY

IN

BIOTECHNOLOGY

BY

TANVI SHARMA

DEPARTEMENT OF BIOTECHNOLOGY AND BIOINFORMATICS

JAYPEE UNIVERSITY OF INFORMATION TECHNOLOGY

WAKNAGHAT, SOLAN, HP-173234, INDIA

FEBRUARY 2024

DECLARATION BY THE SCHOLAR

I hereby declare that the work reported in the Ph.D. thesis entitled **"Molecular characterization, purification, and immobilization of a bacterial carbonic anhydrase for efficient CO_2 conversion"** submitted at **Jaypee University of Information Technology, Waknaghat India,** is an authentic record of my work carried out under the supervision of **Dr. Ashok Kumar Nadda**. I have not submitted this work elsewhere for any other degree or diploma.

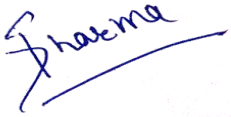

Tanvi Sharma

Enrollment No. 186552

Department of Biotechnology and Bioinformatics

Jaypee University of Information Technology, Waknaghat, India-173234

Date:

SUPERVISOR'S CERTIFICATE

This is to certify that the work reported in the Ph.D. thesis entitled "**Molecular characterization, purification, and immobilization of a bacterial carbonic anhydrase for efficient CO_2 conversion**," submitted by **Tanvi Sharma** at **Jaypee University of Information Technology, Waknaghat**, **India,** is a bonafide record of her original work carried out under my supervision. This work has not been submitted elsewhere for any other degree or diploma.

(**Dr. Ashok Kumar Nadda**)

Assistant Professor

Department of Biotechnology and Bioinformatics

Jaypee University of Information Technology, Waknaghat, India-173234

Date:

ACKNOWLEDGMENTS

I feel remarkably fortunate to have had the opportunities that have brought me to this stage in my life and for the people that have helped shape my journey along the way. "Nothing fruitful can be achieved without the perfect combination of inspiration and perspiration we owe much to inspiration part." This work has the imprint of many people and it is a pleasure for me to thank all those who have made this thesis possible by making their support available to me in several ways. First and foremost, I take this opportunity to extend my profound gratitude and indebtedness to my esteemed supervisor ***Dr. Ashok Kumar Nadda****, for his expert guidance, and unbiased never-ending encouragement at every juncture of the present research work. I will always be indebted to him for his advice, affection, and concern which always showered on me.*

I also owe my sincere thanks to JUIT administration, Vice Chancellor, ***Prof. (Dr.) Rajendra Kumar Sharma****, Dean,* ***Prof. (Dr.) Ashok Kumar Gupta****, Registrar,* ***Maj. Gen. (Retd.) Rakesh Bassi****, and H.O.D, Dept. of Biotechnology and Bioinformatics,* ***Prof. (Dr.) Sudhir Kumar*** *for providing essential amenities, research funding, and infrastructure for pursuing the research work.*

I also express my deep sense of gratitude towards my DPMC member ***Dr. Sudhir Kumar, Dr. Jitendra Vashist,*** *and* ***Dr. Vineet Sharma*** *for their precious suggestion and constant support in the entire work. I want to extend my deep sense of gratitude towards other faculty members of the Department of BT&BI for encouraging deeds and fruitful guidance during my research work. I will always appreciate the help I got from our technical and non-technical staff.*

I am extremely thankful to my colleagues ***Kriti Sharma, Rolika Gupta, Lalita Sharma, Diksha Manhas, Suhani Bhagta,*** *and* ***Megha*** *for their help, cooperation, advice, support, encouragement and for providing a healthy and comfortable workplace.*

It would be incomplete on my part if do not acknowledge the evitable role of my parents for their support and confidence. I can neither compensate nor reimburse the debt of the everlasting affection and blessings of my parents ***Mr. Vijay Sharma, Mrs. Neelam Sharma*** *and* ***Mr. Chaman Lal Sharma****, and* ***Mrs. Surekha Devi*** *for their encouragement, patience and supporting me throughout my life and studies.*

*I would like to express my hearty thanks to my husband **Dr. Abhishek Sharma** for being my reminder that even when all things fail, life is worth living. He profoundly motivated me in every way for opting and accomplish the Ph.D. I wish to express my special thanks to my brother **(Tushar)** for his support and to help me out in the down phases of my life.*

*I wish to express my special thanks to **Dr. Shweta Sharma** (sister-in-law), **Abhilasha Sharma** (sister-in-law), **Mr. Dinesh Sharma** (brother-in-law), for their love, care and moral support that enabled me to do my research work with added enthusiasm and earnestness. A special thanks to **"Dinesh Sharma (uncle)"** for his constant support always. I would like to thank my family members, relatives, cousins who have been extremely supportive to me throughout all my endeavors.*

Last but not least I bow in gratitude to the Almighty whose grace has enabled me to complete various ventures of life. I thank God for all that he does for us. Please always have a hand on me 'God' and I hope with your blessing of yours, I will continue to read this path and make my parents, teachers, friends, and this country proud.

Table of Contents

CONTENTS **PAGE No.**

LIST OF SYMBOLS AND ABBREVIATIONS

%	Percentage
ppm	Parts per million
HCO_3^-	Bicarbonate
s^{-1}	Per second
kDa	Kilodalton
pH	Hydrogen ion concentration
3-D	Three dimensional
RubisCo	Ribulose-1,5-bisphosphate carboxylase/oxygenase
mol /mol	Moles per mole
mol/l	Moles per liter
mmol CO_2/g	Millimoles carbon dioxide per gram
mg/g	Milligrams per gram
cm^3/g	Centimeter cube per gram
m^2/g	Meter per square gram
mmol/g	Millimoles per gram
km^2	Square kilometer
sp.,	Species
mg/L/day	Milligrams per liter per day
m^2 /day	Meter square per day
NADH	Nicotinamide adenine dinucleotide
Min	Minutes
°C	Degree Celsius
mg	Milligrams
H_2O	Water
Ca^{2+}	Calcium ion
α	Alpha
β	Beta
γ	Gamma
ε	Epsilon
δ	Delta
His	Histidine
Cys	Cysteine
Asp	Aspartate

Asn	Asparagine
Tyr	Tyrosine
Thr	Threonine
Val	Valine
Leu	Leucine
mM	Milli Molar
mg/mL	Milligrams per liter
M	Molar
U/mg	Units per milligram
μM/ min/protein	Micromole per minute per protein
PCR	Polymerase chain reaction
DNA	Deoxyribonucleic acid
mg/min	Milligrams per minute
mL	Milliliter
g	Gram
Mt/year	Metric tonne per year
ton/day	Tonne per day
Mtpa	Millions of tonnes per annum
m^2	Square meter
Co^{2+}	Cobalt
Cu^{2+}	Copper
Ni^{2+}	Nickel
g/l	Grams per liter
NaCl	Sodium chloride
$MgSO_4.7H_2O$	Magnesium sulfate heptahydrate
Na_2HPO_4	Disodium hydrogen monophosphate.
$FeCl_3 \cdot 6H_2O$	Ferric chloride hexahydrate
$MgSO_4$	Magnesium Sulfate
$ZnCl_2$	Zinc chloride
$NaNO_3$	Sodium nitrate
$ZnSO_4.7H_2O$	Zinc sulfate heptahydrate
KH_2PO_4	Potassium dihydrogen phosphate
NaH_2PO_4	Sodium dihydrogen phosphate
p-NPA	Para Nitrophenyl acetate

p-NP	Para Nitrophenol
h	Hours
v/v	Volume by volume
rpm	Rotation per minute
kHz	Kilo Hertz
µg/mL	Microgram per milliliter
nm	Nanometer
µL	Microliter
rRNA	Ribosomal RNA
BLAST	*Basic Local Alignment Search Tool*
MEGA X	Molecular Evolutionary Genetics Analysis
K^+	*Potassium*
Mg^{2+}	Magnesium ion
Na^+	Sodium
Zn^{2+}	Zinc (II) ion
Al^{3+}	Aluminum ion
Fe^{3+}	Ferric ion
w/v	Weight by volume
CTAB	Cetyl trimethyl ammonium bromide
mA	*Milliampere*
MALDI-TOF-MS	Matrix-assisted laser desorption/ionization-time of flight-Mass spectrometry
NCBI	National Center for Biotechnology
PDB	Protein Data Bank
DS	Discovery Studio
CHARMm	Chemistry at Harvard Molecular Mechanics
U/mL	Units per millilitre
Tris–SO_4	Tris sulphate
C	Carbon
O	Oxygen
Ca	Calcium
N	Nitrogen
EDX	Energy Dispersive X-Ray
Da	Dalton

NMR	Nuclear magnetic resonance
DOPE	Discrete Optimized Protein Energy
ProSA	Protein Structure Analysis
$Cu_3(PO_4)_2$	Copper (II) phosphate
NH_2	Amine
$Zn_3(PO_4)_2$	Zinc phosphate
µmol /mL/min	Micromoles per milliliter per minute

LIST OF FIGURES

LIST OF TABLES

ABSTRACT

The gradual increase in atmospheric carbon dioxide (CO_2) caused by the use of fossil fuels has recently raised environmental concern. To mitigate the CO_2 level, novel conversion strategies are urgently needed. Numerous biological, physical, and chemical approaches have already been exploited for CO_2 conversion. Among these, the conversion of CO_2 using carbonic anhydrase (CA) is an eco-friendly approach that transform millions of CO_2 molecules into bicarbonate ions (HCO_3^-). Furthermore, HCO_3^- formed during CO_2 conversion can be precipitated into calcium carbonates ($CaCO_3$), which is an essential raw material in various industries.

Thus, a CA-producing bacterium, *Corynebacterium flavescens* T5 was isolated from cow saliva. The maximum CA production was obtained by the optimizing production parameters. The optimum production parameters were media (nutrient broth), temperature (40°C), inoculum volume 4% (v/v), inoculum age (24 h), and agitation speed 120 rpm. The optimized reaction parameters were reaction pH (7.0), buffer molarity (50mM), reaction time (10 min), and temperature (35°C). All the tested organic solvents and denaturing agents inhibits the enzyme activity. As per our knowledge, *C. flavescens was* reported first time for the CA production and found to be promising candidate.

After that, the keratin particles were used to immobilize *C. flavescens* cells to improve the CO_2 conversion efficacy. The optimum glutaraldehyde concentration, temperature, and incubation period were found to be 0.6 % (v/v), 25 h, and 4°C. After 10 cycles, the production of $CaCO_3$ for immobilized cells was found to be 53.46%. The FE-SEM analysis of synthesized $CaCO_3$ showed the main form of crystal was vaterite. The FTIR analysis confirms the functional groups, while the XRD analysis revealed the crystalline structure of $CaCO_3$. The whole cell immobilization on keratin particles proved to be effective for CO_2 conversion.

Furthermore, the CA was purified using column chromatography with 10.4-folds purification having molecular weight approximately 29 kDa on SDS-PAGE. Further, MALDI-TOF-MS analysis confirmed that the purified protein showed 58% of the sequence coverage with *K. pneumoniae*. The purified CA exhibited a slightly basic pH (7.5) and reaction temperature (35°C).

To improve the physiochemical properties and stability of the enzyme, the nanoflower of purified CA was synthesized. The flower-like morphology of carbonic anhydrase

nanoflowers (CANF) was confirmed by FE-SEM. The CANF showed 90% of immobilization yield and a good catalytic activity. The optimal reaction temperature of CANF was 40°C, whereas the optimal pH and reaction time were 7.5 and 10 min, respectively. The CANF has shown improved thermostability and storage stability in comparison to free CA. The CANF exhibited a lower K_m value (4.7 mM) as compared to free CA (5.1 mM), suggesting that CANF has higher accessibility for substrate. Furthermore, the CANF retained 80% of relative activity after nine cycles of reuse. The application of CANF for CO_2 conversion showed higher $CaCO_3$ production (1.71-folds) than free CA. This study proved that CANF has a promising future for converting CO_2 into $CaCO_3$, thus it can utilize to mitigate the CO_2 level in the environment which is one of the major concerns of the 21st century.

Keywords: CO_2, Carbonic anhydrase, isolation, *C. flavescens*, optimization, whole-cell immobilization, purification, CANF, $CaCO_3$

Chapter 1 Introduction

In recent years, one of the serious problems that emerge out is global warming, which protrudes due to the rise in the level of carbon dioxide (CO_2) in the atmosphere. The repercussions of global warming are acidic oceans, deviation in crop patterns, air pollution, and disease patterns. CO_2 is one of the major greenhouse gases (GHGs) emitted by anthropogenic activities and is the main contributor to the climate change [1, 2]. From 2000 to 2014, the CO_2 emission rate increased by 2.6% per year, and its yearly production is nearly 35 gigatons [3]. Indeed, daily worldwide CO_2 emission reduces in 2020 due to Covid -19, but the global CO_2 level increases continuously. In 2020, the CO_2 concentration was reported to be 411ppm, with the majority of CO_2 coming from transportation, industries, electricity generation, and fossil fuel burning. By 2100, the CO_2 concentration could reach approximately 540-970 ppm and may lead to a high rise in the temperature [4, 5]. The mitigation of most GHGs, like CO_2, has been considered an important concern to prevent the irreversible environmental damage. Since, the industrial revolution, GHGs emissions have been growing at an expeditious rate due to the rise in fossil fuel usage and energy demand. Moreover, by evaluating the existing energy need it is not possible to substitute the non-renewable resources with alternate energy [6]. To sustain the carbon cycle, plants transform the CO_2 into organic compounds, this is also affected by the use of fossil fuels [7]. The excessive burning of fossil fuels releases the stored carbon into atmosphere, where it become GHG. The GHGs trap heat in the atmosphere, causes global warming. Indeed, climate change has an impact on plant growth and development, due to the variations in photosynthetic carbon assimilation [8]. In all the sectors of the economy, worldwide CO_2 emissions must be diminished to mitigate the CO_2 level in the atmosphere. Several researchers have been working on capturing and converting CO_2 into industrial products in an economically safe manner [9, 10].

Numerous biological, physical, and chemical approaches have already been exploited for CO_2 conversion. Among these methods, the enzymatic method is recognized as a suitable way for converting CO_2 into high-value products using formate dehydrogenase (FateDH) and carbonic anhydrase (CA), due to the green nature of the biocatalyst. CA rapidly catalyze the hydration of CO_2 in an eco-friendly manner, with a turnover number of approximately 10^6 s^{-1} [11]. Furthermore, HCO_3^- formed during CO_2 conversion can be precipitated by calcium ions into calcium carbonates ($CaCO_3$), that might be used as raw materials in pharmaceuticals, construction materials, and cosmetics [12, 13]. However, the CO_2 conversion using chemicals generally needs high pressure, temperature, and more reaction time, whereas CA can fix CO_2

and shows a higher reaction rate at low-pressure conditions. The main advantages of using CA producing microorganisms to convert CO_2 are economic viability and higher turnover number [14]. CA is the first recognized metalloenzyme that contains mostly zinc in its active site and is one of the utmost catalytically effective biocatalysts [15]. CA is ubiquitous in all domains of life, and the physiological function of CA in different organisms includes the transport of CO_2/HCO_3^-, respiration, photosynthesis, homeostasis, lipogenesis, and ureagenesis, *etc* [2, 16, 17]. Even though CA is omnipresent, CA from microbes has attracted attention due to its easy production. CA- producing bacterial species such as *Neiserria gonorrhoeae, Bacillus subtilis*, *Serratia* sp., *Bacillus schlegelii, Citrobacter freundii,* and *Aeribacillus pallidus* have been explored for converting CO_2 into $CaCO_3$ [2]. In microbes, CA is produced inside the cytoplasm or extracellular spaces. In this context, the purification of CA from bacteria offers immense potential for its CO_2 conversion application. The microbial enzyme can be purified by fractionation, concentration, and chromatographic techniques. The molecular mass of CA varies from species to species, but most CA purified from a microbial source is a monomeric protein and their molecular mass generally lies in the range of 25-35 kDa [18]. The purification of the enzyme is important, as it increases its stability and specific activity [19].

Despite being the fastest known enzyme, the poor stability, sensitivity to the environment, high cost, and fragile nature of native CA severely limit its industrial application. Highly stable CA that can withstand extreme pH(s), high temperature, and high salinity is required to capture CO_2 from industries. As a result, various methods such as directed evolution, genetic engineering, and molecular modification are being used to improve CA's stability and economic productivity. However, these approaches are costly, tedious, and time-consuming. [20, 21]. At the same time, immobilization overcomes these drawbacks, so expanding the possible large-scale industrial applications of CA [22, 23]. In the last decade, various attempts have been made for enhancing the thermal and chemical stabilities of CA using immobilization. Recently, various hybrid, organic, and inorganic matrices have been utilized as a matrix for immobilizing CA, which not only permit its usage in harsh conditions but also improve the recovery and efficiency to diminish the cost of industrial applications [24]. To improve the CA application, the various matrices used for immobilization include alginate, biosilica, glass micropipettes, biochar, metal-organic framework (MOFs), and a variety of nanoparticles [25-28]. The immobilization matrices play a vital role because the properties of the matrices could have a strong impact on thermal stability, immobilization yield, and enzyme activity [29]. Indeed, the development of eco-friendly and low-cost materials for CA immobilization is still needed. Moreover, various parameters that are considered during the

immobilization process are a selection of support material with suitable surface chemistry, pore diameter, mechanical resistance, and evaluation of experimental conditions to optimize enzymatic activity, immobilization yield, and stability under rigorous industrial conditions [30, 31]. The most commonly used enzyme immobilization approaches are adsorption, entrapment (encapsulation), binding to support (carrier), and cross-linking [32]. Importantly, the immobilized biocatalyst shows excellent reusability, improved thermal stability, low levels of leaching, and good storage properties in comparison to the native biocatalyst [33]. Enzyme immobilization is an efficacious method to enhance the stability, reusability, and reduce the biocatalyst cost. Thus, enzyme immobilization has become a mandatory step for creating an enzyme as an industrial biocatalyst.

In some cases, immobilized enzymes show a loss in activity due to alteration in the 3-D structure, and a rise in mass-transfer limitations [34]. Recently, there have been various methods reported for CA immobilization that do not use any preexisting solid matrix, such as cross-linked enzyme aggregates, nanoflowers (NFs), copolymers, and sol-gels [35, 36]. Previously, NFs attracted considerable interest due to their flower-like morphology and combination of organic and inorganic functionalities [37]. The nanoflowers exhibit excellent stability because the inorganic part forms a protective covering for the organic part. This hierarchical porous structure results in a high surface area, cooperative effects among metal ions and enzymes, which boosts the catalytic activity and stability of nanoflowers [38]. However, for large-scale applications, the low mechanical stability of carrier-free immobilized enzymes must be considered. Various methods of immobilization are available each of them has its pros and cons. Furthermore, several pilot plants are installed for capturing and converting CO_2 using immobilized CA. The CO_2 released from the cement industry can be captured and transformed into fine chemicals. In the previous report, for recovering the CO_2 discharged from the cement plant, a CO_2 capturing unit was installed in which immobilized CA was used for converting the CO_2 into $CaCO_3$. The manufactured $CaCO_3$ was utilized as the preliminary material for the manufacture of Portland cement [39]. But, for CO_2 conversion, an inadequate number of industrial methods using CA have been known until now. The goal of CO_2 mitigation approaches is to reduce GHG emissions by up to 40 -70% and achieve neutral emissions by the end of the 21st century.

In light of the above, the present study has been conceived with the aim, of "**Molecular characterization, purification, and immobilization of a bacterial carbonic anhydrase for efficient CO_2 conversion.**" An experimental approach has been designed with the following main objectives:

i) Screening of carbonic anhydrase-producing bacterial isolate from cow saliva.

ii) Whole-cell immobilization and $CaCO_3$ production using keratin particle immobilized cells.

iii) Purification and characterization of carbonic anhydrase from the isolated strain of *Corynebacterium flavescens.*

iv) Synthesis of carbonic anhydrase nanoflowers and its application for CO_2 conversion.

Chapter 2 Review of literature

2.1 Global warming

Global warming is the instant increase in the earth's temperature, mainly due to the release of GHGs. The most emitted GHGs are CO_2 (56%) and CH_4 (17%), whereas CO_2 is the utmost vital gas in terms of the amount emitted and the most widely studied [40]. The upsurge in the atmospheric CO_2 concentration is a severe environmental issue that the whole nation is facing due to anthropogenic activities including fossil fuel combustion, industrialization, transportation, and deforestation [2, 41]. International energy agencies reported that residential, energy, transportation, and industrial sectors are responsible for 7, 20, 22, and 41% of CO_2 emissions, respectively (Figure 2.1) [42]. Among these, energy power plants (41% of overall CO_2 emissions) are the largest contributors of CO_2 emissions, so they are the key targets for CO_2 reduction. Since the industrial era, the CO_2 concentration has increased by 75% [43, 44]. Based on the latest report from the global carbon project, Japan, China, Russia, USA, and India are the top five nations generating the most CO_2 [45]. To save the environment from the harsh effects of GHGs, environmentalists urge people to utilize clean energy sources. Furthermore, to replace fossil fuels, green energy products are in huge demand. In 2015, the United Nations Agreement emphasized the effects of CO_2 emission on the environment mainly referred to fossil fuel combustion, highlighting that this emission raises the level of CO_2 trapped in the troposphere and hence increases the global atmospheric temperature [46]. In the polar area, the temperature rise would be three times more than that of other areas, which can harshly affect the living organisms and their survival on the earth. In the past years, an abnormal variation in the seasonal temperature in different geographical areas has been observed. It is predicted that in 2030, the CO_2 concentration in the atmosphere will touch 600-1500 ppm [47]. Moreover, due to the climate crisis, agricultural production has also been affected, resulting in food shortages and a rise in food prices. The harmful effects of global warming are continuously aggravated due to ozone depletion and the rise in heat waves, which directly or indirectly raise the incidence of heat-related diseases and fatalities [48, 49]. Various marine, terrestrial, and freshwater species are on the verge of extinction.

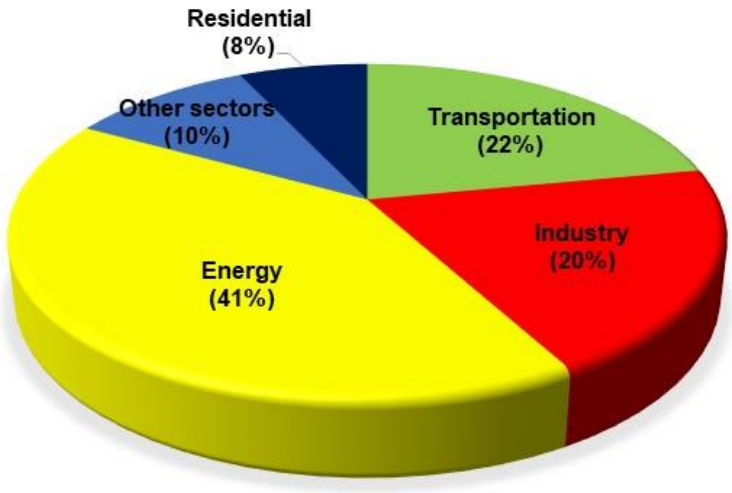

Figure 2.1: CO_2 emission from different sources [50]

Various cities around the world are responsible for GHGs emissions and energy consumption. Therefore, to reduce GHGs, cities will be required to use less energy and utilize renewable energy resources. Nowadays, smart cities are being developed for mitigating the CO_2 footprint. Smart cities are described as the development of an urban area, that usages the internet of things and information communication technology to provide real-time information to efficiently manage resources. The main motive of smart cities is to improve transportation, energy efficiency, security, waste management, and water management [51]. The idea of the smart city includes smart mobility (promoting public transport, electric vehicles, and carpooling as well as traffic management), smart lightening (reducing energy usage by providing a particular amount of light at a particular time), smart buildings (optimizing air conditioning, heating, and energy usage), smart environment (monitoring water and waste management, urbanization, and sustainable processes), smart people (e-learning, connected citizen and e-health), and smart governance (digital process automation, public welfare) [52]. Various smart cities, such as Singapore (36% by 2030), London (60% by 2025) Barcelona (45% by 2030), Amsterdam (60% by 2025), host the project, to reduce CO_2 emissions [53]. The European countries have started a start-up program called Everimpact; they developed software that provides various ways to calculate GHGs continuously. The emission-correct data is the basis for making policies and taking initiatives to cut these emissions. Furthermore, smart cities utilize sensor technology to collect and analyze information regarding crime rates, traffic rush hours, and air quality [54]. The execution of these biosensors requires costly infrastructure and high maintenance. Secondly, urbanization should be considered a priority to

deal with the rising slum population [55]. So, it must be ensured that no residents are excluded from the data collection of smart cities.

In the present scenario, global warming is a threat to mankind's survival as well as ecological and biological systems. So, there has been increased pressure for scientists to develop a novel technology for CO_2 capture and utilization. Till now, several materials, chemicals, enzymes, and plants have been described for CO_2 conversion (Figure 2.2). Nowadays, most research work is focused on how to convert CO_2 into methane, calcium carbonates, organic acids, and methanol. Additionally, utilizing CA for converting CO_2 into a value-added chemical is the utmost effective biological method, as it offers an economical approach to oppose the growing threat of a climatic catastrophe [6]. The main reason is microbial enzymes can be cultured and produced at a large scale for industrial use in a short period of time without any detrimental effect on the environment. However, the CO_2 conversion by non-biological approaches is restricted due to environmental limitations and high operational cost.

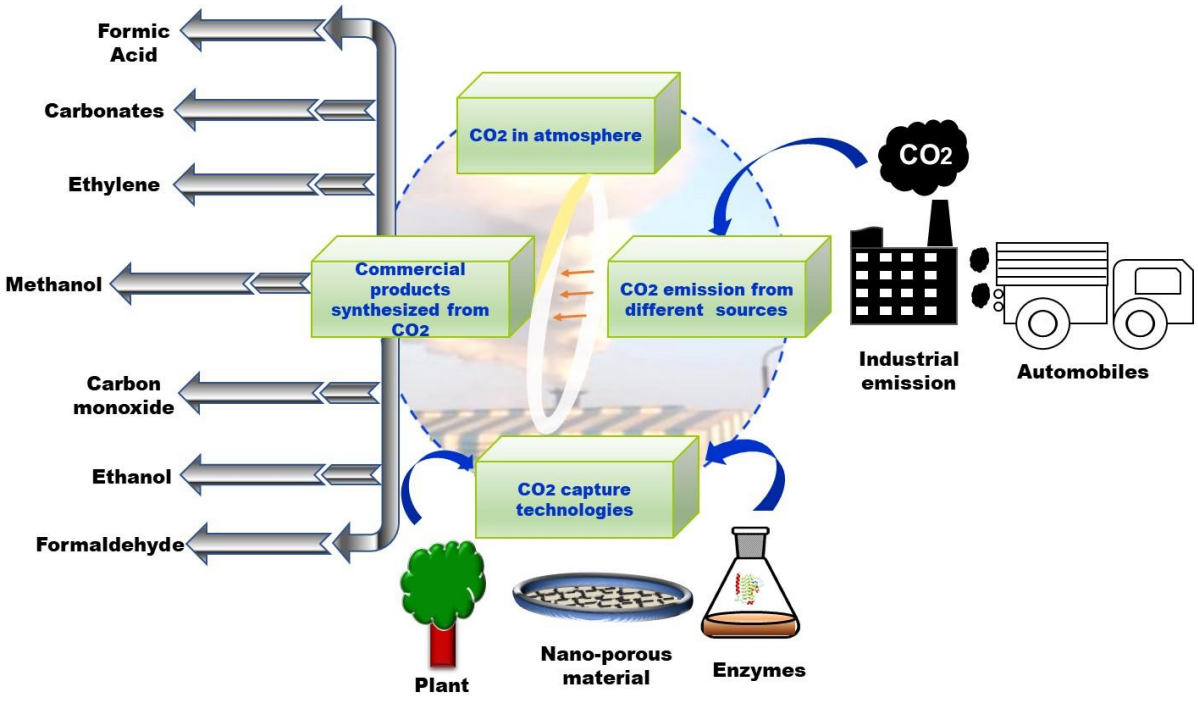

Figure 2.2: Schematic illustration of various systems utilized for the conversion of CO_2 to fine chemicals [56]

2.2 Approaches for mitigating the global warming

For CO_2 conversion, various enzymes (*e.g.*, CA, alcohol dehydrogenase, RubisCo, formate dehydrogenase), materials (biochar, porphyrin, zeolites, metal-organic frameworks), and chemicals (*e.g.*, diethanolamine, monoethanolamine, piperazine) have been used (Figure 2.3). Furthermore, the use of a non-biological approach for mitigating CO_2 has been proven to be efficient but has some drawbacks, including pollutant regeneration and high operational costs. Nowadays, various effective methods are available for CO_2 capture and utilization, but they have not been used on a large scale [40]. If the government would start investing in these strategies, then the execution of CO_2 capture and conversion plants would become operational in a short time.

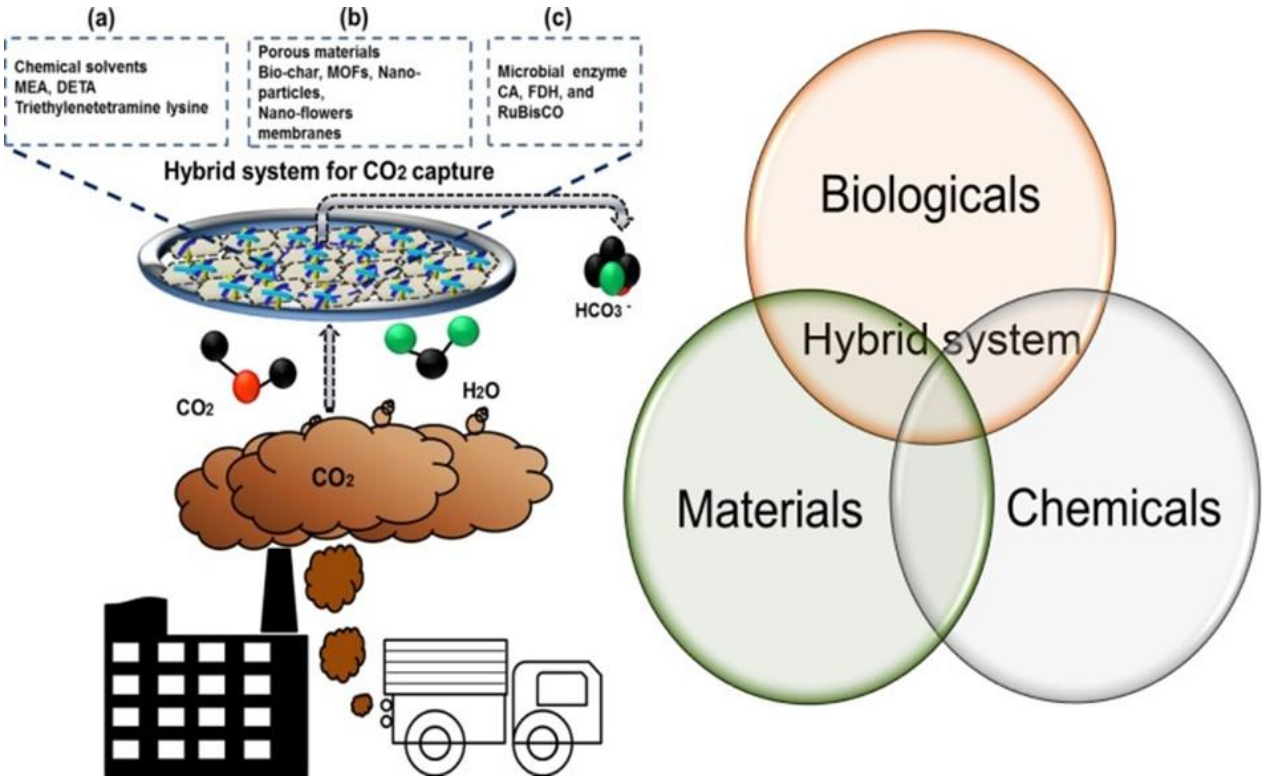

Figure 2.3: Schematic illustration of an integrated system having chemicals, porous material, and microbial enzymes for capturing and converting CO_2 [2]

2.2.1 Chemical fixation of CO_2

Ionic liquids, blended amine solvents, and biphasic solvents are some of the chemicals used for CO_2 capture (Table 2.1). Various chemicals such as dimethylamino-propylamine

acetate (DPA), methylcyclohexyamine (MCA), methyldiethanolamine (MDEA), monoethanolamine (MEA), triethylenetetramine (TETA), diethylenetriamine (DETA), dimethylcyclohexylamine (DMCA), pentamethyldiethylenetriamine (PMDETA), diglycolamine (DGA), dibutylamine (DBA), and piperazine (PZ) are employed for capturing the CO_2, but the main drawback is the high energy need for regeneration [57-59]. Nowadays, researchers are more concerned about studying blended solvents as they need low energy, resistant to solvent degradation, and temperature. In a recent study, MCA was blended with DMCA to capture CO_2, and the CO_2 absorption ability of the DMCA-MCA solvent was higher than MCA [60]. Furthermore, to diminish the energy consumption in the regeneration of the solvents; Wang et al., blended DETA/sulfolane to capture CO_2 and found that at the end of the reaction, two liquid phases were formed and sulfolane easily separated from the reaction mixture [61]. So, during the regeneration process, solvent loss and energy consumption are also reduced.

Table 2.1: Various chemicals reported for the CO_2 capture

S. No	Solvent	CO_2 absorption capability (mol /mol)	Regeneration efficacy (%)	Reference(s)
1.	DETA-Propanol	6.5[a]	NA	[62]
2.	DMCA-MCA	0.9	NA	[60]
3.	Tetraethylenepentamine-Methylimidazolium	1.7	90.7	[63]
4.	TETA-DMCA	0.9	NA	[64]
5.	1-Butyl-3-methylimidazolium tetrafluoroborate-sodium glycinate	0.6[a]	64.0	[65]
6.	DBA	0.8	94.3	[66]
7.	PMDETA-DETA	0.6	NA	[67]
8.	Dual functional ionic liquid	1.3	NA	[68]
9.	MEA/water	0.4	NA	[69]
10.	TETA-hydrobromide-PMDETA	2.6[a]	95.0	[70]
11.	Trihexyl(tetradecyl)ammonium lysinate	2.1	NA	[71]
12.	Tetramethylammonium glycinate	0.6	98.0	[72]
13.	TETA-lysine-ethanol-H_2O	2.3	93.0	[73]
14.	Piperazine/propanol/H_2O	1.2	74.0	[74]

15.	AMP/Piperazine	0.8	57.0	[75]
16.	DPA/ ethylenediamine	0.2[b]	NA	[76]
17.	DPA/Fluorine	0.1[b]	94.0	[77]
18.	DGA-PEG 200	0.4	94.6	[78]
19.	DBA/ethanol/H_2O	0.8	94.3	[66]
20.	Sulfolane/DETA	1.7	NA	[79]

[a]mol/l
[b]g/g

Moreover, ionic liquid (IL) with high polarity, low energy requirement, high thermal stability, and low volatility has attracted the environmental engineer's attention for capturing the CO_2 [76]. Previously, it was found that the addition of hydroxyethyl-3-methylimidazolium lysine [C_2OHmim][Lys] to MDEA enhanced the CO_2 absorption capacity, due to the strong affinity of CO_2 with an amine [80]. Furthermore, to capture the CO_2 from industry, Voskian et al., used the ethylenediamine functionalized IL, which has a CO_2 capture performance of 0.95 mmol CO_2/g IL [81]. From these studies, it can be assumed that the blending of IL with the amino group results in enhanced CO_2 capture capability. However, the prime cost and high viscosity of IL are the main obstacles to its practical usage. The chemicals utilized for CO_2 capture may emit highly toxic compounds into the environment, and the degradation of these products is more difficult. Thus, future studies should be emphasized on blending microbial enzymes with chemicals to decrease the release of toxic compounds into the environment.

2.2.2 Materials for CO_2 capture

Various materials, including porous carbon, porphyrin, MOFs, and zeolites with good absorption capacities, have been used to capture CO_2 (Table 2.2). The CO_2 absorption on the surface of these materials is dependent on structural configuration, surface chemistry, and pore size. Ideal materials for CO_2 absorption should have fast kinetics, high reusability, high selectivity, good thermal stability, and be cost-effective [82]. Previously, N-doped porous carbon was created by the template-free method and the effect of various nitrogen sources such as ethylenediamine, melamine, and hexamethylenetetramine on CO_2 absorption was examined [83]. The porous carbon material having ethylenediamine as a nitrogen source exhibited the highest nitrogen atoms, micropore volume, and CO_2 uptake. Indeed, MOFs having porous crystalline structures and large surface areas have shown applicability for capturing CO_2.

Recently, to improve the performance of MOFs, the doping of metal ions has been widely used. Previously, the MOF (UTSA-16(Zn)) synthesized by replacing cobalt with zinc via microwave irradiation showed improved stability, CO_2 absorption ability, and selectivity as compared to cobalt-containing MOFs [84]. Previously, the porous zeolite-chitosan was synthesized using a solvent exchange technique and showed a CO_2 capture efficiency of 1.70 mmol/g. The zeolite-chitosan having well defined porous structure synthesized using a solvent exchange technique showed 1.70 mmol/g CO_2 capture efficiency. Zeolite-chitosan has interaction sites for CO_2 capture, so it could be explored for CO_2 capture efficiently [85, 86]. Recently, porphyrin emerged as an ideal material for CO_2 capture, having a basic pyrrole cavity and aromatic rings, which allow good binding with CO_2 [87, 88]. Previously, Jiang et al., synthesized porous tetraphenyl porphyrins (POTPPs) to attain high CO_2 absorption ability [89]. The POTPPs with large surface area and nitrogen content showed 3.25 mmol/g of CO_2 absorption ability. Generally, the porosity, morphology, texture, and surface area have an enormous effect on the material CO_2 absorption performance. Therefore, these materials could be utilized for large-scale CO_2 capture as they show higher CO_2 absorption ability. But the further transformation of CO_2 into valuable chemicals is still required to be explored.

Table 2.2: Various materials reported for capturing CO_2

S. No	Material	Temperature	Pressure (bar)	Porosity (cm^3/g)	Surface area (m^2/g)	CO_2 absorption ability (mmol/g)	References
1.	Zeolite-chitosan	NA	4.60	0.06	22.53	1.70	[85]
2.	HKUST-1 MOF	25.00	1.00	0.59	1409.00	4.10	[90]
3.	Porous carbon	25.00	1.00	1.34	2264.00	3.88	[91]
4	Porous carbon	25.00	30	2.03	4196.00	28.30	[92]
5.	UTSA-16 (Zn)	24.85	1.00	0.50	475.38	4.71	[84]
6.	Hierarchically porous carbon	25.00	1.00	10.00	2700.00	3.70	[93]
7.	Porous carbon	25.00	1.00	NA	3260.00	4.30	[94]
8.	Amino-functionalized porphyrin	NA	1.00	0.46	587.00	328.10*	[95]
9.	N-doped Hierarchically porous carbon	30.00	NA	NA	301.00	74.76*	[83]
10.	ZIF-8 MOF	NA	0.15	0.65	1742.00	1.9 *	[96]
11.	PCN-124	0	1.00	0.57	1372.00	9.10	[97]
12.	Porous covalent triazine polymer	25.00	1.00	0.62	1200.00	3.2	[98]
13.	Li-LSX Zeolite	60.00	1.00	0.32	660.00	4.43	[99]
14.	CaCHA Zeolite	25.00	1.00	0.35	660.00	5.90	[100]

*mg/g

2.2.3 Natural ecosystem for CO_2 capture

In plants and algae, enzymes such as CA and Rubisco have been reported to capture CO_2 [101]. Rubisco is a key enzyme for photosynthesis and converts CO_2 into an organic compound, but it shows a low affinity for CO_2 [102]. The *Pinus radiate* tree and Chinese forest were reported to sequester 300 and 41 tons of CO_2 per hectare [103, 104]. Also, mangrove forests can capture 654 tons of carbon per km^2 annually [105]. Coastal ecosystems, such as salt marshes and *Cymodocea nodosa*, are considered good CO_2 sinks [106]. During summers, the Antarctic coastal ecosystem and the coastal ocean have a CO_2 fixation rate of 14 to 34 teragrams of carbon per year [107, 108]. Nowadays, a decline in world carbon storage is reported due to the extinction of some ecosystems, resulting in global warming. The rise in atmospheric CO_2 level results in an increase in photosynthesis rate, but up to some level; thereafter excess CO_2 concentration starts affecting the plant's nutritional level [109]. For example, in China Tiantong National Forest decreases 4.38% carbon storage reported annually and it's affected by climate change [110]. To enhance carbon storage, ecosystem restoration could be a suitable option.

Furthermore, algae are widely exploited for CO_2 fixation because of their biodegradability, higher CO_2 fixation rate, and lack of toxicity. During photosynthesis, algae use CO_2 as a carbon source and transform it into organic compounds via the Calvin-Benson pathway [111]. These compounds can be further converted into value-added compounds, including vitamins, proteins, lipids, oils, and carbohydrates that can be utilized as preliminary materials for biofuel production, functional foods, and animal feed. The CO_2 released from industrial areas can be utilized as a source of carbon for algae production. Algal species including *Chlamydomonas reinhardtii, Nannochloropsis* sp., *Tetraselmis suecica, Nannochloris* sp., *Scenedesmus quadricauda,* and *Chlorella vulgaris*, have been reported for CO_2 sequestration [112]. Kassim and his co-workers reported that the CO_2 capture capacity of *Chlorella* sp., was 95.0 mg/L/day [113]. Also, the CO_2 capture efficiency of *Grasiella* sp., at pH 9.0 was found to be 18.9 g m^{-2} /day [114]. In ponds, microalgae are utilized to capture gaseous CO_2 because they have a greater photosynthetic rate than terrestrial plants. In an open pond, the *Chlorella* sp., showed 46% of CO_2 removal efficiency. Furthermore, temperature variation, pond design, and algal physiology also affects the CO_2 fixation capacity of algae in ponds [45, 115]. The microalga, including *Chlorella vulgaris, Isochrysis galbana, Dunaliella tertiolecta,* and *Thalassiosira weissflogii,* can even grow using CO_2 as a carbon source from the cement industry [116]. In this process, dust present in the emission

source may hinder microalgae growth, so it should be eliminated before being inserted into a culture. The drawbacks of using algae for CO_2 fixation are growth conditions, the need light for growth, and poor usage in industrial reactions. Thus, to enhance the CO_2 fixation efficacy using algae, screening and domestication could be a promising approach.

2.2.4 Enzyme mediated CO_2 conversion

The utilization of enzymes for mitigating the CO_2 is a sustainable solution due to the regio-selectivity and stereo-specificity of enzyme-mediated CO_2 conversion. Various approaches for searching potent enzymes having high CO_2 conversion yield include the isolation of microbial enzymes from various habitats, enzyme immobilization, and directed evolution. Enzyme-mediated CO_2 transformation into valuable products is a green approach to alleviate climatic catastrophe. For example, dehydrogenases such as FateDH and FalDH were reported for methanol synthesis from CO_2 in the presence of NADH as a coenzyme (Figure 2.4) [117]. The methanol production from CO_2 is advantageous because it is cheap, substitutes for petroleum-based fuels, and is less flammable. Furthermore, the multi-enzymatic cascade is beneficial for CO_2 conversion over a single enzymatic reaction due to its high energy capacity. For improving the activity of the biocatalytic cascade, the three dehydrogenases were immobilized in a mesostructured cellular foam of silica [118]. Their studies showed that after immobilization, the methanol yield was 4.5-folds higher than the free enzyme. Previously, Jiang et al., encapsulated the three dehydrogenases in gel beads, and immobilized enzymes showed higher methanol production approximately 12 µmol. Whereas free CA showed 1 µmol methanol production after eight cycle of reuse [119]. The CO_2 reduction using dehydrogenases is NADH-dependent, but NADH is costly and increases the enzymatic reaction cost [120].

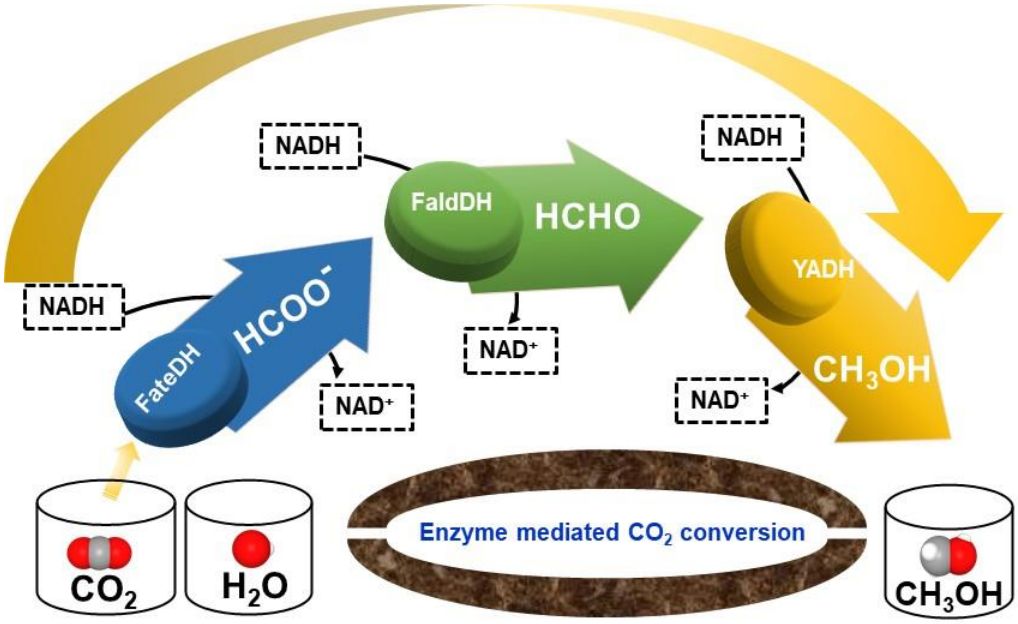

Figure 2.4: Schematic illustration for the conversion of CO_2 to methanol using dehydrogenase enzyme [50]

However, CA is the utmost efficient enzyme for the transformation of CO_2 into valuable products, as it does not require external cofactors [121]. The CA purified from *Bacillus* sp., was studied to produce $CaCO_3$ from CO_2. This CA has a half-life of 54.94 min at 60°C, making it more suitable for large-scale conversion because it saves cooling costs and time [122]. Also, CA from *C. freundii* resulted in 230 mg of $CaCO_3$ production per mg of protein. Moreover, Li et al., cloned the *Lactobacillus delbrueckii* CA, their study showed that the recombinant CA forms 183 mg of $CaCO_3$ at 50°C [123]. These reported studies indicate the utilization of the microbial enzyme as a potent candidate for CO_2 conversion.

2.3 Carbonic anhydrase

CA (E.C. 4.2.1.1) belongs to a class of lyases, having the ability to convert CO_2 into bicarbonate ions [124]. In the presence of calcium ions, the bicarbonate ions can be converted into $CaCO_3$ according to the equation:

$$CO_2 + H_2O \rightarrow HCO_3^- + H^+$$

$$Ca^{2+} + HCO_3^- \rightarrow CaCO_3 + H^+$$

$CaCO_3$ formed through CO_2 conversion can be used for the cement making, antacids, pigments, and others, thus removing the CO_2 in a safe, efficient, stable, and environment-friendly manner [125]. In 1933, CA was initially discovered in red blood cells by Meldrum and

Roughton. In 1963, Blankenship first reported the existence of CA in bacteria. Considering the importance of CA in CO_2 capture and conversion, Smith and Ferry started the purification and characterization of CA in 1994 [126]. Nowadays, the CA has been purified from numerous bacterial species like *B. pumilis, E. coli, N. sicca, A. pallidus, P. fragi* [2]. CA is omnipresent and plays an important role in various physiological processes, including lipogenesis, CO_2/bicarbonate transport, pH homeostasis, secretion of electrolytes, gluconeogenesis, and photosynthesis [127].

2.3.1 CA types and catalytic mechanism

CA has divided into five classes, namely α, β, γ, δ, and ζ on the basis of amino acid homology. Mostly, the metal ion in α, β, γ, δ, class is zinc, however ζ class have cadmium as a metal ion [17, 128]. Structural analysis showed that CA active site differs depending on the class of CA (Table 2.3). The detailed 3-D structure of *Methanosarcina thermophila* CA was shown in (Figure 2.5) using the PyMOL educational version. Generally, α-CA is present in mammals, plants, algae, and bacteria. The structure of α-CA is composed of ten β-strands that surround seven α-helices. The central β-sheets contain active residues of α-CA having water molecules, and three histidines that coordinate with zinc. Mostly, the α-CA are monomeric proteins [129, 130]. Furthermore, β-CA is present in archaea, plants, and bacteria. The structure of β-CA is dominated by α-helices that surround four β-sheets CA, and it can exist as the dimmer, tetramer, and octamer form. The γ-CA are the most ancient CA, having cobalt as a metal ion, and first discovered in *Methanosarcina thermophila* [131, 132]. Indeed, δ-CA was reported in diatom *T. weissflogii* and it showed structural similarity with α and γ-CA [133]. The ζ -CA has been reported in cyanobacteria, and its 3-D structure showed structural similarity with the β-CA [134].

Table 2.3: Various types of CA and its structural composition

S. No	Type	Amino acid residues	Metal ion	Structural composition	Source	Reference
1.	α	3 His	Zinc	Monomer	Bacteria and mammals	[130]
2.	β	2 Cys, Asp, His	Zinc	Dimer or tetramer	Archaea, plant, bacteria	[135]
3.	δ	2 Cys, His	Zinc	Monomer	Diatoms	[133]
4.	γ	3 His	Zinc, cobalt, and iron in anerobic conditions	Homotrimer	Methanogenic archaea	[131]
5.	ζ	2 Cys, His	Cadmium	Monomer	Diatoms and marine cyanobacteria	[134]

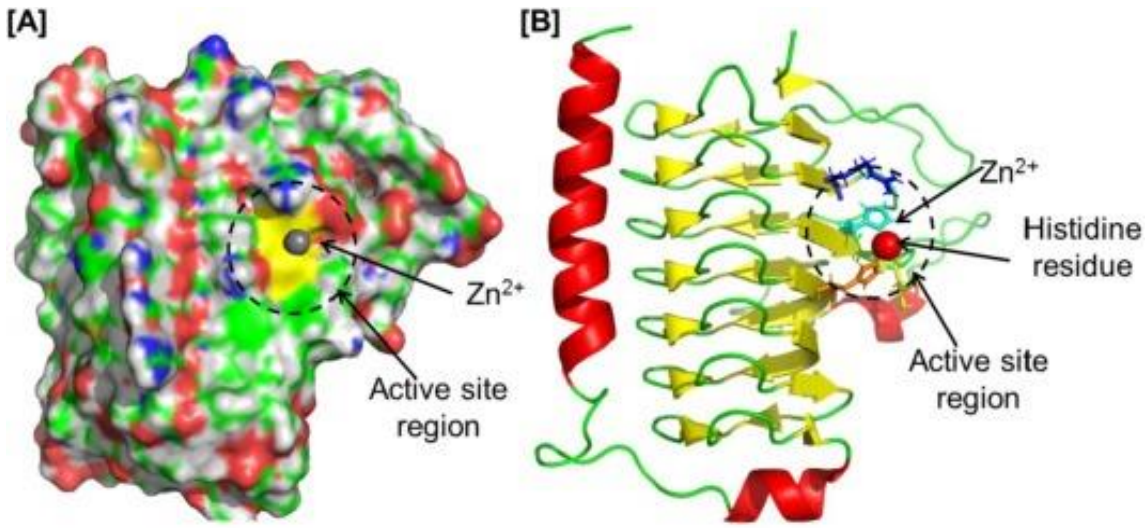

Figure 2.5: The detailed 3-D structure of *Methanosarcina thermophila* CA belongs to γ-class a) surface structure and b) Cartoon structure of CA showing zinc and histidine in the active site [2]

There are two main regions in the CA active site, including the hydrophilic amino acid region (His-64, Asn-67, Tyr-7, Asn-62, Thr-199) responsible for proton movement and the hydrophobic amino acid region (Val-121, Thr-199, Leu-198, Trp-209, Val-207) important for trapping CO_2 [15, 136]. The catalytic mechanism of CA comprises of four stages. The catalytic

triad of CA has histidine residues, water molecules tetrahedrally coordinated with a zinc ion. In the first step, the proton releases from the catalytic triad to form zinc-hydroxide ion (Zn-OH^-); (2) The Zn-OH^- nucleophilically attacks CO_2 to form bicarbonate; (3) The zinc-bound bicarbonate (Zn-HCO_3^-) resulting in the formation of tetrahedral like structure; and (4) In last step, Zn-HCO_3^- is replaced by H_2O, results in completing the catalytic cycle (Figure 2.6) [137]. Moreover, CA also catalyzes the esters hydrolysis, and these reactions occur inside the hydrophobic pockets closer to the zinc [138].

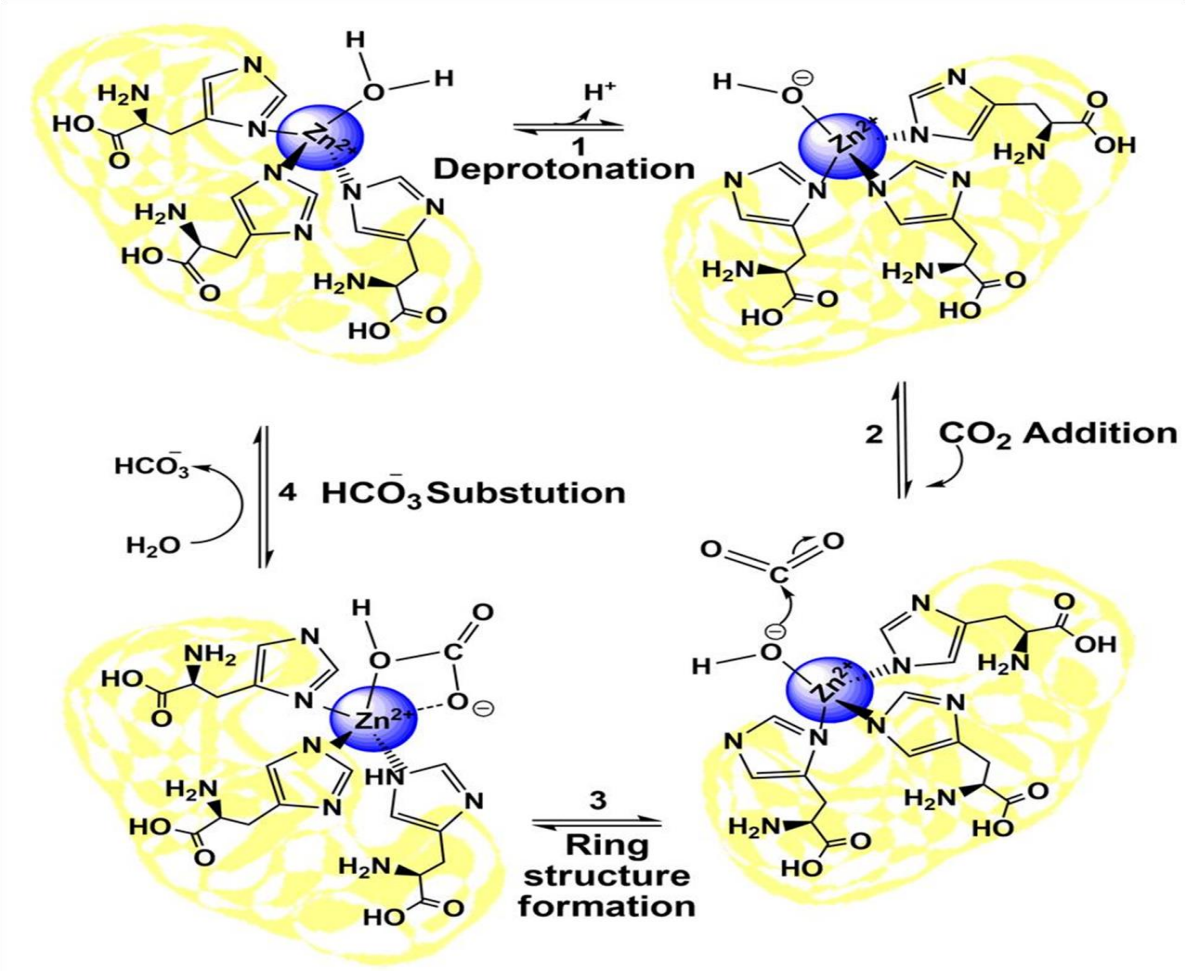

Figure 2.6: Mechanism of action of CA [2]

2.3.2 Potential of purified CA for CO_2 conversion

To meet CO_2 conversion requirements, this method needs CA to have high activity, purity, stability, and the ability to tolerate high concentrations of CO_2. The various methods for purification of CA investigated by researchers include gel filtration, ion exchange, affinity, and

reverse-phase chromatography. Furthermore, protein purification is very vital as it is required to study the enzyme structure, function, and kinetics [139]. The CA has been purified and characterized from mammals, diatoms, bacteria, cyanobacteria, archaea, and algae. Bovine erythrocytes CA was usually utilized for CO_2 conversion studies, but due to the high cost of isolation and purification its practical usage is restricted. Despite this, purified and recombinant CA from bacteria has been generally used for CO_2 conversion owing to its lack of external energy requirement and rapid kinetics [140]. The catalytic properties of CA purified from various bacterial species have been summarized in Table 2.4. Previously, Jaya et al., purified CA of molecular weight 21.0 kDa using affinity chromatography, which sequestered 95.4% (v/w) of CO_2 from soil [141]. Furthermore, CA purified from *L. delbrueckii* had a half-life of 177 h at 50°C, making it more advantageous for industrial processes [123]. Previously, *Aerobacillus pallidus* CA (32.0 kDa) purified using Sepharose column chromatography, was stable at temperatures ranging from 40-60°C [142]. Also, recombinant CA purified by affinity chromatography was reported to produce 95.20 mg of $CaCO_3$ [143]. Furthermore, the molecular mass of *Bacillus* sp., CA purified by Sephadex G-100 and affinity chromatography was reported to be 28.0 kDa [122]. Previously, *Thermovibrio ammonificans and Perse-phonella marina* CA were cloned, and the recombinant enzyme proficiently speeds up $CaCO_3$ formation even at higher temperatures [144]. These reports revealed that CA is a promising candidate for the conversion of CO_2.

Table 2.4: Various CA purified from bacterial source and their catalytic properties

S. No	Source	Molecular weight	Optimum pH	Optimum temperature	K_m (mM)	V_{max}	mg $CaCO_3$/ mg protein	Reference
1.	*Bacillus* sp.,	60.0	8.0	28.0	1.7 [a]	385.9 U/mg	NA	[122]
2.	*Citrobacter frundii*	NA	7.0	37.0	NA	NA	230.0	[145]
3.	*Bacillus* sp.,	27.0	8.0	37.0	1.5	62.75 × 10^{-2} μM/ min	79.8	[143]
4.	*Mesorhizobium loti*	47.0	7.0	50.0	5.6 × 10^{-2}	NA	52.8	[146]

5.	*Serratia* sp.,	29.0	7.6	20.0	12.0	5.2 X 10^{-4} µM /min	31.5	[147]
6.	*L. delbrueckii*	23.8	6.0	50.0	NA	NA	183.0	[123]
7.	*A. pallidus*	32.0	8.0	37.0	NA	NA	42.5	[142]
8.	*B. subtilis*	37.0	8.3	37.0	9.0	714.2 µmol/mg/ protein	NA	[148]
9.	*B. safenis*	21.0	NA	32.0	NA	0.07 µmol/mg/ min	NA	[141]
10.	*Aliivibrio salmonicida*	26.0	8.0	40.0	NA	NA	NA	[149]

[a] mg/mL
[b] M

2.4 Modification of CA for enhanced CO_2 conversion

The CO_2 conversion using CA is the most cost-effective, environment-friendly, and sustainable method. Furthermore, the limitation of the CA isolated from natural sources in applied biocatalysis is that it is not stable under industrially relevant situations such as high temperature, the presence of non-aqueous media, and extreme pH [150]. Therefore, adapting enzymes for reaction environments with unnatural substrates, either to redesign the existing enzyme or design entirely a novel biocatalyst, has become both an opportunity and a challenge for researchers in this field [151]. Fortunately, in a few years, protein engineering and enzyme immobilization (EI) have become powerful tools to modify the enzyme in order to meet industrial demands. Protein engineering (PE) allows producing an enzyme that exhibits desired properties including activity, stability, selectivity, and substrate specificity. Generally, enzyme modifications using PE can be done by directed evolution or rational design. Site-directed mutagenesis, DNA shuffling, and error-prone PCR are most commonly used methods of PE [152, 153]. Moreover, EI allows the enzyme to be imprisoned in its phase, so allows its reuse [154]. EI and PE would be used as a parallel method for enhancing the properties of enzymes.

2.4.1 Protein engineering of CA

The development of CA having enhanced stability is one of the main requirements for capturing and converting CO_2 released from industries. Protein engineering has been utilized to engineer the CA so that it can withstand high temperatures, high salt concentrations, and alkaline conditions. Till now, the thermophilic CA isolated from *T. ammonificans* showed the highest thermal stability. The disulfide bonds between the two cysteine residues stabilize the 3-D structure of this protein and result in enhanced thermostability. Furthermore, the engineering of the disulfide bond of *Neisseria gonorrhoeae* CA results in an 8-folds increase in thermostability [155]. Previously, using molecular dynamic stimulation, mutants of bacterial α-CA with increased stability were created to investigate the relationship between temperature stability and structure flexibility. According to the molecular dynamic stimulation, *T. ammonificans* was the most thermostable CA and has a rigid structure and region with high flexibility [156]. In another study, the expression of *T. ammonificans* CA mutants was created using molecular dynamics (MD) simulations. One of these mutants exhibited 100% of the activity at 90°C compared to the wild type. These outcomes proved that CA mutant can serve as a promising biocatalyst with high thermal stability and activity for CO_2 capture applications [157]. Furthermore, *Thermosulfurimonas dismutans* CA (tdCA) was engineered for high-level expression via periplasmic expression and point mutation. Then the recombinant *E. coli* cells showing higher periplasmic expression were further examined for CO_2 hydration activities. The periplasmic tdCA mutant showed 11.9-folds higher activity as compared to previously reported halophilic CA constructed by engineering the ribosomal binding site [158, 159]. Moreover, the *T. ammonificans* CA was engineered by mutating the N-terminal region, and the new variant showed a three-fold enhancement in half-life at temperatures >70°C and pH 10 [157]. The highly stable variants of *Desulfovibrio vulgaris* CA were created using directed evolution that tolerates the alkaline amine solvent at 107°C. Eventually, this method enhanced the 25-folds CO_2 absorption rate than the noncatalyzed reaction [160]. From these studies, it can be concluded that the methods of PE could be utilized to enhance the stability and catalytic activity of CA for several applications on a large scale.

2.4.2. Immobilized CA for CO_2 conversion

Enzyme immobilization is a technique used in biotechnology to adhere a biocatalyst to an insoluble matrix. Also, the goal of immobilizing an enzyme is to enhance its qualities, such as activity, turnover rate, and stability, in addition to allowing for its continued use [161, 162].

Thus, enzyme immobilization is an effective technology to solve the instability issue of free enzymes and allows their reuse (Figure 2.7). Over the last decade, numerous efforts have been endeavoured for upgrading the thermal and chemical stability of enzymes using immobilization. The immobilization of enzymes has been recognized as valuable, and it was found that 20% of biocatalytic processes use an immobilized enzyme. In this protocol, the enzyme and support material interact either by entrapment, crosslinking, covalent binding, or absorption [163-165] (Figure 2.8). The catalytic features of a biocatalyst rely on the kind of support/matrix used for immobilization. Moreover, various parameters that are considered during the immobilization process include the choice of an ideal matrix having suitable surface chemistry, pore diameter, and mechanical resistance. Still, the selection of a suitable matrix for immobilization is the main task, as it leaves an evident effect on the chemical and physical properties of the enzyme. The support material utilized for immobilizing the enzyme should be biocompatible, stable, inert, cheap, and reusable. Noteworthy efforts have been made to immobilize CA on various matrices, which could not only permit its usage in harsh conditions but also improve the recovery and efficiency to diminish the cost of industrial applications (Figure 2.8). For CA immobilization, mostly utilized support materials are alginate, MOF, nanofibers, biochar, and nanoparticles (Table 2.5) [24, 166].

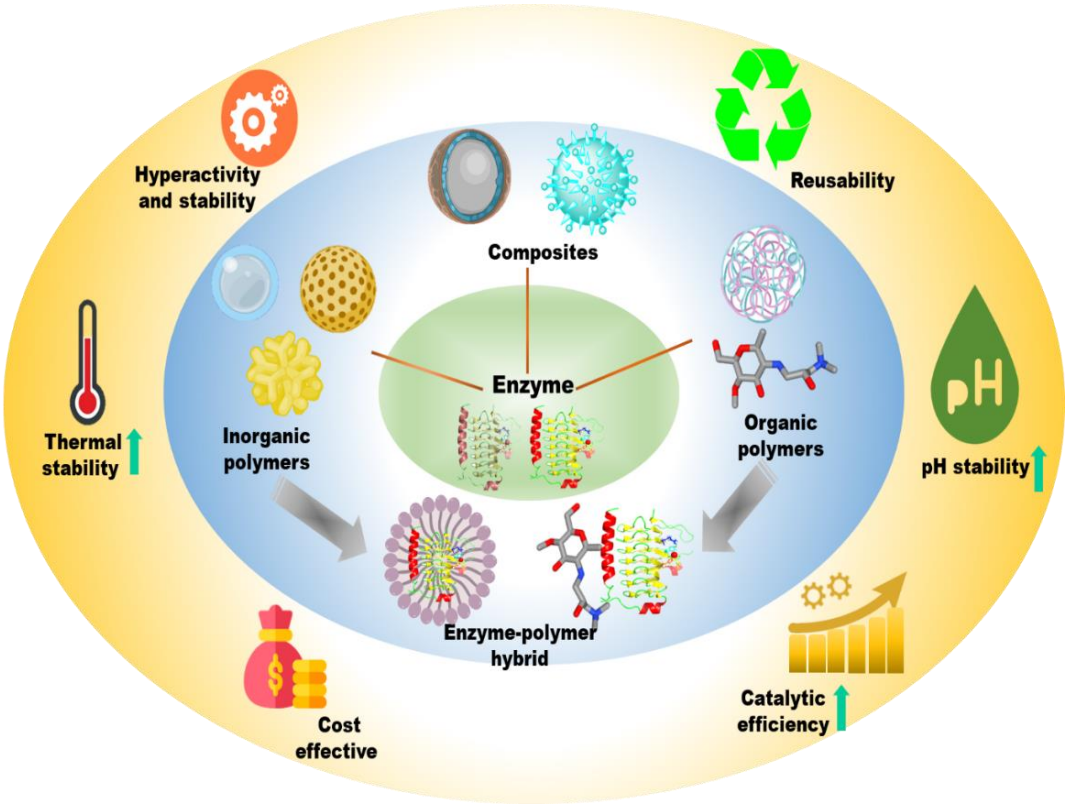

Figure 2.7: Schematic representation showing enzyme immobilization on various matrices and the advantages of the immobilized enzyme [167]

Previously, CA/MOFs were prepared and encapsulated in polyvinyl alcohol chitosan hydrogel (PVA/CS) [168]. The prepared membrane (CA/MOFs/PVA/CS) was stable up to 65°C, and restrict the CA movement in immobilized form. The rate of $CaCO_3$ formation was 20-folds higher using CA/MOFs/PVA/CS membrane than free CA. From this study, it was concluded that CA/MOFs/PVA/CS membranes can be applied for CO_2 capture. Previously, the thermophilic *Sulfurihydrogenibium yellowstonense* CA was immobilized onto nanofibers [169]. These studies revealed that immobilized CA has enhanced $CaCO_3$ yield, *i.e.*, 688.1 mg as compare to free CA (315.9 mg). Furthermore, the immobilized CA was able to withstand the presence of nitrous oxides and sulfur oxide. These outcomes indicate that immobilized CA can be utilized in industrial applications due to its ability to tolerate the presence of toxic compounds. Recently, CA was covalently immobilized on aerogel beads for the conversion of CO_2 into $CaCO_3$. This catalytic system showed only an 18% decline in $CaCO_3$ formation after 10 cycles of reuse [170]. Furthermore, free CA and CA immobilized on polyethylenimine/dopamine showed 72.5 and 61.9 mg of $CaCO_3$ formation. After immobilization, the reusability and storage stability of CA were improved [171]. Moreover, to

enhance the CA activity, magnetic cross-linked aggregates of CA were synthesized, and they were able to enhance the CO_2 absorption rate [172].

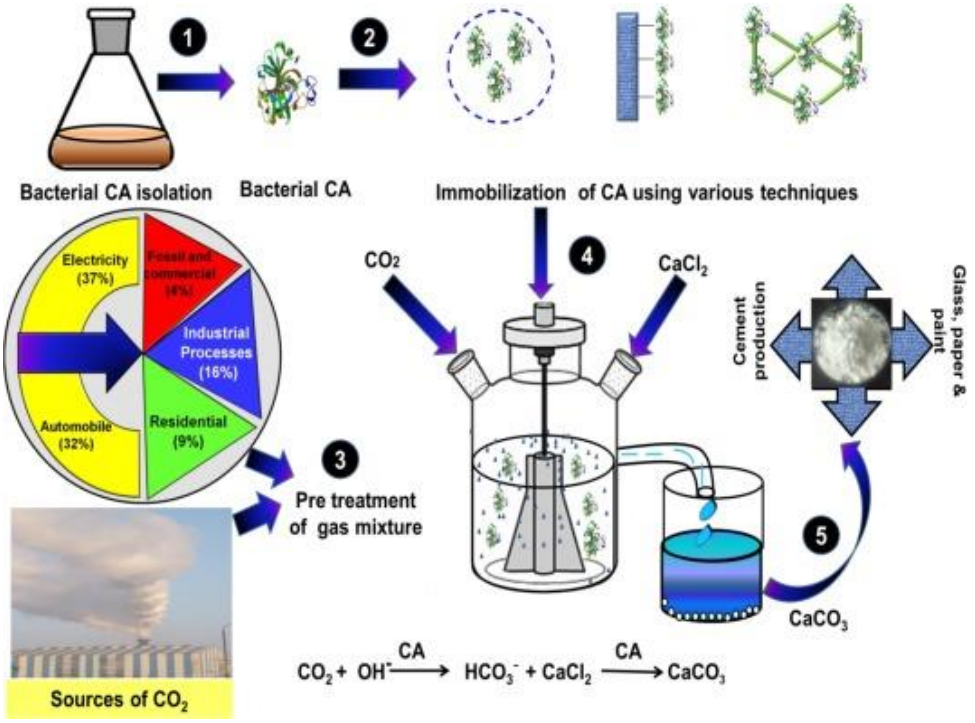

Figure 2.8: Schematic illustration presenting CO_2 conversion into $CaCO_3$ using immobilized CA [2]

The immobilization approach is advantageous because of its directness and convenience. Generally, the enzyme immobilized on the matrix showed lower activity than that of the free enzyme. Recently, there have been various carrier-free methods reported for CA immobilization that showed enhanced activity are cross-linked enzyme aggregates, nanoflowers, copolymers, and sol-gels [36, 173]. The idea behind carrier-free immobilization is to eliminate the support material and to have entirely active enzymes so that higher activity could be achieved. Previously, an elegant method of carrier-free immobilization was reported by Zare [174]. They developed flower-like structures composed of metal ions and proteins that exhibited enhanced stability and catalytic activity, because of their large surface area. A variety of metal ions, such as manganese, copper, zinc, iron, and calcium are used for the synthesis of nanoflowers [35]. Till now, nanoflowers have attracted the interest of researchers due to their ability to integrate the inorganic and organic parts, in addition to their rapid and eco-friendly preparation. For instance, Duan's group has synthesized CA-inorganic nanoflowers with good catalytic activity and recyclability. The synthesized CA-nanoflowers showed approximately 35 g of $CaCO_3$ check protein content production after five cycles of reuse. The improved activity

after immobilization might be due to nanoscale enzyme confinement and the high specific area of nanoflowers [175]. The nanoflowers exhibit remarkable enzymatic activity and stability, as well as relatively inexpensive, which greatly enhances their applicability in pharmaceutical science and biochemistry [176, 177]. Indeed, nanoflowers are very delicate, so their industrial applications are severely limited. Because of their nano size, it is also difficult to separate them from a substrate [178].

These studies concluded that the CA immobilized on various matrices enhanced the production of $CaCO_3$. In this regard, CO_2 conversion using immobilized enzymes seems to be one of the promising low-cost methods for mitigating CO_2. The industrial CO_2 conversion trials used flue gases, and the enzyme performance may have been affected by contaminants present in these gases. These difficulties should be overcome in the future, and more exhaustive research work is required.

Table 2.5: Immobilization of CA on various supports for $CaCO_3$ production

S. No	CA	Immobilization material	Immobilization method	CO_2 concentration (mL)	Reusability	$CaCO_3$ production (mg $CaCO_3$/mg protein)	References
1.	Bovine	Zeolite imidazolate framework (ZIF-8)	Encapsulation	20.0	12.0	34.3	[179]
2.	*Sulfurihydrogenibium yellowstonense*	Nanofibres	Covalent binding	NA	5.0	688.1[a]	[169]
3.	Bovine	Amine-functionalized aerogel beads	Covalent binding	NA	10.0	12[a]	[170]
4.	Bovine	TiO_2 coated membrane	NA	25.0	20.0	101.1	[180]
5.	Bovine	NA	Nanoflowers	20.0	5.0	35.0[b]	[175]
6.	Bovine	Alginate	Entrapment	2.0	6.0	39.0	[26]
7.	*B. pumilis*	Nanoparticles	Covalent	10.0	NA	61.0	[181]
8.	*B. subtilis*	Chitosan/alginate hydrogel	Entrapment	10.0	NA	480.0	[182]

9.	Bovine	Geopolymers microsphere	Covalent binding	10.0	8.0	62.5[a]	[183]
10.	Bovine	ZIF-8	NA	NA	9.0	5.5[g]	[184]
11.	*N. gonorrhoeae*	Hydrogel	Encapsulation	5.0	6.0	5.4[a]	[185]
12.	Bovine	Polyethylimine/ dopamine	Covalent binding	25.0	10.0	61.9[c]	[22]
13.	Bovine	NA	Cross linked enzyme aggregates	NA	30.0	145.0[a]	[186]
14.	*B. halodurans*	Magnetic iron nanoparticles	Covalent	0.5	22.0	138.0[a]	[187]
15.	Bovine	Liposomes	Covalent	8.3	NA	9.1[a]	[188]
16.	Bovine	Bimetallic hybrid nanoflowers	NA	NA	8.0	76.27[a]	[35]
17.	Bovine	Polymerized ionic liquid	NA	NA	5.0	NA	[28]
18.	Human	Mesoporous material	Covalent	100.0	40.0	160.5[a]	[189]

[a] mg
[b] g
[c]mg/min

2.5 CO_2 capture technologies in different countries

Several countries have set targets for mitigating GHGs emissions by capturing and transforming CO_2 into industrial products. The CO_2 released from industries could be captured at a particular point using chemicals, CA, and materials. In 1999, Petronas Fertilizer built the first pilot-scale CO_2 recovery plant and utilized the recovered CO_2 for urea manufacturing. The protocol for urea manufacturing comprises two stages, firstly the CO_2 is absorbed into a proprietary solvent (KS-1) and then reacted with ammonia to make urea. In India, Mitsubishi Heavy Industries recovers 450 tons of CO_2/day and produces urea from the recovered CO_2 [190]. Furthermore, direct air capture (DAC) is a method for removing CO_2 directly from the air. In this method air passes through chemical or sorbent filter material, the CO_2 is absorbed in it. Then heat is applied to liberate CO_2, recovered CO_2 is purified and collected for further use. In the world, Climeworks is known as the first firm to commercially capture CO_2 using the DAC method. They installed a commercial plant at Dresden that can capture 80% of CO_2 and then turn it into fuel [2]. Another DAC firm is Global thermostat, which has a power plant in California. These pilot plants use porous material covered by amines so that when air pass

through it, then it can capture approximately 98% of pure CO_2. Pure CO_2 can be used in plastics, beverages, and synthetic fuels. The global thermostat is operating six commercial projects, with several industries having approximately 2 Mt of CO_2 capturing capacity per year [191]. Moreover, the Canadian firm Carbon Engineering, partially sponsored by Bill Gates, uses the DAC method for capturing CO_2 and has a CO_2-capturing capacity of 1 ton/day [192]. A detailed explanation of how various firms capture CO_2 and convert it into value-added chemicals has been listed in Table 2.6. The drawbacks of the DAC method are its high cost and a lot of energy is needed to liberate CO_2 from the air.

Table 2.6: List of various commercial CO_2 capture plants

S. No	Source of CO_2 emission	Country	Industry	Reaction mediators	Products formed	CO_2 capture capacity (Tons CO_2/day	References
1.	Power generation	United States	Dave Johnston	NM	Enhanced oil recovery	6.0 [a]	[193]
2.	Air	California	Global Thermostat	DAC	Beverages	109.5	[191]
3.	Air	Switzerland	Climeworks	DAC	Carbonates	NM	[194]
4.	Power generation	Netherlands	Hydrogen 2 magnum	NM	Geological storage	2.0 [a]	[195]
5.	Air	Canada	Carbon Engineering	DAC	Synthetic fuels	1.0	[192]
6.	Cement industry	Canada	CO_2 solution Inc	CA	Calcium carbonate	10.0	[196]
7.	Coal plant	Wilsonville	Codexis Inc	CA, MDEA	NM	63.6[b]	[197]
8.	Coal flue gas	United State	Akermin Inc.	CA, K_2CO_3,	NM	80.0[b]	[198]
9.	NG-fired flue gas	India	Mitsubishi Heavy Industries	KS-1	Urea	450.0	[190]
10.	Coal plant	Japan	Toshiba corporation	Amine	NM	10.0	[199]
11.	NG-fired flue gas	Malaysia	Mitsubishi Heavy Industries	KS-1	Urea	160.0	[190]
12.	Air	Germany	Climeworks	NM	Synthetic diesel	80.0[c]	[2]

[a] Mtpa CO_2
[b] %

Until now, very few efforts have been made to use CA for capturing and converting CO_2 at an industrial scale. For large-scale applications, CA should be able to tolerate harsh conditions. The CO_2 capture plant was established by Codexis Inc. at Wilsonville, in which *D. vulgaris*-engineered CA was utilized and the CO_2 capture rate was enhanced 25 times as compared to the non-catalyzed reaction [197]. Furthermore, Akermin Inc. used immobilized CA for capturing CO_2 at its pilot plant in the USA. The absorber column of the plant comprises a nonvolatile alkaline solution, potassium carbonate (K_2CO_3), and immobilized CA, and showed 80% CO_2 capture efficiency [198]. Moreover, CO_2 Solution Inc. tested K_2CO_3 and CA at Salaberry-de-Valleyfield, Canada, for capturing and turning CO_2 into several products of industrial value [196]. There is still a need to explore the conversion of captured CO_2 on a large scale to protect the environment and meet energy demand.

2.6 Other applications of CA

The CA has been widely studied due to its broad physiological importance in all forms of life. The high turnover number, relatively easy purification, and stability make it a promising candidate to be utilized in several biomedical applications including biosensors, drug design, and artificial lungs (Figure 2.9).

2.6.1 Artificial Lungs

Respiratory failures are current health issues that affect several thousand individuals each year. Medical treatment for this disease includes mechanical ventilation, which can sometimes contribute to the worsening of lung injury in the form of barotraumas[200]. The artificial lung is a device made up of hollow fiber membranes (HFM) and responsible for providing oxygen to the blood and removing CO_2 from the blood. Presently, gas exchange is comparatively inefficient in these artificial lungs, so approximately 1-2 m^2 of the surface area is required for adequate gas exchange by the membrane. In the human body, a surface area of this size is not able to perform efficiently [201]. One way to offset these challenges involves immobilizing CA onto the HFM, allowing "facilitated diffusion" of CO_2 as bicarbonate towards the fibers and enhancing CO_2 removal. The concept of immobilizing CA onto HFM was initially described by Karr and his co-workers, and they found the rates of CO_2 exchange were increased by 75%, with no leaching of CA in the device [202]. In another study, immobilization of CA onto chitosan-coated HFM membrane was reported, which results in enhanced CO_2 removal efficiency [203]. Previously, the kinetics of CA for CO_2 exchange in artificial lungs was studied using immobilized CA on a fiber membrane [204]. These findings

indicate noteworthy progress towards the development of new respiratory devices using CA and improved CO_2 exchange capability.

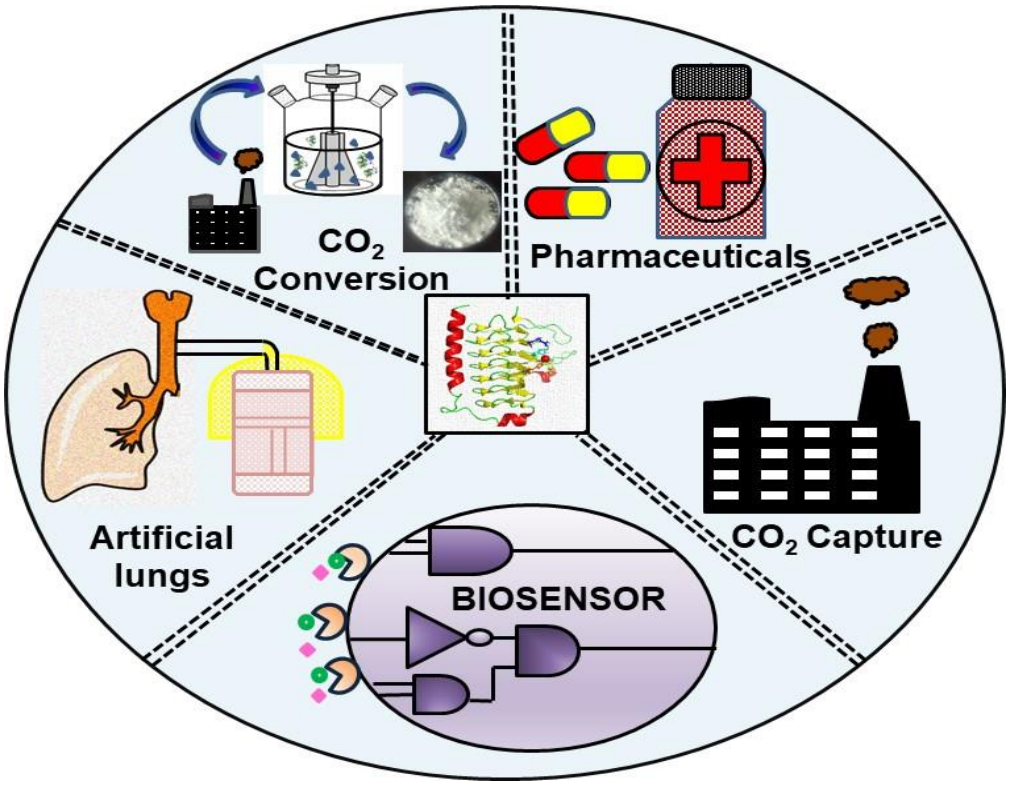

Figure 2.9: Schematic representation of various applications of CA

2.6.2 Biosensor

A biosensor is a device that is useful for detecting the existence of bio-molecules. Various enzyme-based biosensors are present in the market for checking clinically important factors like urea, blood glucose, metal ions, uric acid, cholesterol, *etc.* Human CA II (HCA II) was reported to have a high affinity for zinc and utilized to determine the toxic effect of zinc on certain fish, invertebrates, and plants [205, 206]. Indeed, to enhance the affinity and sensitivity of CA-based biosensors for detecting heavy metals, including Co^{2+}, Cu^{2+}, Ni^{2+}, and Co^{2+}, site-directed mutagenesis can be used to create mutants of HCA II [207]. For detecting the presence of Cd^{2+} in a marine environment, CDCA1 isolated from *Thalassiosira weissflogii* has a high affinity for cadmium, and it could represent a fascinating substitute for the CA biosensor [208]. Furthermore, Caricato et. al. [209]., demonstrated that when *Mytilus galloprovincialis* was exposed to pollution, CA activity increased in the digestive gland. Consequently, they also determined its suitability to be incorporated in multi-marker methods, for detecting environmental pollution. Previously, the biosensor was developed by

immobilizing CA on a combined electrode assembly for diagnosing respiratory health [210]. The characteristic features of this device were sensitivity, fast response, selectivity, portability, and reproducibility. This biosensor offers a valuable, non-invasive diagnostic approach for evaluating respiratory health by analyzing exhaled breath. From these studies, it can be assumed that CA biosensors can be exploited in the future for monitoring the metal ion presence in the environment and for the diagnosis of respiratory health.

2.6.3 Drugs Design

The CA inhibitors have been exploited clinically in the treatment of diseases because of their presence in both eukaryotes and prokaryotes. In humans, various isoforms of CA are present in tissues, and their inhibition leads to physiological and pharmacological responses [211]. CA inhibitors attack the Zn^{2+} ion in the active site of CA either by replacing the non-protein zinc ion to form a tetrahedral intermediate or by binding to a metal coordination sphere to form a trigonal bipyramidal sphere [212]. The most effective CA inhibitors known for pharmaceutical properties are sulfonamides, sulthiame, coumarins, acetazolamide, ethoxzolamide, methazolamide, *etc.* (Figure 2.10). Coumarins are used as agents for the treatment of rheumatoid arthritis; brinzolamide and dorzolamide are used as antiglaucoma agents; sulfamic acid, sulthiame, and zonisamide are commonly used as antiepileptic drugs; acetazolamide and methazolamide exhibit inhibitory activity against bacterial growth in cell cultures [213, 214].

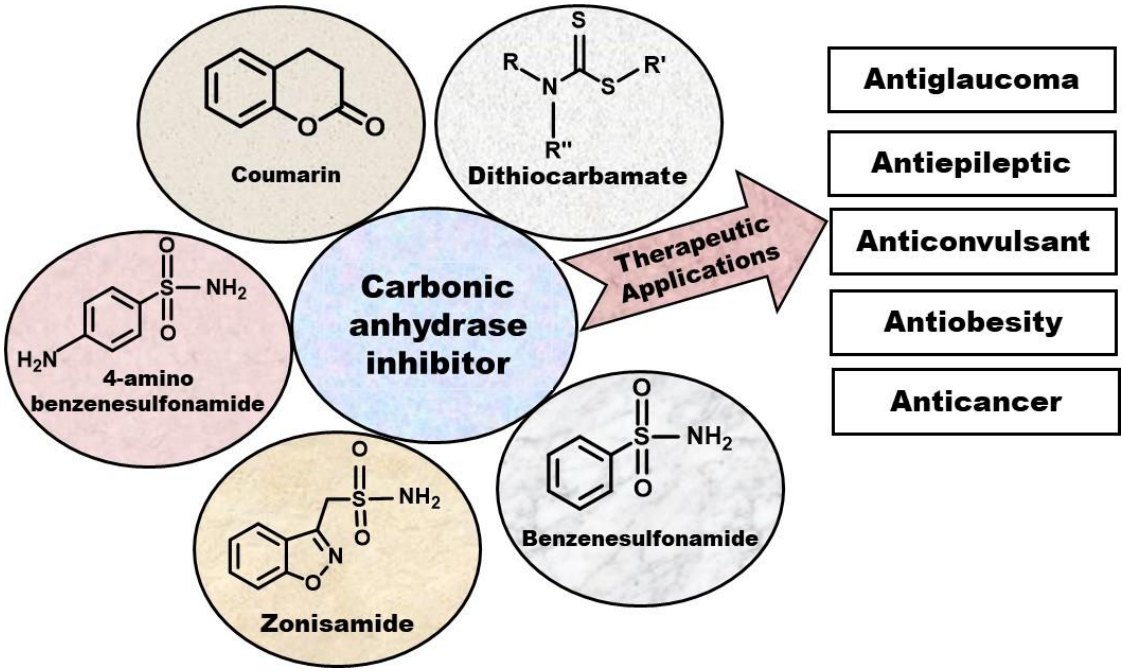

Figure 2.10: Schematic representation of various CA inhibitors and their therapeutic applications

The inhibitors of CA may be used the synthesize antibiotics having novel mechanisms of action, deprived of the antibiotic resistance mostly faced with the many clinically used agents [215]. These inhibitors can perform as a potent drug target for disease.

2.7 Significance of current study

The main aim of the current study was to convert the CO_2 into $CaCO_3$ using a CA from *C. flavescens*. Microbes are commonly utilized to produce the industrially useful enzymes. The CA isolation from cow saliva is economical because there is a price limitation for employing BCA in CO_2 conversion applications. The enhanced CA production from *C. flavescens* was achieved by the optimizing the various reaction and production parameters. The operational stability of the CA is also very important for its economically feasible production. Thus, the CA was purified and characterized. The purified CA was used to synthesize the NFs with the self-assembly of CA and metal phosphate. The synthesized flowerlike nanostructures enhance the enzyme's operational stability, tolerance to prolonged storage, and continuous reusability as compared to free CA. Furthermore, purified CA and CANF were used for the conversion of CO_2 to yield $CaCO_3$. The conversion of CO_2 into $CaCO_3$ using CA is a cost-

effective way to mitigate the CO_2, as the final product, $CaCO_3$ can be further used in the various manufacturing industries.

3.1 Chemicals

In the present study, all the chemicals of analytical grade were used from reputed manufacturing companies such as Himedia, Sisco research laboratory (SRL), Sigma Aldrich, Merck Life Sciences, Thermo Fischer Scientific, *etc*. These include nutrient broth, nutrient agar, Muller Hinton broth, Peptone broth (g/l): NaCl 5.0, peptone 5.0, beef extract 3.0, $CaCO_3$ 6.0, glucose 1.0; and basal salt media (g/l): $CaCO_3$ 0.1, $MgSO_4.7H_2O$ 0.5, Na_2HPO_4 2.0, sucrose 5.0, $FeCl_3.6H_2O$ 0.005, minimal salt media (g/l): $MgSO_4$ 0.2, $ZnCl_2$ 0.02, $NaNO_3$ 0.085, Na_2HPO_4 7.8, $ZnSO_4.7H_2O$ 0.05, KH_2PO_4 6.8, Luria broth, ethanol, Bradford reagent, $CaCO_3$, Bovine serum Albumin (BSA), Na_2HPO_4, NaH_2PO_4, petroleum ether, phosphate buffer saline (PBS), ultrapure water, Sephadex G-100, para-nitrophenyl acetate (*p*-NPA), para nitrophenol (*p*-NP), copper sulfate, glutaraldehyde, magnesium chloride, isopropanol, aluminum chloride, sodium citrate dehydrate, Tris-HCl, potassium chloride, propanediol, ethanediol, calcium chloride, sodium chloride, ferric chloride, zinc chloride, butanol, acetonitrile, acetone, ethylenediaminetetraacetic acid (EDTA), sodium dodecyl sulfate (SDS), cetrimonium bromide (CTAB), dithiothreitol (DTT), phenylmethylsulfonyl, fluoride (PMSF), ammonium-persulfate, acrylamide, protein marker, bromophenol blue (BPB), *bis*-acrylamide, glycerol, Tris, glycine, *N, N, N', N'*-tetramethylene-diamine (TEMED), mercaptoethanol, methanol, Coomassie Brilliant Blue, glacial acetic acid.

3.2 Isolation and screening of CA-producing bacteria

3.2.1 Sample collection

The CA from salivary glands of humans, dogs, cattle, pigs, and sheep have been purified previously [216]. Thus, in the current study, the six years old cow was selected for a sample collection from Mandi district, Himachal Pradesh, India. The cow saliva was taken with sterilized bud and stored in a sealed glass vial, at 4°C, until further use.

3.2.2 Primary screening

For isolating the CA-producing bacteria from cow saliva, 1 mL of a saliva sample was inoculated into the nutrient broth and then diluted serially up to 10^{-9}. The 0.1 mL of the diluted sample was spread on the agar plates containing 3mM *p*-NPA (Figure 3.1). The plates were kept for 48h at 30°C. The CA-producing bacterial isolate was chosen based on colonies of yellow color on the *p*-NPA agar plate [217].

3.2.3 Secondary screening

The bacterial isolates obtained from primary screening were subjected to a CA activity assay. A loopful culture of bacterial isolates was transferred into 50 mL of sterile seed media, *i.e.*, nutrient broth, and kept at 30°C for 24 h. Once the seed culture turns turbid and cell density reached ~3×10^8/ml, the production media was inoculated with 2 ml (2% v/v) of culture. The production media was incubated at 30°C for 24 h at 120 rpm. After 24 h, the culture was centrifuged at 8,000 rpm for 10 min. The pellet was dissolved in phosphate buffer (pH 7.0), then sonicated for 5 min at 35% amplitude, to release the intracellular enzyme. The culture was then centrifuged for 20 min to obtain cell lysate as supernatant and separated from cell debris. The cell lysate was used as a crude enzyme to analyze the enzyme activity. The enzyme activity was recorded under standard assay conditions using *p*-NPA as substrate as reported previously [218], with some modification. The bacterial strain showing the highest activity was selected for identification and further study. The bacterial strain showing the highest activity was selected for identification and further study.

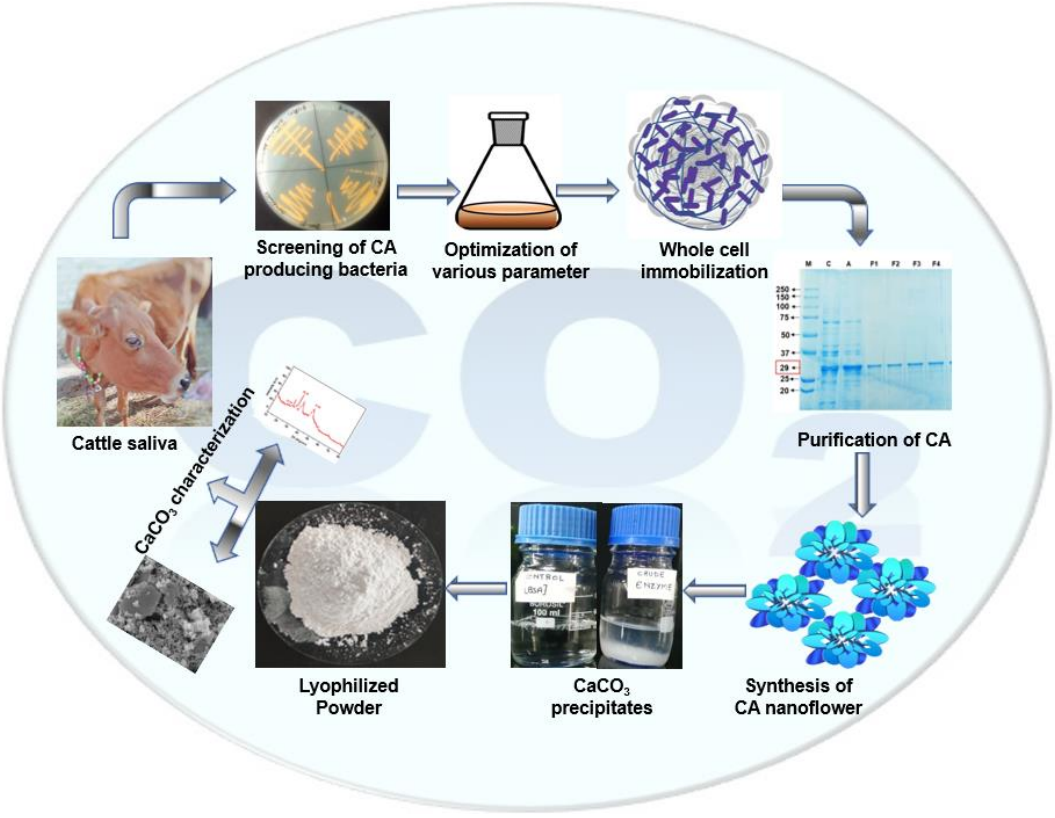

Figure 3.1: Schematic representation of optimization, immobilization, and purification of CA for CO_2 conversion into $CaCO_3$

3.2.4 Activity assay of CA

The activity assay was carried out to determine the µmol of *p*-nitrophenol liberated from *p*-NPA per minute [218]. In an eppendorf tube, 0.825 mL of phosphate buffer (50 mM, pH 7.0) and 0.175 mL of *p*-NPA (10 mM) were added and kept at 37°C for 5 min in a shaking water bath. Then, the enzyme (0.25 mL) was added to eppendorf tube and kept at 37°C for 5 min. The reaction mixture was kept at -20°C for 2 min to stop the reaction. The absorbance of *p*-nitrophenol was measured with a microplate reader at 410 nm. All the experiment was performed in triplicate and the mean value was calculated using standard.

3.2.5 Protein estimation

The protein concentration in the sample was estimated by the Bradford method [219]. To start the reaction,100 µL of protein sample was added to Bradford reagent (900 µL) and mixed properly. Then, absorbance was taken at 595nm and the protein concentrations of the samples were calculated from a reference profile of BSA.

3.2.6 Staining of bacterial culture

Based on activity, the T5 isolate was selected as a potent producer of CA. The gram staining of the T5 isolate was done under a microscope at 100 X, and biochemical characterization was carried out using Bergey's Manual of Systemic Bacteriology [220, 221].

3.2.7 Identification using 16S rRNA gene sequencing

For the identification of the T5 isolate, 16S rRNA gene sequencing was performed by B. Biotech (Bioreserve Biotechnologies) Limited, Telangana, India. The phylogenetic and comparative analysis of the nucleotide sequence was carried out using BLAST and MEGA X [222, 223]. Then, a neighbor-tree joining method was used for making a phylogenetic tree [224].

3.2.8 Optimization of production parameters

Optimization is essential for attaining maximum enzyme production and cutting the overall process cost (Figure 3.2). Effect of various production parameters, including media (Muller Hinton broth, basal salt media, Luria broth, minimal salt media, nutrient broth, and peptone broth), temperature (20-70°C), inoculum size (2-12% v/v), agitation speed (80-180 rpm), and inoculum age (6-36 h), was studied. The activity was calculated for each parameter by standard activity assay described in section 3.2.4 [225].

3.2.9 Characterization of the enzyme

Furthermore, to optimize the various parameters, the reaction mixture was kept at different temperatures (25 to 60°C), reaction time (2 to18 min), buffers (Tris-HCl buffer, citrate buffer, and phosphate buffer, 50 mM), buffer molarity (10-70 mM, Phosphate buffer). Subsequently, the activity was calculated for each parameter by standard activity assay described in section 3.2.4. Moreover, to examine the effect of metal ions (Ca^{2+}, K^{+}, Mg^{2+}, Na^{+}, Zn^{2+}, Al^{3+}, and Fe^{3+}; 1 & 5 mM), denaturing agents (SDS, EDTA, urea, and PMSF; 5mM), and organic solvents (ethanediol, acetonitrile, propanediol, n-butanol, ethanol, and isopropanol; 2% v/v) on the enzyme activity, the enzyme was pre-incubated for 10 min separately with each of the selected metal-ions, denaturing agents, and organic solvents. Then, the reaction was performed using 25 µL of crude CA in phosphate buffer (50 mM) of pH 7.0 at 35ºC, respectively. All the experiments were carried out in three replicates and average values were calculated with standard deviation shown in the error bar.

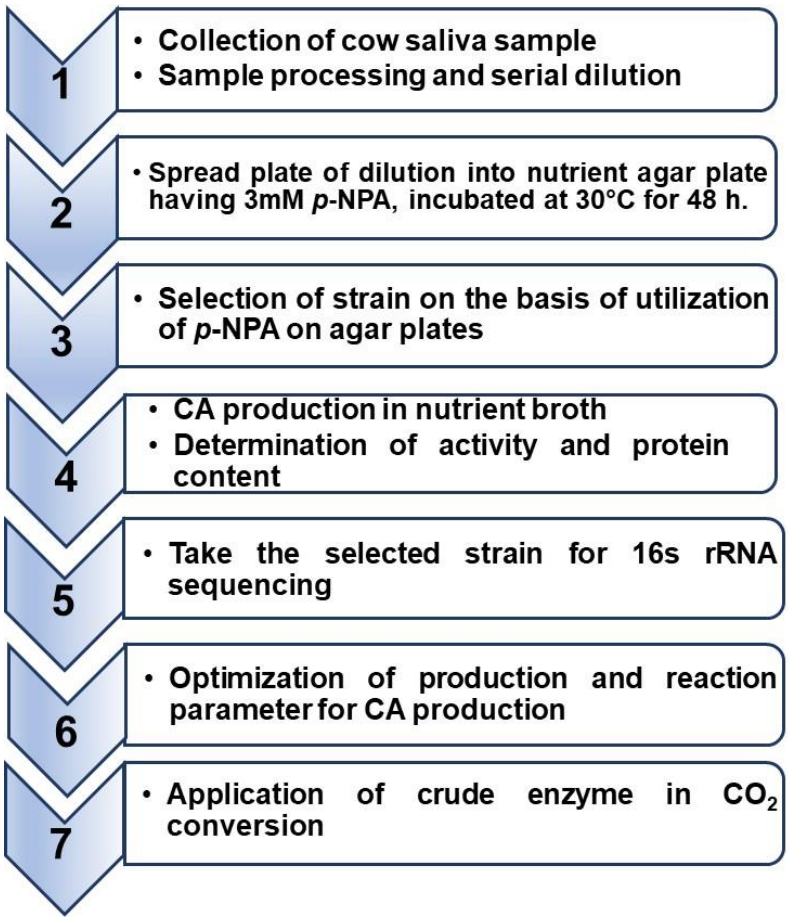

Figure 3.2: Flowchart showing the research methodology for isolation and optimization of CA-producing bacteria

3.2.10 Conversion of CO_2 into $CaCO_3$ using crude CA

The potential of crude CA for the converting the CO_2 into $CaCO_3$ was evaluated using a three-mouthed bottle via an earlier reported method [145]. Firstly, CO_2-saturated water was made by sparging the CO_2 gas into deionized water. To start the reaction, 2000 µL of the crude enzyme was added to CO_2-saturated water, 1 M Tris-HCl (pH 8.0), and calcium chloride (2% w/v). The reaction was carried out for 10 min at room temperature. After 10 min, the $CaCO_3$ precipitates were collected by centrifugation and lyophilized to get a dry powder. The dried powder was weighed to determine the amount of $CaCO_3$ synthesized in the enzymatic reactions.

3.3 Whole-cell immobilization on keratin particles

Immobilized cells impart special stability to bacteria against environmental changes, including salts, self-destruction, pH, solvents, and temperature [226]. The viability and activity of immobilized cells can be preserved for a longer period. For whole-cell immobilization, *C. flavescens* was cultured overnight in nutrient broth at 40°C under continuous shaking at 120 rpm. When the absorbance (Ab_{600}) of the cell culture reached between 0.7-1.20, the cells were harvested by centrifugation at 8000 rpm at 4°C [227]. Afterward, the pellet was collected and kept at 4°C, till further usage.

3.3.1 Preparation of keratin particles

The feathers of the chicken were procured from the chicken processing unit at Solan, Himachal Pradesh, India. Wet feathers were wiped and dried for 72 h at 40°C in an oven, after that chicken feathers were immersed in petroleum ether for degreasing. CTAB was used to remove microbial contamination from the chicken feathers after they were cleaned with distilled water. The feathers were chopped into small slices and dehydrated under sunlight. The chicken feathers were chemically hydrolyzed under alkaline circumstances, as reported earlier [228]. The synthesized keratin particles were used for the immobilization of cells. The scanning electron microscope (SEM) was used to examine the surface morphology of keratin particles.

3.3.2 Whole-cell immobilization protocol

One gram of keratin particles was functionalized by glutaraldehyde (0.2% v/v) for cell immobilization. After functionalization, the keratin particles were kept at 25°C for 2 h and rinsed using phosphate buffer. This method inserts two glutaraldehyde molecules per amino group in the matrices. Afterward, the *C. flavescens* cells at a concentration of 0.5 g cell pellet

per gram of matrix were immobilized and kept at 4°C for 30 h. Afterward, the cell immobilization yield was calculated using the previously reported method [229].

3.3.3 Optimization of immobilization parameters

The optimization of various parameters was done to get the maximum viability and activity of immobilized cells [227]. The optimization of immobilized cells was performed at different temperatures (4-55°C), glutaraldehyde concentrations (0.2-1.4%), and incubation times (5 to 35 h).

3.3.4 Reusability of immobilized cells

The reusability of immobilized cells for the transformation of CO_2 into $CaCO_3$ was estimated for 10 cycles [175]. The immobilized cells were washed with distilled water after each cycle and utilized for the next cycle.

3.3.5 $CaCO_3$ instrumental analysis

The morphology of $CaCO_3$ was investigated by field emission scanning electron microscopy (FE-SEM) using the JSM7401F (JEOL). The $CaCO_3$ composition was determined using XRD in the 400-4,000 cm^{-1} range. Chemical bonds present in $CaCO_3$ were studied by FTIR spectra (model Varian 7000 FTIR). $CaCO_3$ procured from Himedia was used as a control.

3.4. Enzyme purification

The crude CA was purified by acetone precipitation and size exclusion chromatography (Sephadex G-100).

3.4.1 Protein precipitation

The crude enzyme was precipitated with 50% (v/v) acetone in stirring conditions at 4°C [142]. After overnight incubation, the precipitated protein was separated by centrifugation at 8,000 rpm for 15 min. The separated protein was dissolved in a minimum volume of phosphate buffer (pH 7.0). The obtained precipitates and supernatant were analyzed for protein concentration and enzyme activity.

3.4.2 Size exclusion chromatography

A pre-swollen Sephadex G-100 column (Sigma Chemical Co., U.S.A) was equilibrated with 50 mM phosphate buffer (pH 7.0). The protein sample was loaded onto the column and

elution was done with the same buffer at a flow rate of 1.0 mL/min. The fractions were checked for protein content and assayed for activity. The fractions showing adequate enzyme activity were pooled [230]. At each step of purification, the yield and folds of CA were evaluated. Purified CA was store at -20°C, for subsequent use.

3.4.3 Molecular mass [*M*r] determination of purified *C. flavescens* using SDS-PAGE

The SDS-PAGE (12%) was performed to determine the purity and molecular mass of the purified enzyme. The electrophoresis was done using a method given by Laemmli [231].

3.4.3.1 SDS-PAGE stock solutions

I. Tris-HCl (1.0 mM, pH 6.8)

II. Tris-HCl (2.0 M, pH 8.8)

III. 50.0 % (v/v) Glycerol

IV. 10.0 % (w/v) SDS

V. 1.0% (w/v) BPB

VI. 2-Mercaptoethanol

3.4.3.2 SDS-PAGE working solutions

All the SDS-PAGE working solutions were kept at 4°C.

Solution I

Acrylamide (29.2 g) and bis-acrylamide (0.8 g) were added to 100 mL of distilled water and stirred continuously.

Solution II

Tris-HCl (75 mL, 2M, pH 8.8), 4 mL SDS (10%) was added to 21 mL of distilled water and stirred to dissolve it completely.

Solution III

50 mL of 1M Tris-HCl (pH 6.8) and 4 mL SDS (10%) were added to 46 mL H_2O. The prepared solution was stored at 4°C for further use.

Ammonium persulfate (10%, w/v)

1.0 g of ammonium persulphate was added to 10 mL of double-distilled water.

Electrophoresis buffer

Tris-base (3.0 g), SDS (1.0 g), and glycine (14.4 g) were dissolved in 1000mL of distilled water. The pH of the buffer was adjusted to 8.3.

5x Sample buffer

Sample buffer (10.0 mL) was prepared by dissolving 2.0mL of SDS (10%, w/v), 0.5 mL of 2-mercaptoethanol, 0.6 mL of 1 M Tris-HCl (pH 6.8), 1 mL of bromophenol blue, 5 mL of glycerol (50%, v/v) to 0.9 mL of distilled water.

3.4.3.3 SDS-PAGE Preparation

The glass plates (8 cm X 8 cm) of the gel electrophoresis system (Bio-Rad Mini Gel) were cleaned with 95% ethanol and air dried. To make separating gel, separating (12%) gel mixture was added to the glass plates and then over-layered with distilled water. The acrylamide mixture was allowed to polymerize for 30-35 min. After polymerization of the gel, the overlay was removed by tilting the glass plates followed by their inversion on the tissue paper. The separating gel was then covered with 1 mL of the stacking (4%) gel mixture, and a comb was carefully inserted. The complete polymerization of the upper (staking) gel was achieved in 30 min. The composition of SDS-PAGE was as follows (Table 3.1).

Table 3.1: Composition of SDS PAGE

Reagents	**Stacking gel (4%)**	**Separating gel (12%)**
Solution I	670 µL	4000 µL
Solution II	-	2500 µL
Solution III	1000 µL	-
Distilled water	2300 µL	3500 µL

10 % APS	30.00 µL	50.00 µL
TEMED	5.00 µL	5.00 µL

3.4.3.4 SDS-protein molecular weight markers

The molecular mass of protein was determined using a commercial marker (Bio-Rad) ranging from 10.0 to 250.0 kDa.

3.4.3.5 Sample loading dye preparation and electrophoresis

The sample loading buffer and purified protein were blended in 4: 1 and heated at 100°C for 5-10 min. Then, 40 µL of protein sample was loaded into each well and electrophoresis was run at a constant voltage (100 mA). When the dye reached about 1.0 cm away from the anodic end, the power was switched off. The gel was carefully removed from the glass plates and subjected to staining with Coomassie Brilliant Blue to visualize the bands of proteins.

3.4.3.6 Gel Staining

The destain and staining solution of polyacrylamide gel were as follow (Table 3.2 and Table 3.3).

Table 3.2: Reagents for staining of polyacrylamide gel

Staining solution (1 L)	
Coomassie Brilliant Blue R-250	1.0 g
Methanol	450.0 mL
H_2O	450.0 mL
Glacial acetic acid	100.0 mL

Table 3.3: Destain for polyacrylamide gel

Destain solution (1 L)	
Methanol	100.0 mL
H_2O	800.0 mL
Glacial acetic acid	100.0 mL

After electrophoresis, the gel was shifted to a staining box having Coomassie containing 50 mL of Brilliant Blue Stain for 2 h of agitation. The stain solution was decanted, and the gel was washed gently with distilled water. The gel was transferred into the destain solution (about 50 mL) under vigorous shaking. The gel was extensively destained to obtain distinctly resolved protein bands.

3.4.4 MALDI-TOF-MS of purified *C. flavescens* CA

The SDS band of purified CA was subjected to digestion processed with trypsin and kept for 16 h at 37 ºC. The digested peptides were reconstituted in trifluoroacetic acid (0.1%). This mixture was added to cyano-4-hydroxycinnamic and loaded onto a MALDI plate for further evaluation [232]. The obtained peptides were analyzed by MALDI-TOF-MS (BrukerDaltonics) and their spectra were elucidated using BrukarBioTools. The cladogram was created using a CLC workbench to examine the relatedness of an organism.

3.4.5 Bioinformatics study of purified CA

A BLAST search in NCBI (www.ncbi.nlm.nih.gov) was performed to confirm the homologous sequence of the known structure for the template protein, *i.e., C. flavescens* CA. The CA purified from *C. flavescens* showed the highest sequence identity (48%) with *T. ammonificans* (PDB: 4C3T) CA. For homology modelling, *T. ammonificans* CA was chosen as a template. Subsequently, the Clustal Omega program was used to align the sequences between the template and *C. flavescens* CA [232]. Ten model structures of *C. flavescens* CA were created using the *Build Homology Models* tool in the DS software. Based on the lowest discrete optimized protein energy (DOPE) score and probability density function energy value, a final model was chosen [233]. A final model was improved by the CHARMm forcefield in DS through energy minimization. Furthermore, the binding site residues of side chains were refined by the *Side-Chain Refinement* Protocol of DS, which improves the selected amino acids chain confirmation by the ChiRotor algorithm. The stereochemical features of the model structure were validated using the Protein Structure Analysis (ProSA) and PROCHECK programs [234, 235].

3.5 Synthesis of carbonic anhydrase nanoflower (CANF)

To enhance the stability and activity of an enzyme, nanoflowers were synthesized using copper ions as the inorganic and purified CA as an organic part [236]. For the CANF synthesis,

purified CA was added to PBS (pH 7.5, 10mM) and $CuSO_4$ (1.0 mM) and kept at 4°C for 24 h, under constant shaking. After 24 h of incubation, the blue precipitated protein was collected by centrifugation at 10,000 rpm and washed three times with deionized water. The CANF were dried and kept at 4°C till further usage. Additionally, the effect of protein (0.1-0.5 mg/mL) and $CuSO_4$ concentration (0.5-3.0 mM) was investigated on the CANF formation (Figure 3.3).

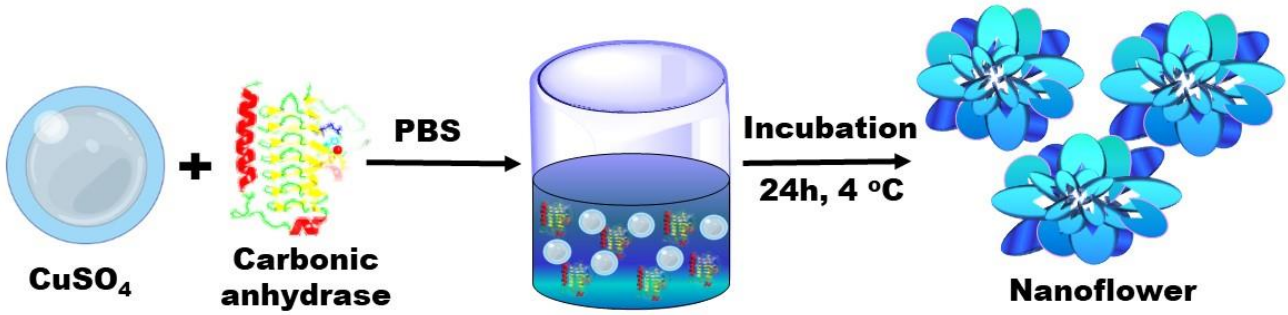

Figure 3.3: Schematic representation for the synthesis of CANF

3.5.1 Characterization of synthesized CANF and free CA

Effect of various reaction parameters, including reaction temperature (25-60°C), reaction pH (4-9.5), reaction time (2-18 min), denaturing agents (urea, SDS, EDTA, and PMSF), storage stability, and thermostability, was studied. All the experiments were carried out in three replicates and average values were calculated with standard deviation shown in the error bar.

3.5.1.1 Effect of reaction temperature

The optimum temperature of free CA and CANF was measured at various temperatures ranging from 25-60°C. The CANF and free CA activity were determined separately for each of the specified temperatures. The reaction was performed separately by using 25 µL of CANF and free CA in phosphate buffer (50 mM) of pH 7.0 for 10 min.

3.5.1.2 Effect of reaction pH

The optimum pH of CANF and free CA was measured by incubating them in different buffer systems having pH ranging from 4.0-9.5 at optimum temperature. The reaction was

performed separately by using 25 μL of free CA and CANF at 35 and 45°C, respectively, for 10 min.

3.5.1.3 Effect of reaction time

To study the reaction time effect, enzyme activity was assayed at a selected reaction time (2-18 min). The reaction was performed separately using 25 μL of CANF and free CA in phosphate buffer of pH 7.5 at 35 and 45°C, respectively, for 10 min.

3.5.2.4 Effect of denaturing agents

The effect of denaturing agents (urea, SDS, EDTA, and PMSF) on the CA activity was determined. Each of the chosen denaturing agents was pre-incubated with the biocatalyst for 10 min before the activity was assessed. The control without any treatment was considered 100%.

3.5.2.5 Temperature stability

The thermostability of enzyme is vital for its practical applications. Thus, the thermal stability of CANF and free CA was determined by incubating them at 50°C, and the residual activity was calculated after each 2 h by the same method as described above. The activity calculated before incubating the enzyme was taken as 100% of activity in all the cases.

3.5.2.6 Storage stability

The enzyme sample was stored at 4°C and the enzyme activity was studied after a regular interval of 5 days by withdrawing the samples over the incubation of 20 days.

3.5.2.7 Reusability

The reusability of CANF was evaluated using *p*-NPA as a substrate for ten cycles under standard assay conditions. After completion of each cycle, the CANF was separated by centrifugation and washed with deionized water, then used again in the next reaction. The initial activity of CANF was considered as 100%.

3.5.2.8 Kinetic study

The kinetic parameters such as V_{max}, K_{cat}, and K_m, of free enzyme and CANF, were calculated by the Lineweaver-Burk plot between 1-20 mM *p*-NPA concentrations using standard assay conditions [237]. The K_m, V_{max}, K_{cat}, and specificity constant was determined

values by the Lineweaver-Burk plot (Equation 1). The reaction was performed using the assay method.

$$\frac{1}{V} = \frac{1}{V\max} + \frac{1}{[S].Km} \quad \text{… …. Equation 1}$$

3.6 Instrumental study of CANF

3.6.1 FE-SEM analysis

The FE-SEM was used to determine the morphology of CANF (FE-SEM, JSM7401). The elemental components of CANF were determined by dot mapping.

3.6.2 FTIR analysis

The FTIR spectra were used to observe the presence of functional moieties and chemical bonds in the CANF. The FTIR spectra were observed in the wavelength ranging 400-4000 cm^{-1} range using FTIR spectroscopy (FTIR, NEXUS 870).

3.7 Conversion of CO_2 into $CaCO_3$ using CANF and free enzyme

The potential of CANF and free CA for the conversion of CO_2 into $CaCO_3$ was further evaluated by the same method as described above.

The carboxylating enzymes are receiving much attention these days, because of their role for the conversion of CO_2 into fine chemicals. CA is found in all forms of life, but CA isolated from microbes is more attractive owing to their easy production. In the present study, the first objective is to isolate CA-producing bacterial strains and optimize various physiological parameters for maximum CA production.

4.1 Isolation and screening of CA-producing bacteria

The cow saliva was used to isolate the CA-producing bacteria. The cow saliva was diluted serially up to 10^{-9}. The diluted sample was spread on the agar plates containing 3mM *p*-NPA. The plates were kept for 48h at 30°C. The bacterial isolates were screened based on the formation of yellow-color colonies. The 10 bacterial isolates were selected from primary screening and cultivated in nutrient broth (Figure 4.1A-D). Furthermore, secondary screening was done using an activity assay described in section 3.2.4., which showed that the T5 isolate was the most potent CA-producing bacterium and selected for further work (Figure 4.1E). In mammalian saliva, CA plays an important role to maintain the saliva pH. Indeed, the isolation of CA-producing bacteria from cow saliva is rapid and economic. Previously, *Microcoleus cathonoplastes* was isolated from a soda lake produce a potent CA, and *Bacillus safensis* isolated from a water sample was reported to show the presence of CA [141, 238]. In addition, CA was also produced by *Psychrobacter* sp., isolated from frozen soil having an alkaline pH [239].

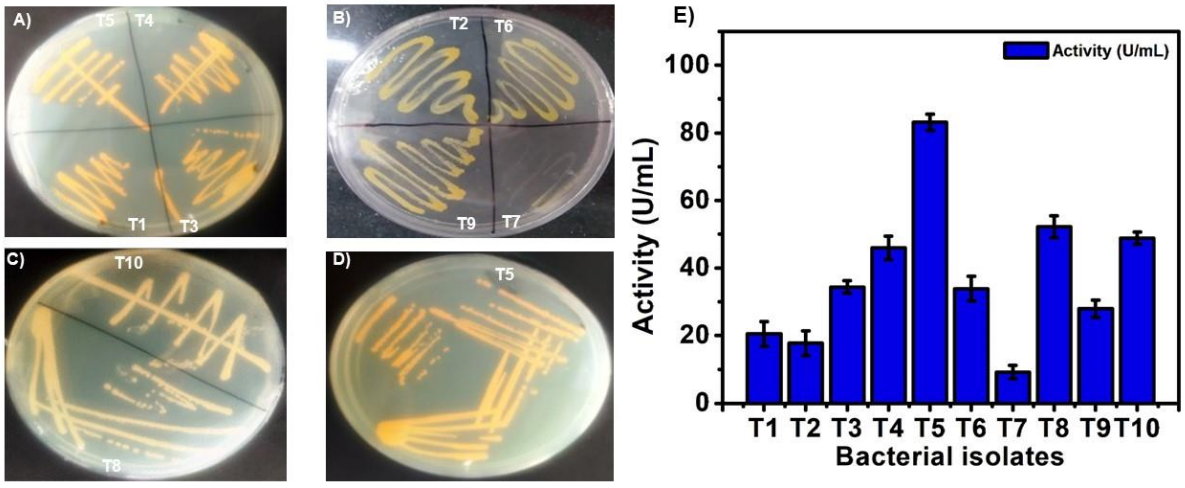

Figure 4.1: A-D) Isolation of CA producing bacterial isolates from cow saliva using (*p*-NPA). E) Selection of bacterial isolate based on CA activity assay

4.2 Morphological characteristics and strain identification

The T5 isolate was found to be gram-positive and rod-shaped (Figure 4.2A). The biochemical analysis showed nitrate reduction, glucose, Voges-Proskauer, and sucrose positive. Further, the identification of isolated strain was performed using 16s rRNA sequencing. The DNA was extracted from the T5 isolate and analyzed by agarose gel electrophoresis (Figure 4.2B). After 16s rRNA gene sequencing using nucleotide homology and phylogenetic analysis, the T5 isolate was recognized as *Corynebacterium flavescens.* Subsequently, a phylogenetic tree was designed *via* the neighbor tree joining method, showing 99.4% sequence homology with *C. flavescens* HBUM07012 (Figure 4.2C). The strain's gene accession number was MN982752, and it was deposited in NCBI.

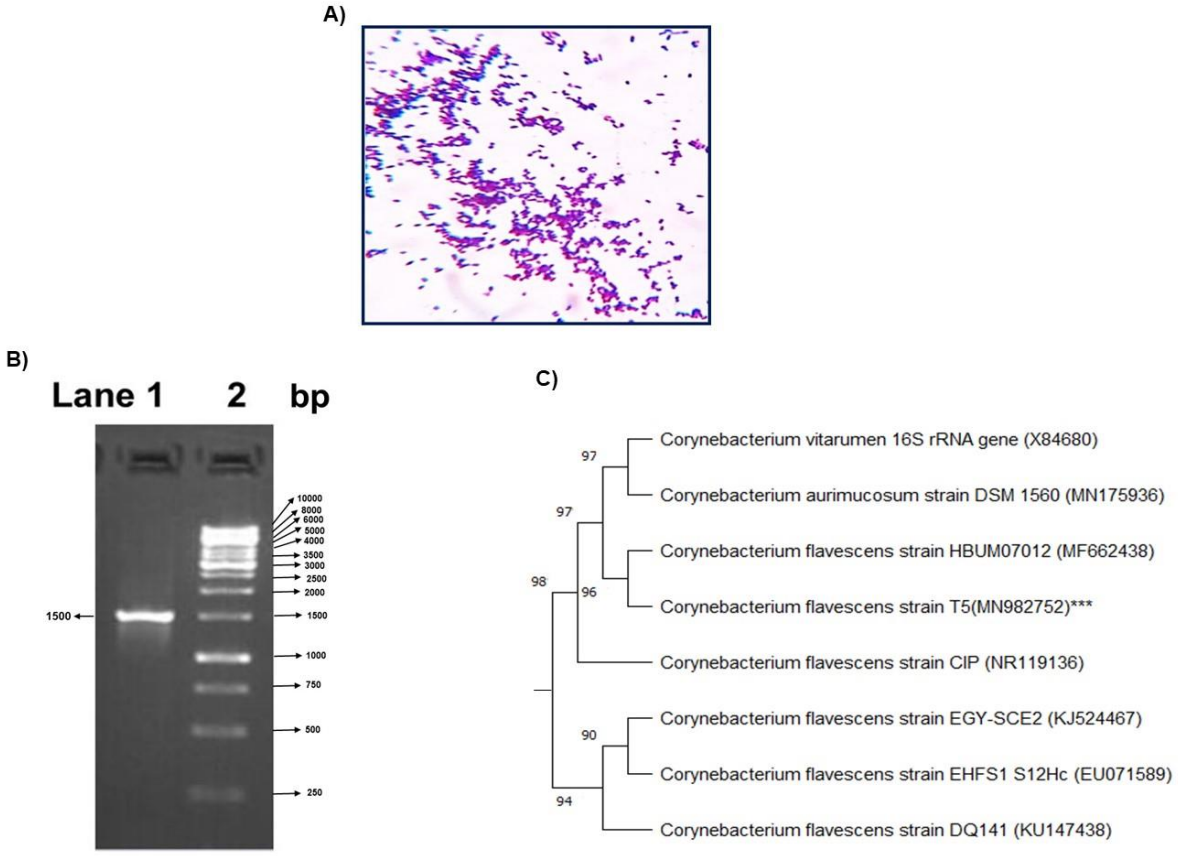

Figure 4.2: A) Gram staining of T5 isolate at 100X; B) Agarose gel electrophoresis image [Lane 1: T5 isolate PCR product, and Lane 2: DNA markers] C) Phylogenetic tree of T5 isolate identified as *Corynebacterium flavescens*

4.3 Optimization of production parameters

To raise the production of CA by *C. flavescens*, the various process parameters were optimized.

4.3.1 Selection of culture medium

Among the six media i.e., Muller Hinton broth, basal salt media, Luria broth, minimal salt media, nutrient broth, and peptone broth tested for CA production, the nutrient broth was found to be the best media with a maximum activity of 84.9 U/mL (Figure 4.3). However, the lowest activity (38.6 U/mL) was detected in the Muller-Hinton broth. Therefore, the nutrient broth was selected for CA production in further studies. Previously, Ramanan et al., also reported the same medium for *Nocardiopsis lucentensis* CA production [240]. In another study, peptone broth was selected as the suitable media for CA production from the *Pseudomonas fragi* [225].

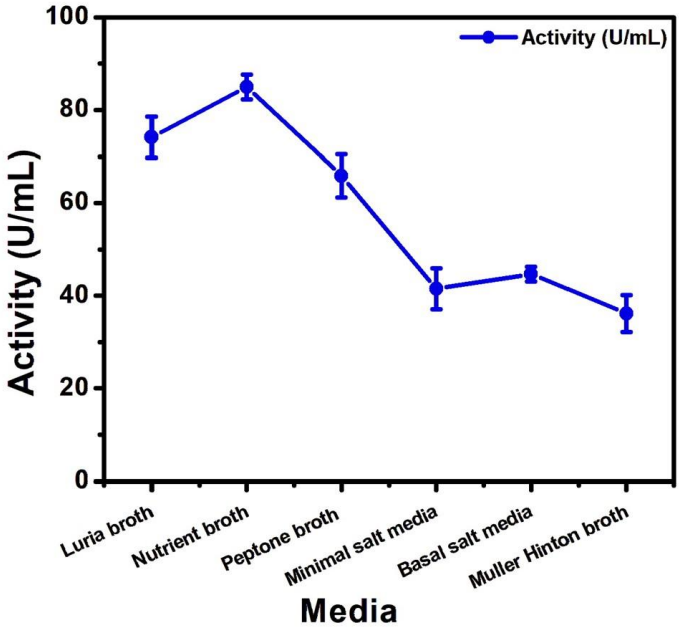

Figure 4.3: Effect of various media on CA production by *C. flavescens*

4.3.2 Optimum temperature and agitation rate

The incubation temperature is an important factor because it affects the metabolic activity of microbes and their enzymes [241]. The effect of temperature on the production of CA was determined by incubating the production media at various temperatures ranging from 20 to 70°C for 24 h at 120 rpm. The maximum production (85.5 U/mL) of CA was recorded at 40°C (Figure 4.4). Then, CA activity starts declining with a further rise in temperature. Approximately 50% of CA activity was lost at 70°C. Similarly, Jaya et al., reported the

optimum production of *B. safenis* CA at 40°C [141]. Previously, the optimal temperature for *C. freundii* CA production was reported at 37°C [145]. However, *Methanobacterium thermoautotrophicum* exhibited optimum activity at 75°C [242]. Whereas, *Bacillus mucilaginosus* showed higher CA production at 32°C [243]. Therefore, from these outcomes, it can be concluded that temperature optima for CA production varies among the different genera and species.

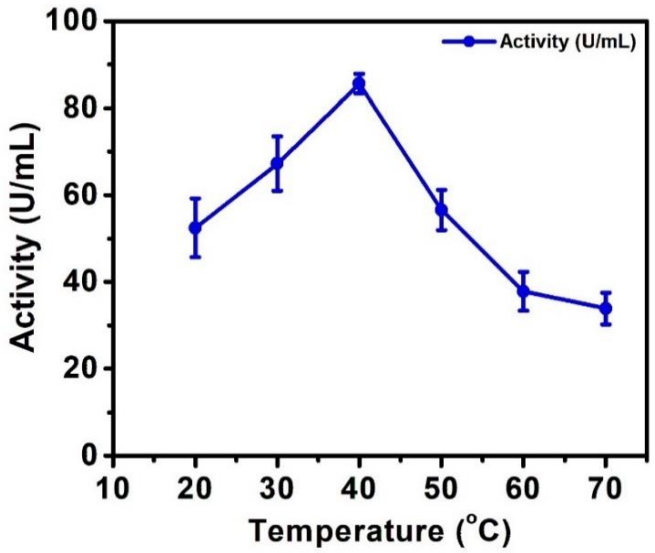

Figure 4.4: Effect of temperature on CA production by *C. flavescens* was performed using nutrient broth as production media

Agitation plays a key role in enzyme production as it ensures the proper nutrient and air distribution, which affects bacterial growth and product yield. Also, the production of enzymes is reported to be higher under constant shaking in contrast to static conditions. Thus, the role of agitation speed on the enzyme production was also examined, and it was observed that CA activity reached 86.5 U/mL at 120 rpm (Figure 4.5). The decline in activity was detected at higher agitation speed due to the reduction in the viability of microbial cells. Almost 40% of activity was lost at 180 rpm. Furthermore, the deactivation effect has also been attributed to the shearing forces generated due to mixing and the entrapment of air bubbles in the medium [244]. Bose et al., have optimized 150 rpm to culture *A. pallidus* for CA production [245]. Previously, CA from *Bacillus mucilaginosus* showed maximum CA production at 200 rpm [243].

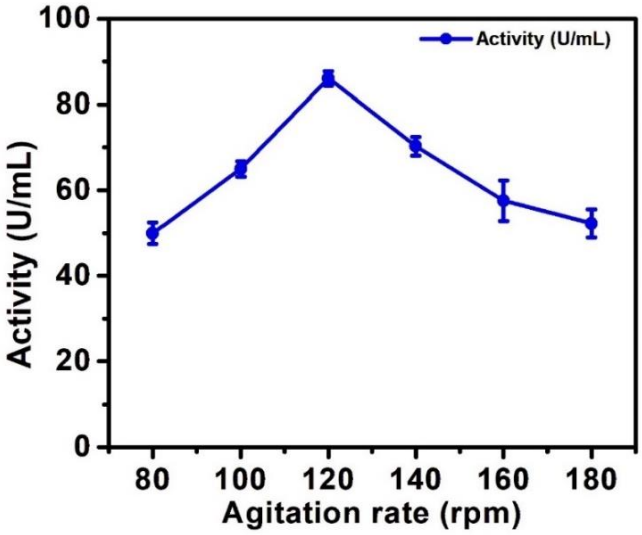

Figure 4.5: Effect of agitation rate on CA production by *C. flavescens* was performed using nutrient broth as production media at 40°C

4.3.3 Inoculum volume and inoculum age

The optimization of inoculum volume and age is a very vital parameter as it affects the final product cost and production rate. The seed culture was prepared in nutrient broth (50 mL) by adding a loopful culture of *C. flavescens* and kept at 40°C for 24 h. For CA production, inoculum volume was varied from 2 to 12% v/v for 100 mL of production medium. The inoculated production media was kept at 40°C for 24 h at 120 rpm. The results exhibited that a rise in the production of CA was noticed with 4% v/v inoculum volume (Figure 4.6). However, a further rise in inoculum volume above 4% v/v led to a decrease in CA activity. Earlier reports depicted that an inoculum size of 1.5% was best suited for *A. pallidus* CA production [245]. Generally, the higher inoculum volume enhances bacterial growth up to some level, and afterward, the growth starts declining due to the depletion of nutrients. When an inoculum size is low, the bacterial cells are lesser in the medium and thus take more time to divide [246]. So, the inoculation of an optimal number of cells in the media plays an essential role in CA production. The age and quantity of the inoculum have a significant effect on the growth and metabolic rate of bacteria.

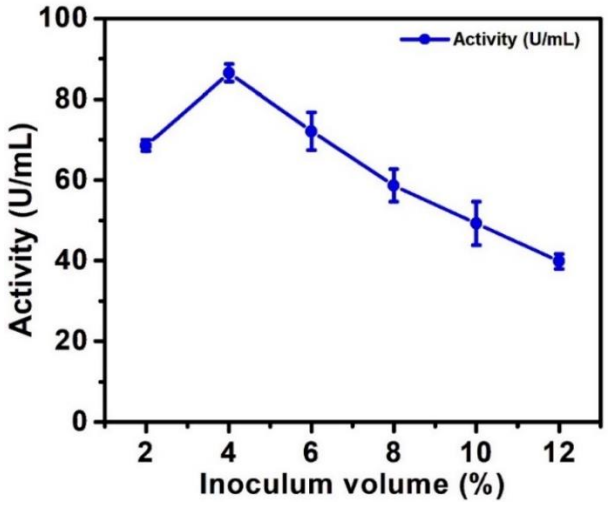

Figure 4.6: Effect of inoculum volume on CA production by *C. flavescens* was performed using nutrient broth as production media, 40°C temperature, and 120 rpm agitation rate

To study the effect of inoculum age, the nutrient broth was inoculated with 4% (v/v) seed cultures of varying ages (6, 12, 18, 24, 30, 36 h) and incubated at 40°C. The highest CA production was observed when 24 h old culture was used (Figure 4.7). With a further increase in inoculum age, a decline in enzyme productivity was observed that might be due to the accumulation of secondary and tertiary metabolites [247]. The lowest activity (49.2 U/mL) was observed when 36 h old culture was used. Thus, the study concluded that the 24 h old culture is more active than that of the aged inoculum, Thus, the *C. flavescens* produced maximum CA during the early phase of growth, and afterward, it starts declining.

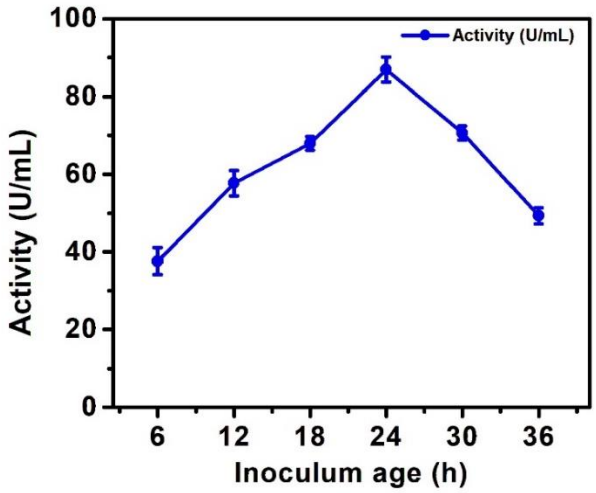

Figure 4.7: Effect of inoculum age on CA production by *C. flavescens* was performed using nutrient broth as production media, 2% v/v inoculum size, 40°C temperature, and 120 rpm agitation rate

4.4 Characterization of the enzyme

Various physical parameters, such as, cultivation temperature, agitation rate, and aeration are essential for promoting, stimulating, enhancing, and optimizing enzyme production. However, the optimization of various reaction parameters is important to improve the activity of crude enzyme mixtures. Thus, reaction conditions of crude CA isolated from *C. flavescens* were optimized to determine the most favorable reaction conditions, including buffer pH, buffer molarity, reaction temperature, reaction time, and the presence of denaturing agents, metal ions, and organic solvents, *etc.*

4.4.1 Buffer pH and buffer molarity

pH is an important reaction parameter because the ionization state of amino acids present in the active site of enzymes is pH-dependent. At optimum pH, enzymes are mostly active; when the reaction pH rises, the charged amino acids of the enzyme become deprotonated, and their ionic potential changes [248]. The different buffers of varying pH were individually assayed to examine the CA activity. In the present study, the CA is active at neutral pH (Figure 4.8), but when the pH is increased the CA activity starts decreasing due to changes in the ionization of catalytically important amino acids. This result coincided with the findings of *T. ammonificans* CA in which a phosphate buffer of pH 7.0 was used for the activity assay [157]. Previously, *Helicobacter pylori* CA exhibited maximum activity in an acidic condition [249]. Furthermore, Li et al., have used the phosphate buffer (pH 6.0) for activity assay [123]. The CA purified from *Mytilus galloprovincialis* showed optimal activity in a Tris-sulfate buffer having a pH 7.6 [250]. At high or low pH, the active sites of enzyme lose their affinity towards the substrate which results in the decline of enzyme activity too.

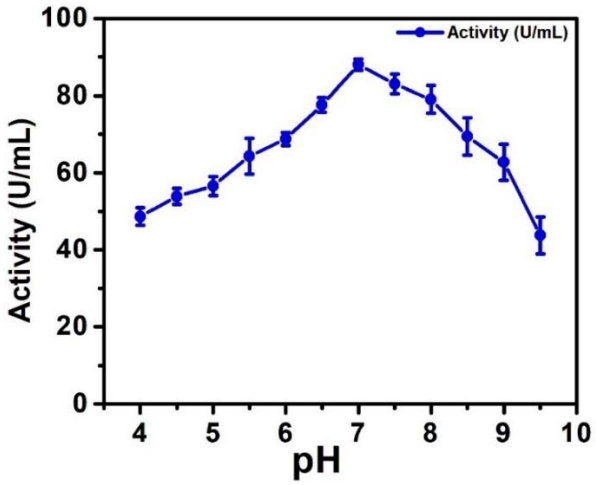

Figure 4.8: Effect of buffer pH on CA activity was performed at 37°C for 10 min

Furthermore, the different concentrations (20-70 mM) of phosphate buffer were utilized to select the optimal molarity of the buffer. The activity was found to be the highest when a phosphate buffer of 50 mM concentration was used (Figure 4.9). The enzyme activity starts decreasing when the ionic strength of the buffer is increased, which may be because the enzyme-substrate complex becomes unstable at higher buffer molarities [251]. However, Jun et al., have used Tris-SO_4 buffer (50 mM) for the activity assay [149]. Previously, 1.0 M of Tris-SO_4 buffer was optimized for CA purified from sheep [252]. Moreover, Jo et al, while carrying out their work on CA production from recombinant *T. ammonificans* and *P. marina*, found 50 mM of potassium phosphate buffer optimal for the activity assay [144]. In one of the previous study, 1 M of glycine/NaOH buffer was optimized for CA purified from fish muscle [253].

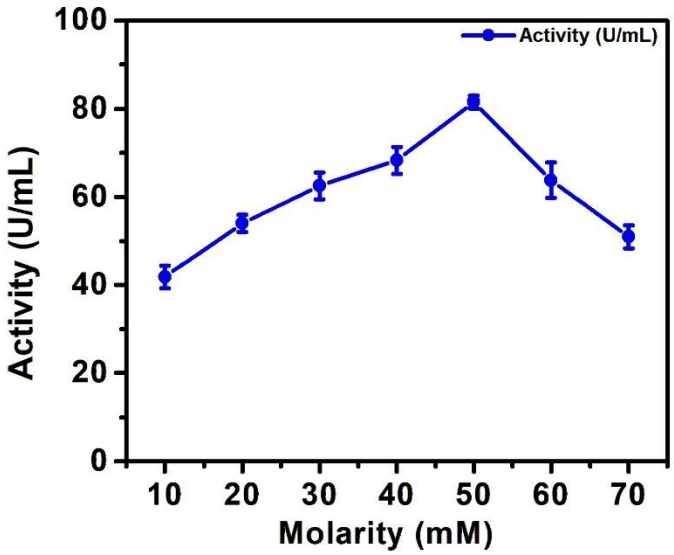

Figure 4.9: Effect of different buffer molarity on CA activity was performed in phosphate buffer of pH 7.0 at 37°C for 10 min

4.4.2 Reaction time and temperature

The optimum reaction time for CA activity was evaluated by keeping the reaction mixture at various time intervals (2-18 min). The maximal activity of 88.3 U/mL was recorded when the reaction mixture was incubated for 10 min (Figure 4.10). After 10 min, due to the denaturation of protein, the activity starts decreasing. Previous results showed that 5 min is an optimal time for activity assay [250].

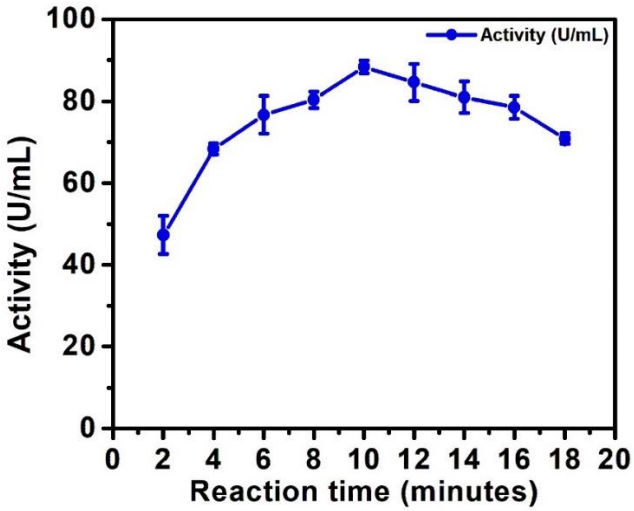

Figure 4.10: Effect of reaction time on CA activity was performed in phosphate buffer (50mM) of pH 7.0 at 37°C

The enzymatic reaction was carried out at different temperatures (25-60ºC), to find out the optimum reaction temperature (Figure 4.11). A temperature of 35ºC was found to be optimum for CA activity from crude cell lysate. Afterward, enzyme activity starts decreasing due to the disruption of intermolecular interaction (dipole-dipole interaction and hydrogen bonding) and hydrophobic interactions within the protein structure. When these forces are altered, protein secondary and 3-D structures also change [254]. The results of the present finding, coincided with the work of Sundaram and Thakur, as they also found 35°C temperature suitable for activity assay [122]. While CA from *Methanosarcina thermophila* was reported to exhibit maximum activity at 75ºC [242]. The optimal temperature for CA from *Trachurus trachurus*, *Mesorhizobium loti*, and *Bacillus* sp., were reported to be 30, 40, and 37°C, respectively [143, 146, 253]. Moreover, the optimal temperature for *Bacillus* sp., CA, was reported to be 60°C [122]. These outcomes showed the ability of CA to play a diverse role in the microorganisms existing in an extreme environment.

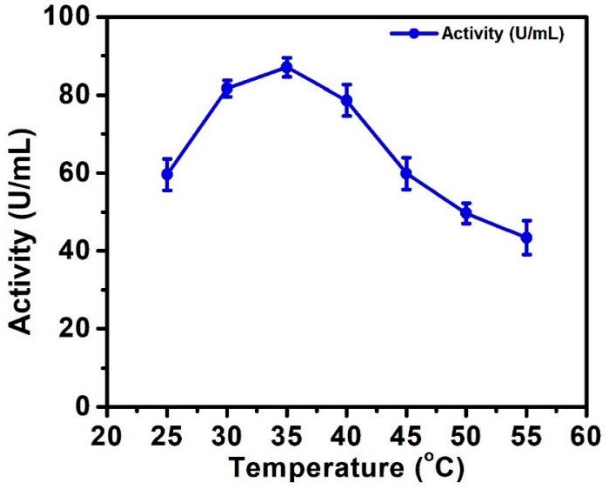

Figure 4.11: Effect of temperature on CA activity was performed in phosphate buffer (50 mM) of pH 7.0 for 10 min

4.4.3 Metal ions affecting CA activity

Metal ions form complex with proteins that either maintain or disrupt the three-dimensional structure and confirmation. The activity of crude CA was determined in the presence of 1 and 5 mM concentrations of metal ions. The untreated enzyme was used as control and defined as 100% relative activity. These metal ions of different concentrations were added to the reaction mixture, and the CA activity was evaluated in each case. The metal ions Zn^{2+} and Fe^{3+} showed an increase in CA activity. These outcomes suggested that the CA from *C. flavescens* is a metalloprotein (Table 4.1). On the other hand, Na^{2+}, Mg^{2+}, Al^{3+}, and K^{+} strongly inhibit the CA activity. The interaction of metal ions with carboxylic acid and the amine group of proteins can either promote or inhibit enzyme activity. However, various metal ions denature the enzyme by attaching to its sulfhydryl group, which leads to a decline in enzyme activity [255]. Previously CA purified from *Dicentrarchus labrax* was inhibited in the presence of Zn^{2+}, Co^{2+}, and Al^{3+} [256]. The inhibition of activity might be due to the formation of metal complexes in the enzyme active site, thus preventing the catalytic reaction. In contrast, *P. fragi* CA activity was improved in the presence of Na^{2+}, Zn^{2+}, and Fe^{3+} [225].

Table 4.1: Effect of various metal ions

Metal ion	Concentration	Relative Activity (%)
NaCl	1	87.4
	5	82.1
KCl	1	66.7
	5	70.6
$MgCl_2$	1	54.4
	5	48.8
$ZnCl_2$	1	103.7
	5	106.0
$CaCl_2$	1	100.4
	5	99.3
$FeCl_3$	1	101.6
	5	103.7
$AlCl_3$	1	44.4
	5	37.4

4.4.4 Organic solvents and denaturing agents

Most of the time, the organic solvents denature the CA by disrupting the hydrogen bond, which is required for maintaining the functional group of the enzyme. To examine the effect of selected organic solvents (2% v/v) on the CA activity, the crude CA was pre-incubated for 10 min at 35°C with selected organic solvents. It was observed that all the tested organic solvents decreased the CA activity (Figure 4.12). Previously, ethanol was found to inhibit the activity of CA purified from human erythrocytes [257]. The solvent might have distorted the active site of the enzyme, hence preventing the substrate to enter the active site of the enzyme [258].

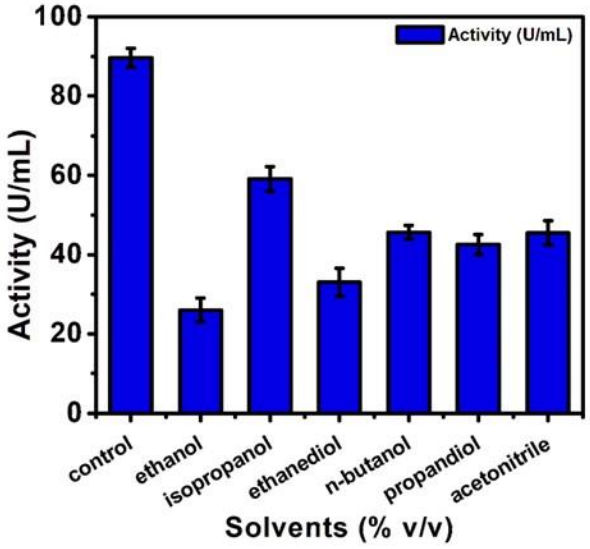

Figure 4.12: Effect of different solvents on CA activity was performed in phosphate buffer (50mM) of pH 7.0 at 35°C for 10 min

Furthermore, to study the effect of SDS, EDTA, urea, and PMSF, on CA activity, these were preincubated separately at 5 mM concentration with the crude CA at 35°C for 10 min, respectively. All the chelating agents had a severe inhibitory effect on CA activity (Figure 4.13). Among them, EDTA and SDS strongly inhibited the CA activity. Previously, the CA activity of *B. subtilis* was completely inhibited by EDTA [148]. Also, EDTA had shown an inhibitory effect on the CA obtained from *P. fragi* [225]. Generally, detergents disrupt the 3-D structure of the enzyme, which results in protein denaturation [259]. The binding of SDS with CA may result in the formation of unfavorable electrostatic interactions that induced the unfolding of CA, and thus a decline in CA activity was observed [260].

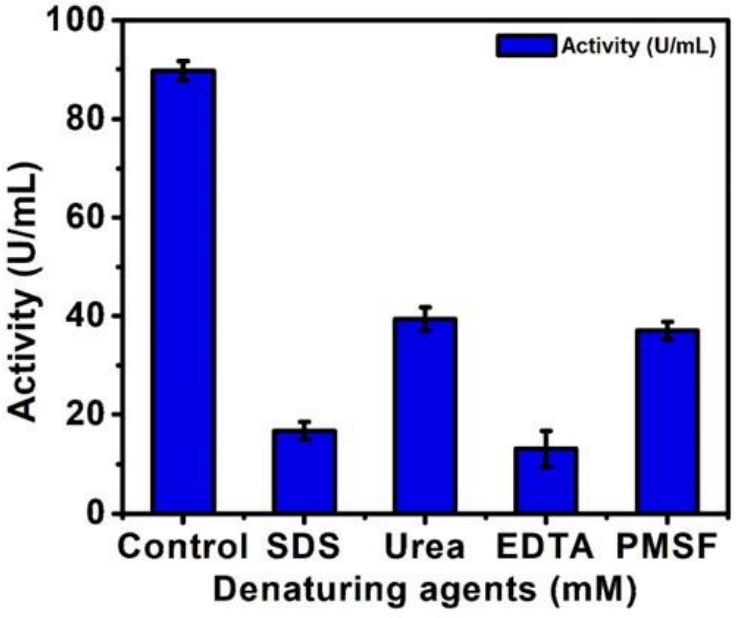

Figure 4.13: Effect of denaturing agents on CA activity was performed in phosphate buffer (50mM) of pH 7.0 at 35°C for 10 min

4.4.5 Conversion of CO_2 into $CaCO_3$ using crude CA

The biomimetic conversion of CO_2 using crude CA is an economic and eco-friendly approach. The control reaction was conducted using BSA, which showed no precipitation. The crude CA exhibited higher CO_2 conversion *i.e.,* 45.0 mg $CaCO_3$/mg protein, as compared to the partially purified *B. pumilus* CA (33.0 mg $CaCO_3$/mg protein) [261]. The control reaction was carried out using BSA, which showed no precipitation. Thus, *C. flavescens* CA represents a promising candidate for the conversion of CO_2.

4.5 Immobilization of *C. flavescens* cells on keratin particles

Whole-cell immobilization reduces the expensive and laborious steps needed for enzyme purification. Previously, whole cells of *Chlorella* and *Geobacillus thermoglucosidasius* also exhibited the production of $CaCO_3$ [262, 263]. Thus, the immobilization of whole cells of *C. flavescens* was performed covalently on keratin particles to enhance the whole cells' stability and CO_2 conversion efficacy. The keratin particles morphology was analyzed by SEM (Figure 4.14A). The diameter of keratin particles was approximately 0.5 µm. The SEM images revealed that the small pores were present on the keratin particles, and these pores were enough to immobilize the whole cells of *C. flavescens*. The SEM image of *C. flavescens* cells immobilized onto keratin particles was shown in (Fig. 4.14B). The image showed that *C. flavescens* cells were uniformly bound with keratin particles.

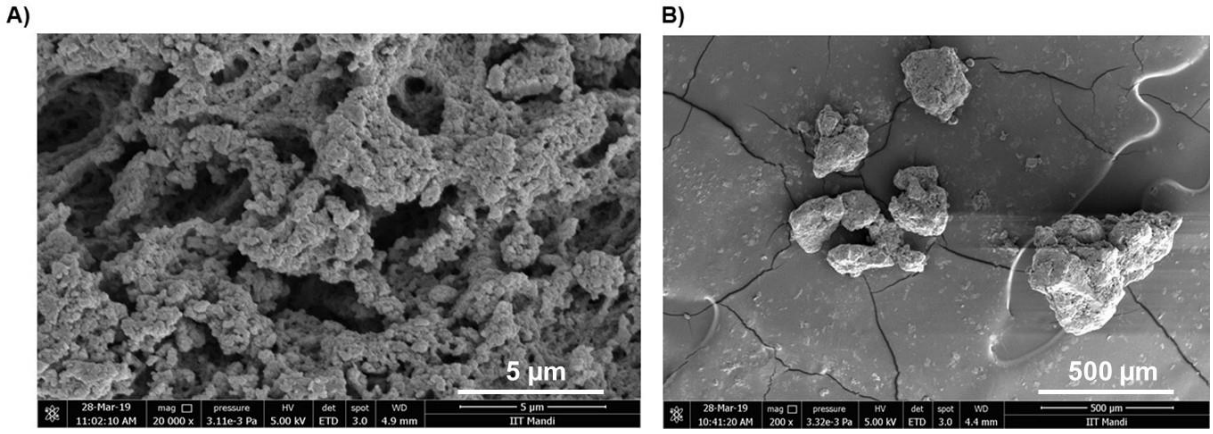

Figure 4.14: SEM images showing the morphology of A) keratin particles, B) *C. flavescens* cells immobilized onto keratin particles

4.6 Optimization of parameters affecting whole-cell immobilization

4.6.1 Glutaraldehyde concentration

Glutaraldehyde has been reported as the most reliable cross-linker in previous studies. The glutaraldehyde was used to introduce aldehyde moieties into the matrix. To attain efficient bio-catalysis, the optimization of various immobilization parameters is required. Among the various glutaraldehyde concentrations (0.2-1.4% v/v) used, 0.6% v/v was found to be optimal for whole-cell immobilization (Figure 4.15). At higher glutaraldehyde concentrations, the immobilization yield decreased. A very high glutaraldehyde concentration led to spatial hindrance between cell aggregates due to the formation of several cross-linking points on the keratin particles [264]. Whereas, a low concentration of glutaraldehyde results in insufficient cross-linking and low immobilization yield. At low concentrations, both aldehyde groups of glutaraldehyde may get cross-linked with amino groups of keratin particles, leaving a few free aldehyde groups accessible for interaction with the cells. In contrast, *E.coli* cells entrapped in chitosan have shown a 5.0% glutaraldehyde concentration optimal for immobilization [265]. Moreover, Zhang and his co-workers used 0.1% glutaraldehyde for immobilization of recombinant whole-cell having isomerase onto alginate beads [266].

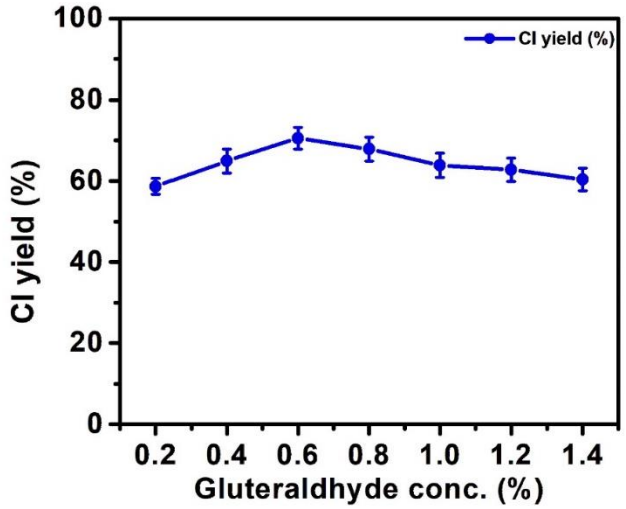

Figure 4.15: Effect of glutaraldehyde concentration on CI yield was determined for 30 h at 4°C

4.6.2. Incubation temperature

Initially, with a rise in temperature from 4 to 55°C, the CI yield decreased from 72.5 to 46.0% (Figure 4.16). Thus, the optimal temperature for cell immobilization was 4°C. These outcomes exhibited that a low temperature is more advantageous for cell immobilization than a higher temperature. Previously, 4°C temperature was reported optimal for the immobilization of methanotrophs on coconut coir [267]. Indeed, the *Bacillus circulans* cells immobilized on a palm curtain showed 40°C temperature optimal for immobilization [268].

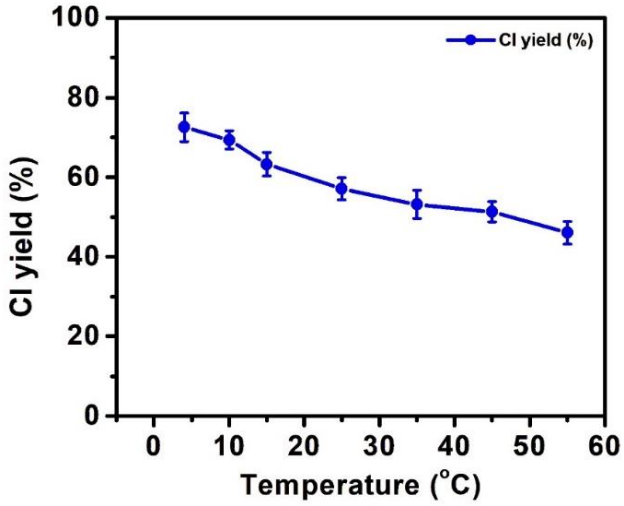

Figure 4.16: Effect of temperature on CI yield was determined using 0.6% (v/v) glutaraldehyde concertation for 30 h

4.6.3 Incubation time

In fact, the CI yield of immobilized cells was evaluated for 5 to 35 h of incubation. In the current study, the CI yield was enhanced with an increase in the time of incubation up to 25 h (Figure 4.17). After 35 h of incubation, the CI yield decreased slightly. After prolonged exposure to the reaction system, the cells begin to degrade, resulting in a loss of CI yield [218]. Previously, an incubation period of 24 h was reported as optimal for the immobilization of *Methylocella tundrae* cells on chitosan [227]. Furthermore, 48 h of incubation time was found optimal for the immobilization of *Bacillus* sp., cells on sodium alginate [269]. Moreover, the *Bacillus circulans* cells entrapped in alginate beads showed maximum relative activity at 36 h of incubation [270].

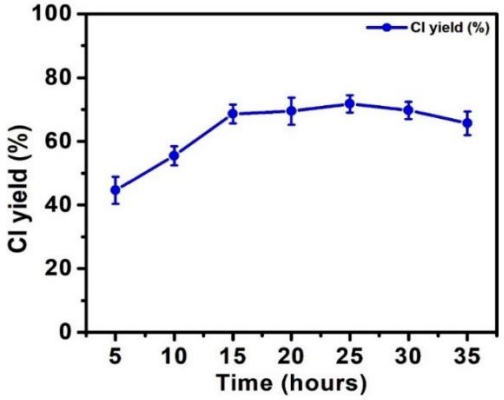

Figure 4.17: Effect of incubation time on CI yield was determined using 0.6% (v/v) glutaraldehyde concertation

4.6.4 Reusability

The reusability of immobilized cells is an important parameter to be widely used in the industrial sector. Immobilized *C. flavescens* cells show noteworthy differences in their catalytic activity after repetitive use. The amount of calcium carbonate formed by the immobilized cells in the first cycle of reuse was 86.71 mg. After 10 consecutive cycles, the $CaCO_3$ production by immobilized cells was 14.1 mg. A decrease in $CaCO_3$ production was observed with an increasing number of cycles (Figure 4.18). The decrease in $CaCO_3$ production is because of the leaching of cells, and the loss of immobilized cells during washing after each cycle of reuse [229]. These outcomes recommend that the immobilization of *C. flavescens* cells is an effective method for CO_2 conversion. Moreover, the $CaCO_3$ formed after each cycle will also provide a valuable chemical that can be utilized in the manufacture of antacids, chemicals, white paints, calcium supplements, and other construction materials [271].

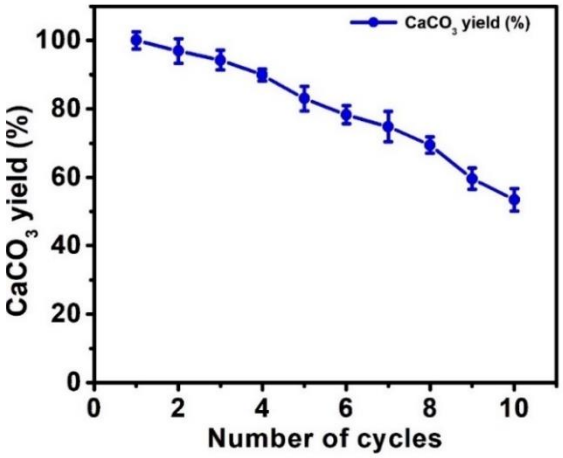

Figure 4.18: Reusability of immobilized cells

4.6.5 Instrumental analysis of $CaCO_3$

4.6.5.1 FE-SEM analysis of $CaCO_3$

The $CaCO_3$ was further characterized by SEM, XRD, and FTIR. The results of SEM micrographs exhibited that $CaCO_3$ is mainly comprised of the vaterite form, although a few calcites were also observed (Figure 4.19A-B). Furthermore, it was reported that $CaCO_3$ exists in calcite and vaterite forms in the presence of CA [123]. The different crystal forms of $CaCO_3$ are vaterite (spherical), aragonite (needle-like), and calcite (rhombic). Moreover, the EDX experiment confirmed that the formed precipitates were $CaCO_3$ (Figure 4.19C-F). The resulting images showed that $CaCO_3$ precipitates consisted of C, O, and Ca respectively.

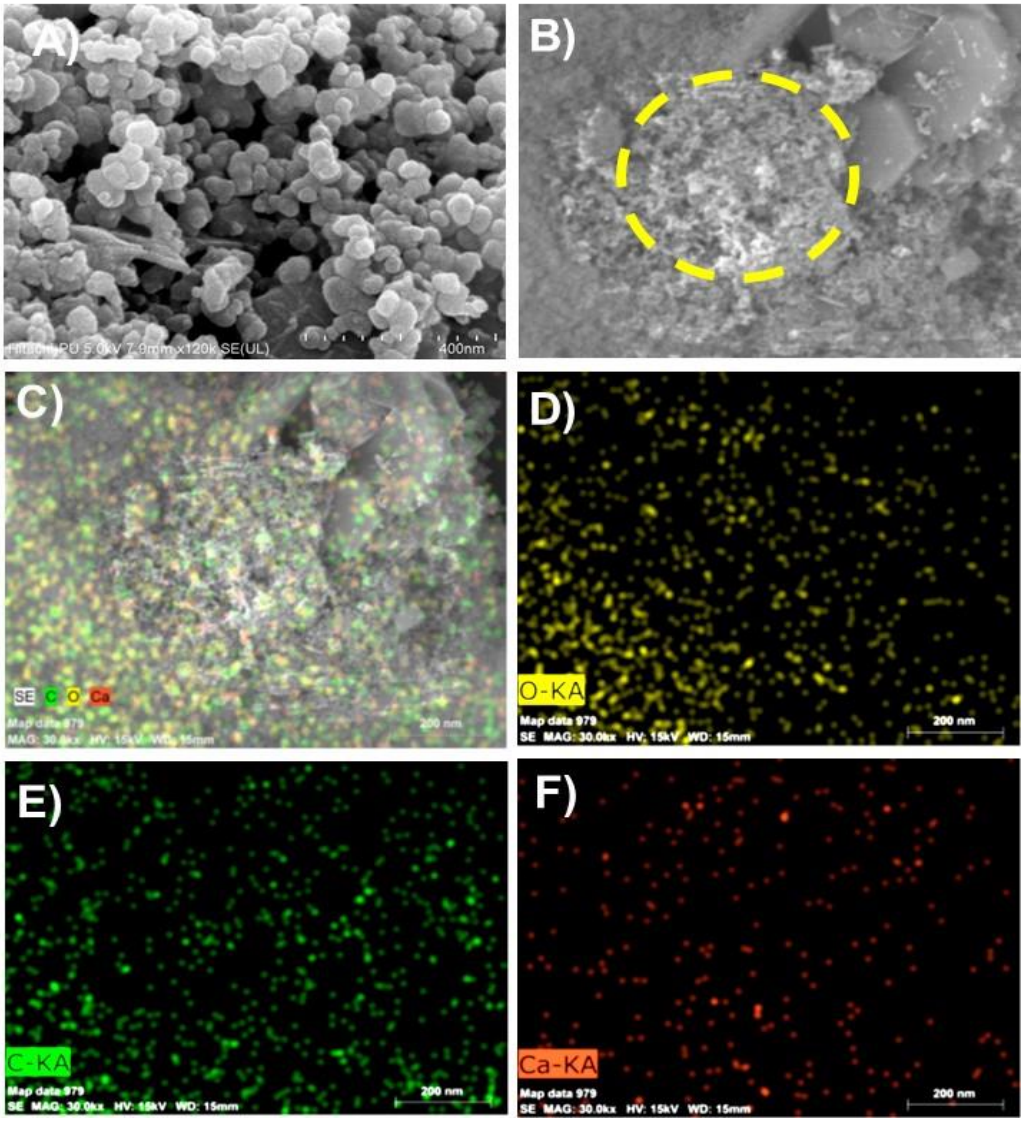

Figure 4.19: FE-SEM images of $CaCO_3$ A) Morphology of $CaCO_3$ B-F) Elemental images of $CaCO_3$ showing the existence of D) oxygen E) carbon and, F) calcium

4.6.5.2 FTIR analysis of $CaCO_3$

In addition, FTIR analysis provided the chemical structure of $CaCO_3$. As shown in (Figure 4.20), the test sample shows peaks at 712, 874, 1465, and 1420 cm^{-1}, and the control sample also showed peaks at nearly the same wavenumber that confirm the formation of $CaCO_3$.

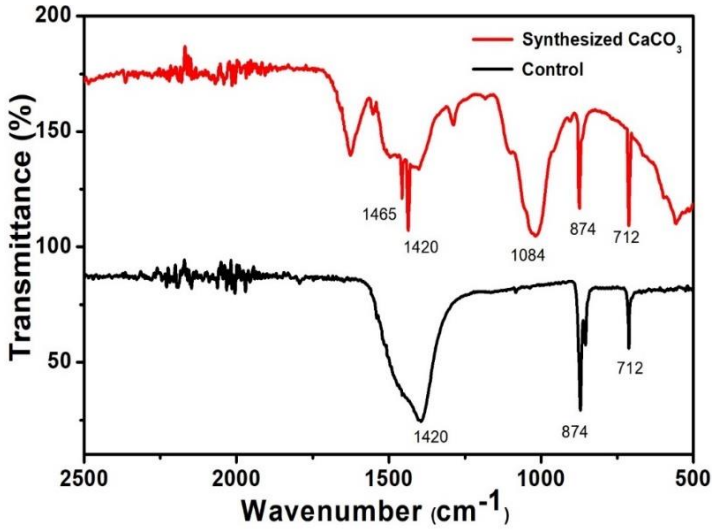

Figure 4.20: FTIR analysis of control and synthesized $CaCO_3$ in the 500-2500 cm^{-1} region

4.6.5.3 XRD analysis of $CaCO_3$

Moreover, the crystallographic structures of the $CaCO_3$ were analyzed by XRD (Figure 4.21). The diffraction peaks at 25.46 and 29.48 correspond to vaterite and calcite, respectively. Previously, the diffraction peaks at 29, 43, 47, and 57 corresponded to the calcite form of $CaCO_3$, whereas the peaks for the vaterite form appeared at 25, 27, 33, and 50 [272].

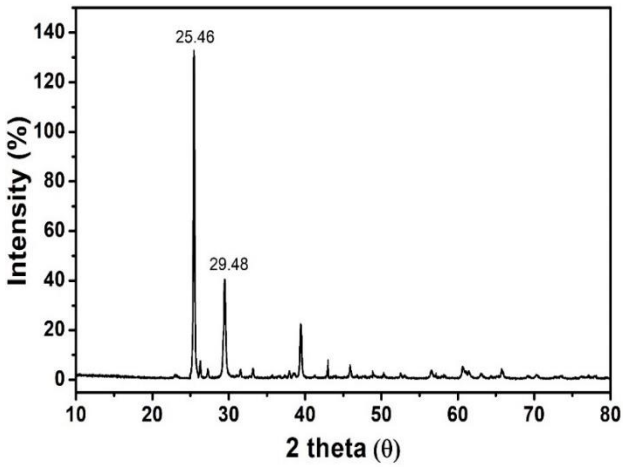

Figure 4.21: XRD analysis of $CaCO_3$

4.7 CA purification

4.7.1 Purification and molecular weight determination

The crude CA having an activity 91.9 U/mL was concentrated using acetone precipitation. The precipitates having 1.4-fold purification were loaded on Sephadex G-100 to separate the proteins on the basis of size. The fractions having higher activity and protein content were pooled and used for further studies. This chromatographic step showed 10.7% yield of CA (Table 4.2). The Sephadex G100-column purified fractions were further examined using denaturing SDS-PAGE (12%). Furthermore, the SDS-PAGE analysis revealed the single band of purified enzyme (29.0 kDa) (Figure 4.22A-B). The single band of protein on SDS-PAGE indicated that the enzyme may be a monomeric protein. Previously, an extracellular *P. fragi* CA purified using affinity chromatography showed a molecular weight of 31.0 kDa and 4.5-folds purification [225]. In another study, CA purified from bovine erythrocytes by Sephadex G-150 chromatography exhibited a molecular weight of 29.8 kDa [273]. Furthermore, the CA isolated from camel liver resulted in a 45.2% yield by affinity chromatography [139]. Indeed, bacterial CA possesses a molecular weight of 28.0 kDa in *Bacillus* sp., 25.0 kDa in *N. gonorrhoeae,* 23.0 kDa in *Helicobacter pylori,* 29.0 kDa in *N. sicca* [2, 122, 143].

Table 4.2: Summary of protein purification

Purification step	Volume (mL)	Activity (U)	Protein (mg)	Specific activity (U/mg)	Fold purification	Recovery (%)
Crude	250.0	22975.0	483.7	47.4	1.0	100.0
Aectone precipitation (%)	30.0	2838.0	42.0	67.5	1.4	12.3
Sephadex G-100	15.0	2462.4	4.98	494.4	10.4	10.7

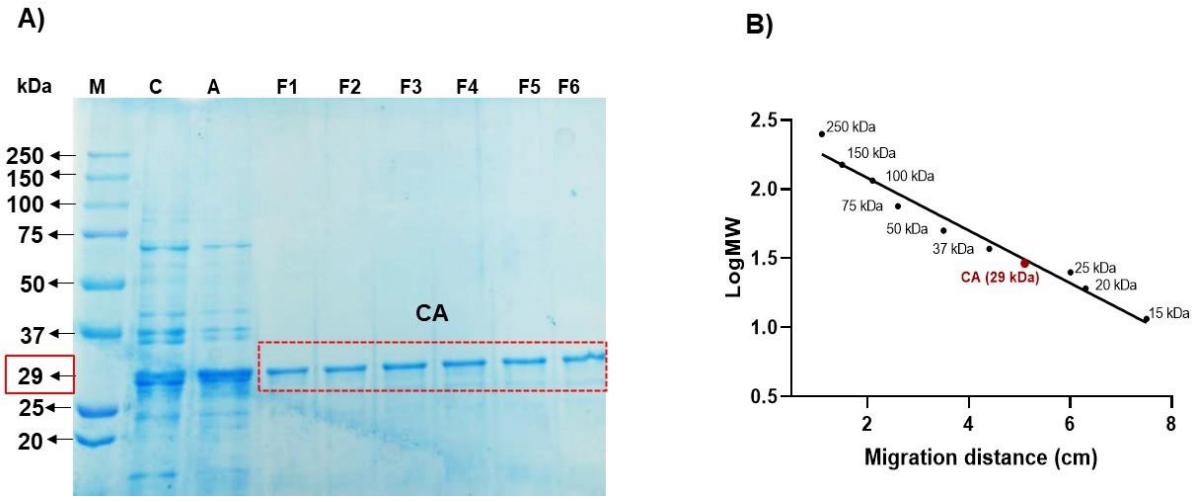

Figure 4.22: A) Molecular weight determination of *C. flavescens* CA on 12 % SDS-PAGE, Lane M: protein marker, lane C: crude CA, lane A: precipitated protein; lane F1-F6: purified CA using Sephadex G-100 B) Calibration curve for calculating the molecular mass of protein

4.7.2 MALDI-TOF-MS of purified CA

The protein band was cut from the gel surface and analyzed using MALDI-TOF-MS. The Mascot search analysis of the peptide fragments acquired from MALDI-TOF-MS confirms that the purified protein was CA, which had a high score (95) and a sequence from a CA related to *K. pneumoniae* that covered 58% of the sequence coverage. (Figure 4.23A). A higher score in MASCOT indicates that more peptides were recognized from an actual protein [274]. Therefore, the results attained from MALDI-TOF-MS analysis in the present study confirmed that the purified protein of *C. flavescens* was CA. The nominal mass of CA from *K. pneumoniae* was 27.24 kDa. The CA molecular mass predicted by SDS-PAGE and MALDI-TOF-MS was roughly similar. The molecular mass of CA varies depending on the source of isolation and CA having the same molecular weight has also been reported from different sources. Furthermore, the Multiple Sequence Alignment results were used to create a Cladogram that authenticated the relatedness of purified CA with *K. pneumoniae* CA (Figure 4.23B).

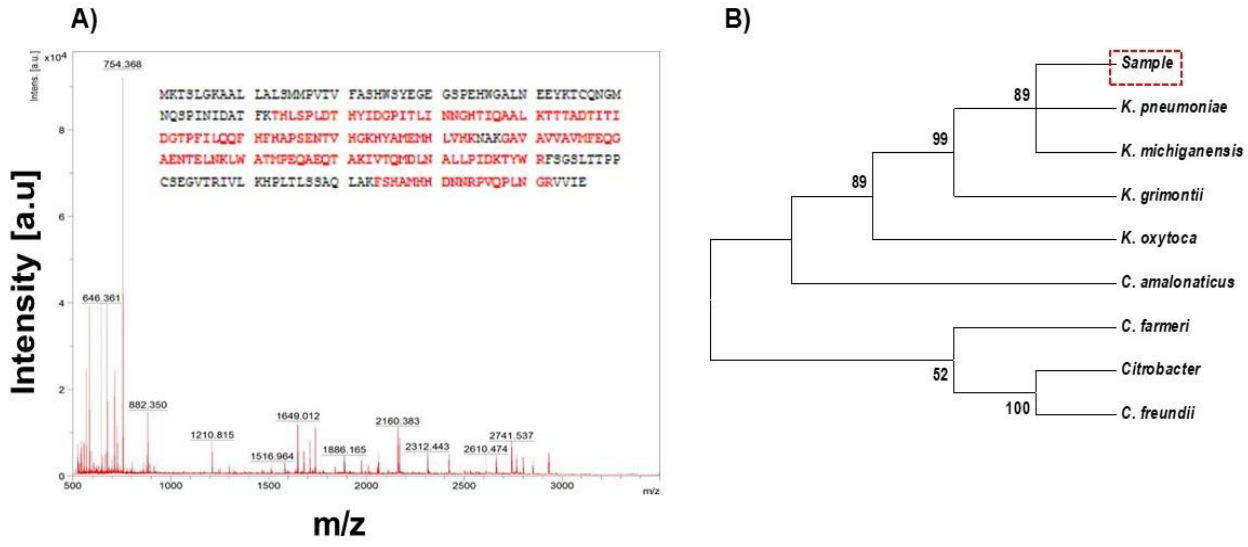

Figure 4.23: A) MALDI TOF-MS analysis of tryptic digested peptides fragments of purified CA B) Cladogram of purified CA with related protein(s)

4.7.3 Modelling and validation of CA structure

The main goal of homology modelling is to create the 3-D structure of a protein from experimentally known structures of related homologs as templates. To verify the homologs sequence of known structure for template protein *i.e., C. flavescens* CA, a BLAST search was performed in NCBI (www.ncbi.nlm.nih.gov). A blast search revealed that *T. ammonificans* (PDB: 4C3T) CA exhibits 48% of sequence identity with *C. flavescens* CA. Thus, *C. flavescens* CA structure was built using *T. ammonificans* CA as template (Figure 4.24a-b). The homology model of CA were generated by MODELLER using the *Build Homology Models* protocol applied in DS software. The best model showed a DOPE score of -23400.61 and PDF energy of 1278.53. Homology modelling-based protein structure prediction of protein structure is a quicker strategy of structural analysis as compared to X-ray diffraction or NMR. In comparison to NMR or XRD, homology modelling-based protein structure prediction is a faster method of structural investigation.

To validate the CA model Ramachandran plot was constructed representing that 12% of residue was in the additionally allowed region, 88% in the allowed region, and no residue was present in the disallowed region (Figure 4.24c). The Z-score of protein was -6.18 predicted by the ProSA program (Figure 4.24d). This score is within the range usually reported for

numerous native proteins of similar size. Thus, these findings show *C. flavescens* CA structure has good stereochemical characteristics.

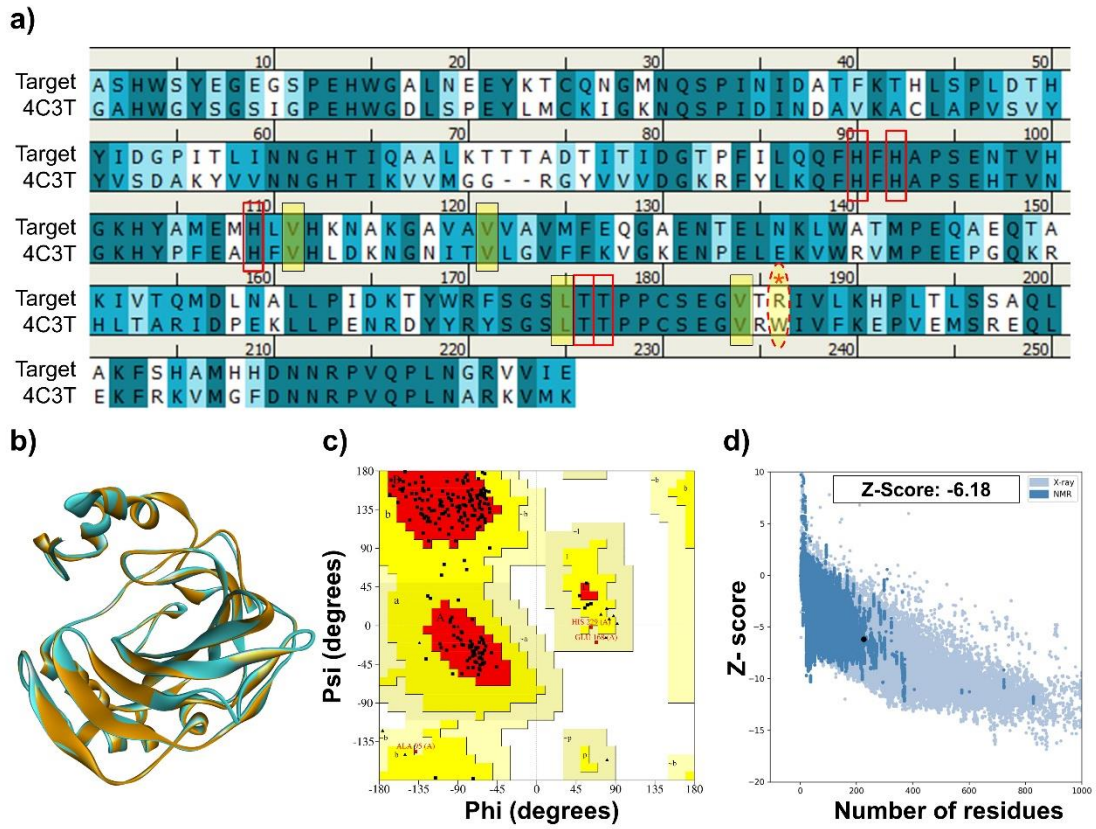

Figure 4.24: Homology modelling of *C. flavescens* CA a) Sequence alignment of CA from *C. flavescens* aligned with *T. ammonificans* CA sequence. Red boxes represent histidines that coordinate the zinc ion and conserved binding site amino acids. Yellow boxes indicate the residues that bind CO_2. A red dotted circle with an asterisk denotes mutation in the CO_2 binding area; b) Homology model (cyan) superimposed with *T. ammonificans* (orange) CA structure; c) Ramachandran plot showed that 88.8% of structure residues occur in allowed regions, d) The Z-score of protein was -6.18 predicted by the ProSA program.

The structural and sequence analysis of *T. ammonificans* and *C. flavescens* shows the hydrophilic region is conserved, which is responsible for the binding of the Zn^{2+} ion binding. Most of the CO_2 binding residues present in hydrophobic regions including Val142, Thr197, Val205, Val132, and Leu196 are also conserved. Additionally, in the hydrophilic region metal coordinating residues such as His130, His111, His111, Thr197, and Thr198 are conserved

(Figure 4.25). Moreover, the *C. flavescens* CA Arg207 is replaced with *T. ammonificans* CA Trp208, thus the local region of *C. flavescens* CA shows slightly hydrophilic content.

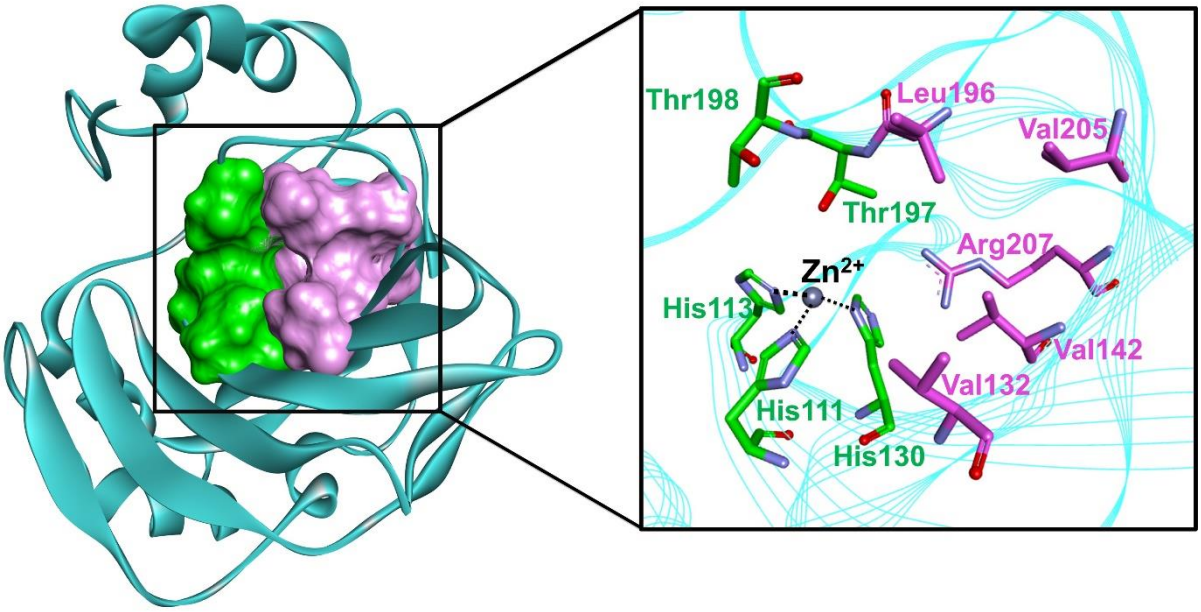

Figure 4.25: The overall structure of homology modelled of *C. flavescens* CA.

4.8 Synthesis of CANF

The outline for CANF synthesis is shown in Figure 4.26. The first step in the synthesis of hybrid nanoflowers (NFs) involves the formation of primary crystals, in which the phosphate group of the buffer binds electrostatically to the metal ions. Then, primary nanoplates were produced due to the formation of coordination bonds between the metal ions and amine groups found in the protein backbone. The formed nanoplates look like flower petals and begin to aggregate together, forming a flower-like shape [275, 276].

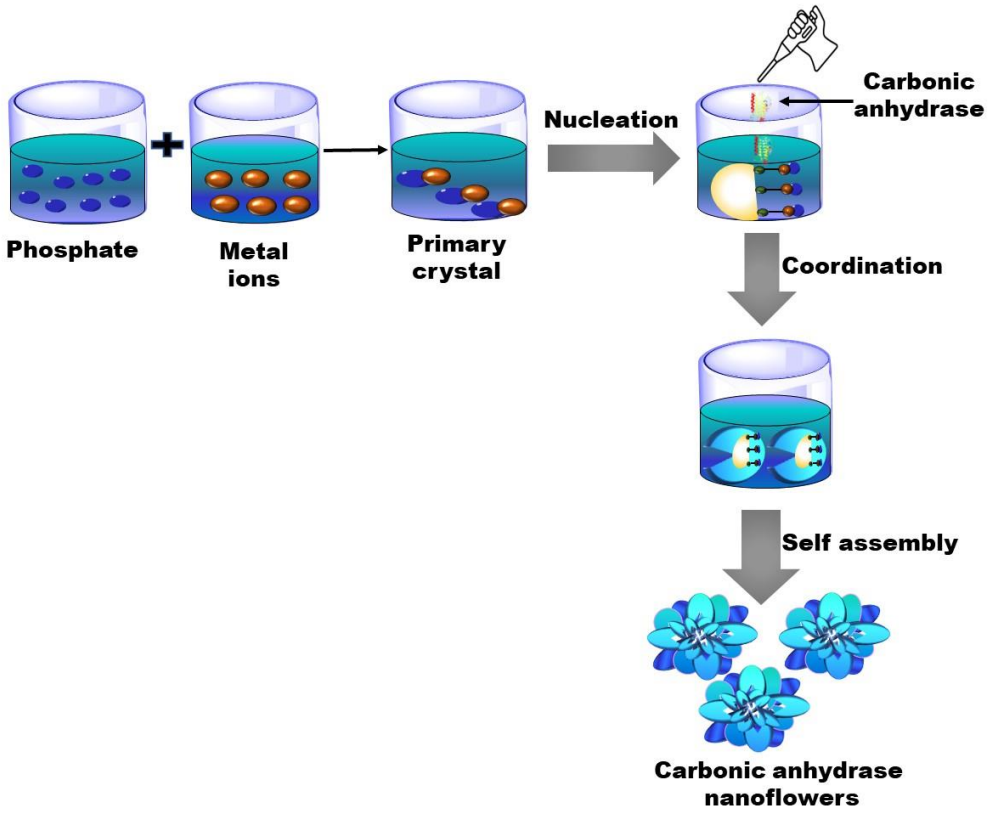

Figure 4.26: Schematic representation of various steps involves in NFs synthesis

The enzyme is the major component during hybrid NFs synthesis, and enzyme concentration plays an important role in the nucleation, growth, and activity of NFs. In addition, the enzyme serves as a "glue" to keep the metal phosphate crystals intact [275]. The purified enzyme having activity 494.4 U/mg was utilized for NFs synthesis. Thus, the protein concentration was varied, and the maximum residual activity was observed at 0.2 mg/mL of protein. Also, the highest immobilization yield (90%) was observed at 0.2 mg/mL of protein concentration. As the concentration of protein increased from 0.2 to 0.5 mg/mL, the residual activity started decreasing from 100 to 61% (Figure 4.27). Previously, the optimized protein concentration for the synthesis of xylanase hybrid NFs was found to be 0.25 mg/mL [277]. At lower protein concentrations, the higher residual activity of CANF was observed which might be due to the high surface area and favourable confirmation of the immobilized enzyme.

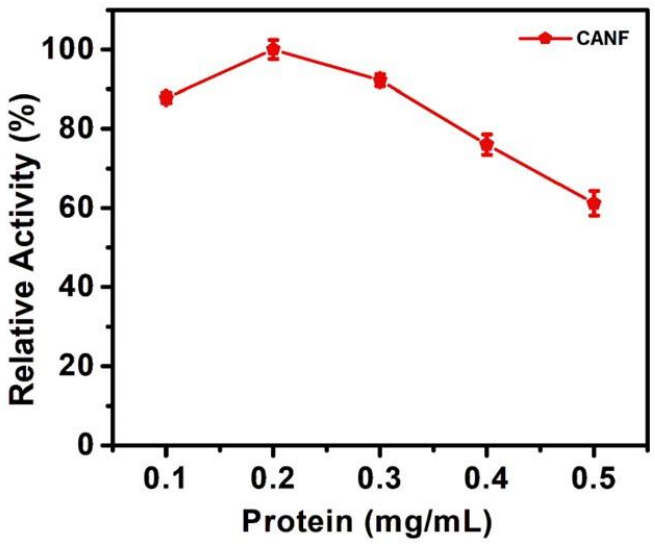

Figure 4.27: Effect of protein concentration on CANF synthesis

The various amino acid residues present in the protein structure provide different affinities for various metals. During the synthesis of NFs, metal ions are widely employed as a precursor for the nucleation of metal phosphate crystals and inorganic-organic coordination. Various enzymes, including trypsin, catalase, and lactoperoxidase, were used to synthesize copper-based NFs [276, 278]. Therefore, $CuSO_4$ concentration was varied and CANF exhibited maximal relative activity (100%) while using a 2.0 mM $CuSO_4$ concentration. Indeed, the synthesis of CANF using $CuSO_4$ (3.0 mM) showed a decline in the activity (77.8 %) (Figure 4.28). Previously, 0.8 mM was the optimum $CuSO_4$ concentration to synthesize the uniform urease hybrid NFs [279]. Coordination bond among the metal ion and enzyme functional group strengthens the structural stiffness during nanoflowers formation, limiting the extent of conformational changes and prevents the enzyme denaturation in extreme reaction conditions [280, 281].

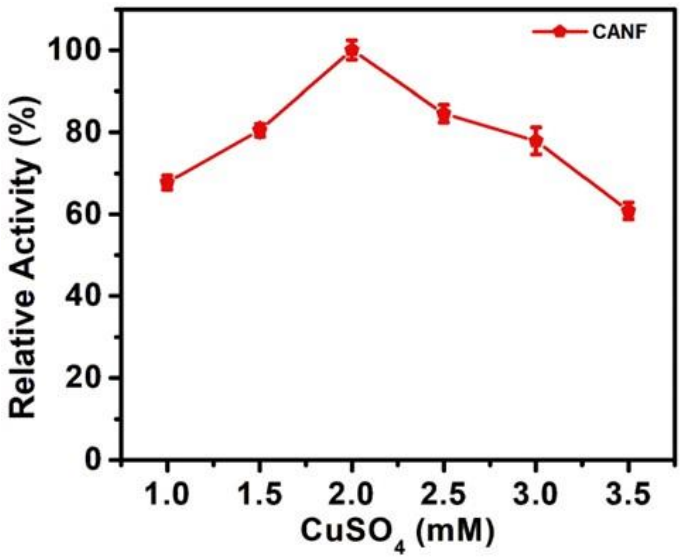

Figure 4.28: The effect of varied $CuSO_4$ concentration on CANF synthesis

4.8.2 Characterization of CANF and free CA

4.8.2.1 Temperature

Enzymes are often temperature and pH sensitive, and they become inactive when exposed outside of their ideal range. This is due to changes in enzyme structure at various pH and temperatures. Thus, the enzyme activity of CANF and free CA was measured at different temperatures (25-60°C) (Figure 4.29). The CANF showed maximum residual activity at 40°C, whereas the free enzyme exhibited maximal activity at 35°C. The free enzyme showed a relative activity of 93.37% after 35°C. The loss in CA activity at higher temperatures might be attributed to a significant change in the enzyme structure that could have limited the availability of the active sites for the substrate molecule. However, the CANF showed higher activity at 40°C, because of strong cross-linking within the nanoflowers, which prevents the CA from denaturation [282]. The CANF showed a 1.0-fold higher RA than the free CA at 40°C. Generally, the optimal enzyme activity is shifted to higher temperatures in immobilized conditions. NFs have a greater temperature optimum than their free counterparts because enzyme molecules in NFs are encapsulated inside the nano-porous structures, and prevent the thermolabile amino acids from being exposed to heat directly. In contrast, at higher temperature the free CA is exposed directly to heat shock, which causes the denaturation or a drop-in activity. Similarly, the optimal temperature for lipase NFs and free lipase was found to be 40 and 30°C, respectively [283]. In contrast, CANF and free CA exhibited the optimal temperature of 56°C [35]. The increased CANF activity could be due to the nanoflower's high surface area or the cooperative action of the encapsulated CA, which overcomes the mass transfer barrier.

CA showed variable activity profiles at various temperature ranges after immobilization by entrapment, encapsulation, and covalent binding method on bioinspired silica, silk hydrogel, and Fe_3O_4 magnetic microspheres, respectively [185, 284].

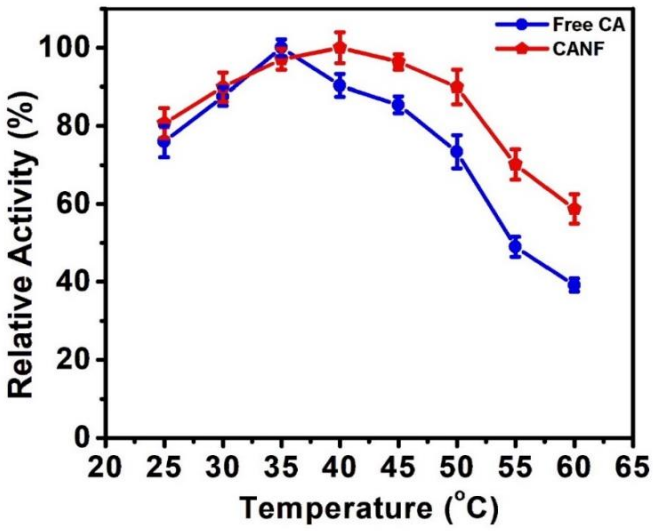

Figure 4.29: Activity profile of purified CA and CANF at different temperatures was performed in phosphate buffer (50 mM) of pH 7.0 for 10 min

4.8.2.2 Reaction pH

The effect of reaction pH on the CANF and free CA activity was also examined (Figure 4.30). The CANF and free CA exhibited similar pH optima; the highest relative activity was observed at pH 7.5. The free CA retained nearly 68% of activity at pH 5.5 and 49% at pH 9.5. Whereas, the CANF showed the relative activities of 80.20 and 65.17% at pH 5.0 and 9.5, respectively. The enzyme activity starts decreasing as the buffer pH was altered from the optimal value. Any change in pH optima may lead to the breaking of an ionic bond that destabilizes the enzyme's tertiary structure, and the enzyme begins to lose its shape and active sites. In addition, a change in pH not only alters the shape of the enzyme's active site, but it may alter the charge present on the substrate, making it impossible for the substrate to bind to the active site or prevents catalysis. At optimal pH, the enzyme maintains a perfect conformation and ionization state, which promotes optimal catalysis [285]. In the present study, pH optima for CANF and free CA are identical; that might be due to there is negligible changes in the microenvironment around the active site of CANF. In a previous study, the optimal pH of free and CA immobilized on aerogel beads were 8.0 and 8.5 [286]. Indeed, the optimal pH of free and $Zn_3(PO_4)_2$/lipase hybrid NFs was 7.6 [287]. Furthermore, Chang et al., reported that immobilized CA and free CA showed higher activity at 8.0 and 7.5 [183]. Overall, these results

showed that CANF is very efficient, retaining higher stability and activity than a purified enzyme.

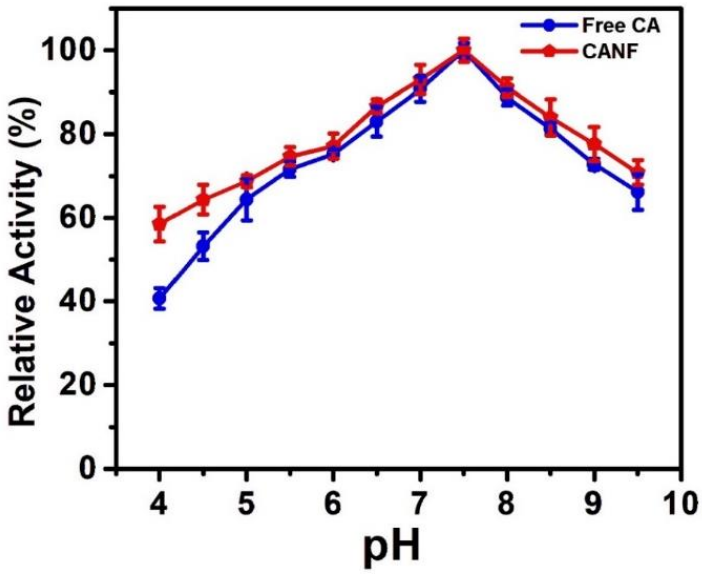

Figure 4.30: Activity profile of CANF and free CA at different pH was performed at 35 and 40°C for 10 min

Table 4.3: Various immobilized and free CA and their catalytic properties

S.no	Enzyme source	Enzyme state	Optimum temperature (°C)	Optimum pH	K_m (mM)	V_{max} µmol/min/mg)	Reference
1.	*C. flavescens*	Free	35	7.5	5.1	166.6 [a]	Present study
		Immobilized	40	7.5	4.7	185.1	
2.	Bovine erythrocyte	Free	25	7.5	7.6	1.6 [b]	[183]
		Immobilized	30	8.0	21.5	5.0	
3.	*E. coli*	Free	37	8.2	18.2	416.6[c]	[182]
		Immobilized	37	8.2	19.1	434.7	
4.	*Azadirachta indica*	Free	30	8.0	0.8	0.11	[288]
		Immobilized	40	9.0	1.0	0.08	
5.	*B. pumilis*	Free	25	7.0	1.2	1.12	[26]
		Immobilized	35	7.0	4.5	1.01	
6.	Bovine erythrocyte	Free	25	8.0	11.7	-	[170]
		Immobilized	30	8.5	11.5	-	

[a]µmol/ml/min
[b]mM/min
[c]umol/min

4.8.2.3 Reaction time

The effect of reaction time on the CANF and free CA was also studied by measuring enzyme activity at various time intervals (2-18 min). The CANF and free CA showed that 10 min of reaction time is optimum for enzyme activity assay (Figure 4.31). Furthermore, the CANF and free CA exhibited residual activity of approximately 98 and 81% after 10 min of incubation. With the subsequent increase in reaction time, enzyme activity declined due to product inhibition and enzyme denaturation. Previously, the best reaction time for CA bound to the magnetic microspheres and free CA was 3 min [289]. Indeed, the CA immobilized on the polyester and free CA were reported to have a 5 min reaction time optimum for activity assay [218].

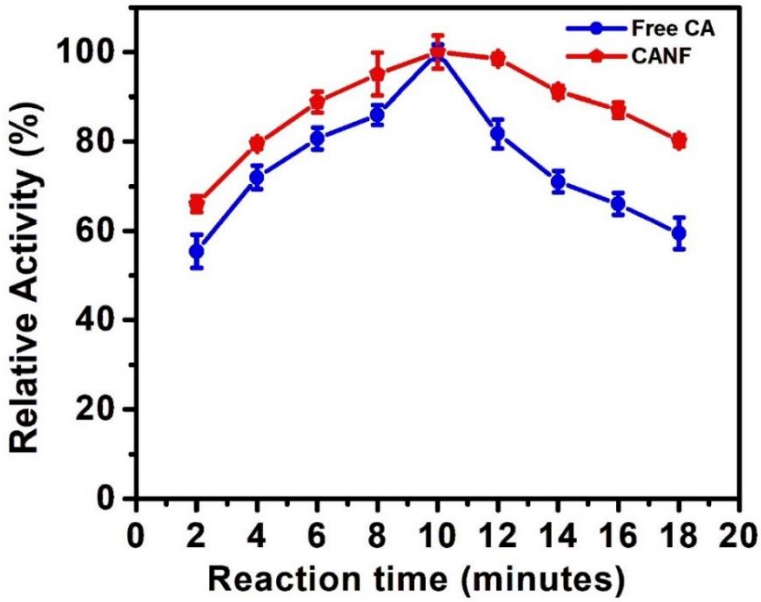

Figure 4.31: Activity profile of CANF and free CA at different reaction times was performed in phosphate buffer of pH 7.5 at 35 and 40°C

4.8.2.4 Denaturing agent

Inhibitors of enzymes have been employed to study the mechanistic and structural features of the enzymes. Thus, the effect of various denaturing agents on the CANF and free CA activity was studied (Figure 4.32). All denaturing agents showed an inhibitory effect on the CANF and free CA. In the presence of SDS, the CANF, and free CA exhibited relative activity of 25 and 16%, respectively. Whereas, the CANF and free CA exhibited relative activities of 18 and 14%, in the presence of EDTA as compared to the control. Thus, EDTA

and SDS were found to be the most effective inhibitors of the enzyme. The inhibition of enzyme activity in the presence of denaturing agents such as SDS could be attributed to the unfavorable electrostatic interactions that result in the unfolding of CA and hence its inactivation [290]. Furthermore, SDS breaks the ionic bonds, hydrophobic interactions, and hydrogen bonds, thus leading to enzyme inactivation [291]. Previously, CA purified from *P. fragi* exhibited an inhibitory effect in the presence of EDTA [225]. Furthermore, the activity of CA from *A. pallidus* was inhibited in the presence of EDTA and PMSF [142]. Indeed, the CA-immobilized ZIF-8 composite retained 93% of activity in the presence of SDS whereas free CA exhibited only 8% of relative activity [184].

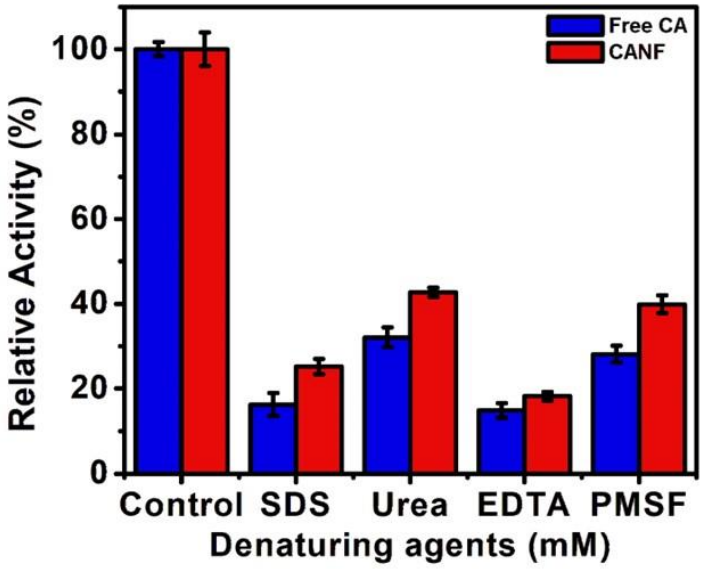

Figure 4.32: Activity of CANF and free CA in the presence of the denaturing agent was performed in phosphate buffer of pH 7.5 at 35 and 40°C

4.8.2.5 Thermo-stability

The stabilization of enzymes at high temperature is required for its practical applications [292]. Thus, the stability of CANF and free CA was also studied by incubating them at 50°C for 8 h. The thermal stability experiment showed that the CANF perform well as compared to the free enzyme at 50°C (Figure 4.33). For example, CANF still retained 51% of activity at 50°C after 4 h, while free CA lost 66% of activity under the similar conditions. The half-life was of CA and CANF was approximately 2.5 h and 4 h at 50°C. We expect that *C. flavescens* CA immobilization could further raise the thermal stability at elevated temperatures. In summary, the increase in temperature causes a sudden decline in the thermo-stability of free enzyme, but the CANF has shown relatively moderate thermal stability so far. Previously,

calcium-based CANF retained 45% of its activity at 80°C [175]. Indeed, BCA encapsulated in ZIF-8 showed a decline in 14% of its activity at 55°C, whereas the free CA lost 45% of activity [179]. The studies showed that the introduction of metal ions may slightly change the conformation of enzyme that results in enhanced stability at elevated temperature [276]. The higher thermostability of CANF is due to the presence of CA molecules inside the nano-porous structures, which results in increased enzyme rigidity.

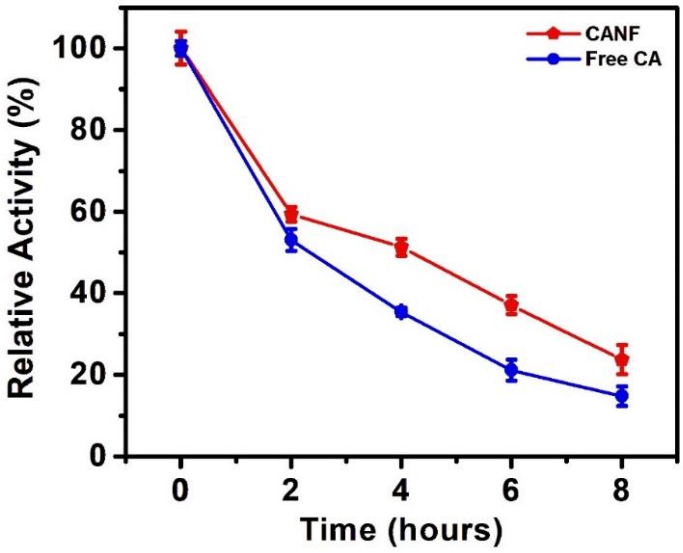

Figure 4.33: Thermal stability of purified CA and CANF at 50°C for 8 hr

4.8.2.6 Storage-stability

The storage-stability profile of CANF and free CA at 4°C (Figure 4.34). The CANF and free CA exhibited a relative activity of 74.0 and 7.4% at 4°C after 20 days of incubation, respectively. The findings revealed that low temperatures (4°C) were favourable for long time preservation of enzymes. CA storage stability and adaptability to environmental fluctuations were improved after immobilization. The CANF showed enhanced storage stability attributed to the efficient entrapment of the CA in the NFs, which restricts its leakage [218]. In a previous study, the immobilized CA on modified magnetic particles preserved a residual activity of 80% after 40 days [293]. Indeed, NADH oxidase NFs showed 72.6% relative activity after 30 days, whereas free oxidase lost complete activity [294]. Moreover, CA immobilized on a flat sheet membrane retains 82.3% of activity, while free CA loses 38% activity after 40 days of incubation [295].

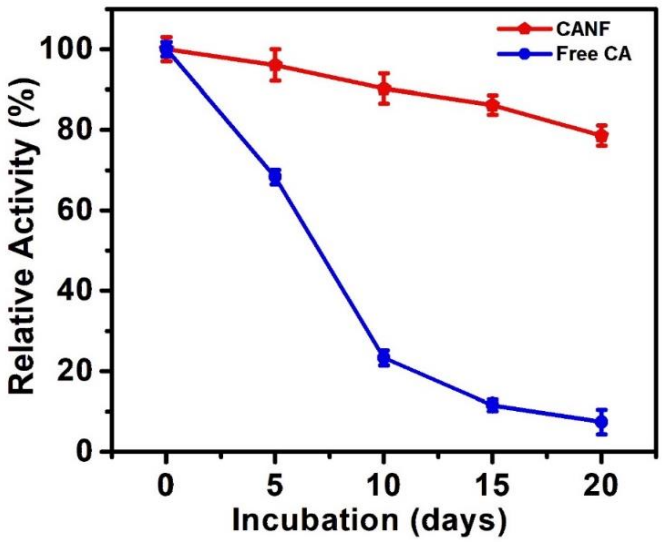

Figure 4.34: Storage stability of CANF and free CA at 4°C was measured for 20 days of incubation

4.8.2.7 Reusability

The reusability of CANF is an essential parameter to be widely used in the industry in terms of CA cost. Thus, the reusability of CANF was examined. Although CANF activity reduced significantly as the number of cycles increased, they still retained more than 80% of residual activity until 9 cycles (Figure 4.35). These results suggest that the CA were tightly entrapped in NFS after eight cycles of reuse, thus exhibiting excellent reusability. The reusability of CANF was better than that of bimetallic CANF, as they exhibited 13% of residual activity after being used for 8 cycles [35]. Subsequently, the reusability of CANF was much enhanced in comparison to lactoperoxidase NFs, having 15% relative activity after 6 cycles [296]. Moreover, the CA encapsulated in bioinspired silica maintained 87% of activity after 4 cycles of reuse [297]. The loss of CA activity after successive cycles of reuse might be related to the leaching of the enzyme and the destruction of the immobilized enzyme during washing and centrifugation [298].

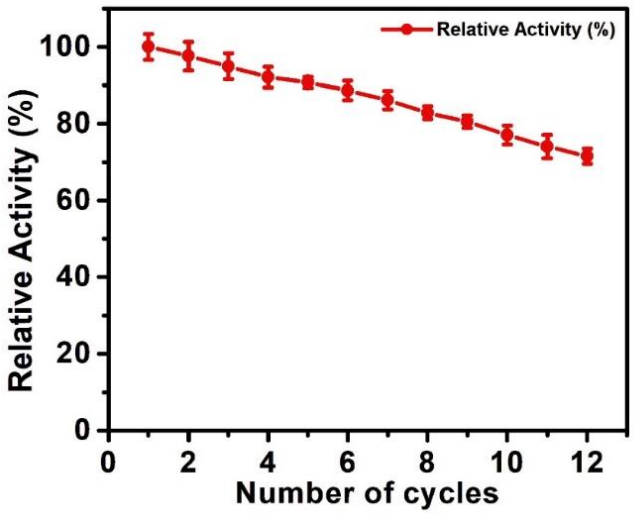

Figure 4.35: Stability of CANF during repeated cycles

4.8.2.8 Kinetic study of free CA and CANF

The kinetics of CANF and free CA were analyzed at different substrate concentrations of *p*-NPA via the Lineweaver-Burk plot [299]. The V_{max} and K_m for free CA were 5.1 mM and 166.6 µmol/mL/min, respectively, compared with 4.7 mM and 185.1 µmol/mL/min for CANF, respectively (Table 4.4). The CANF showed a lower K_m value as compared to free CA, indicating that CANF has higher accessibility for substrate, which could be attributed to the fact that a larger surface area provided by NFs or the enzyme might have reorganized itself to give a better shape. The 3-D structure of CA is important to retain its activity and during CANF synthesis the minor change in active site results in the increased availability of active sites to the substrate molecules [300]. Moreover, the decline in V_{max} during immobilization is possibly due to the interaction of CA with the functional groups on the matrices. Earlier, the K_m of calcium-based CANF and free CA was reported to be 19.23 and 30.56 µM, respectively [175]. Furthermore, the CA immobilized on the magnetic nanoparticles exhibited a significant rise in K_m value (from 0.48 mM to 1.02 mM) and a decrease in V_{max} value (from 1.53 to 0.098 µmol $min^{-1}mL^{-1}$) [301]. The K_{spec} and K_{cat} for free CA were observed to be 15.6 $M^{-1}s^{-1}$, and 80.5 s^{-1} respectively, compared with 18.9 $M^{-1}s^{-1}$ and 89.5 s^{-1} for CANF. Previously, the K_{cat} for CA immobilized on aerogel beads and free CA was reported to be 3.18 and 6.97 s^{-1}, respectively [286]. The kinetic durability of the biocatalyst might be enhanced by increasing the rigidity of flexible regions found in the active site of the biocatalyst. The active site is important in enzyme catalysis for keeping the right conformation and for engineering the enzyme's durability [302].

Developments in structural biology and bioinformatics aid in analyzing the flexibility of active site residues and identifying the important mutation sites for protein stabilization.

Table 4.4: Kinetic parameters of CANF and free CA

Carbonic anhydrase	V_{max} (µmol /mL/min)	K_m (mM)	K_{cat} (sec^{-1})	K_{spec} ($mM^{-1}s^{-1}$)
Free	166.6	5.1	80.5	15.6
CANF	185.1	4.7	89.5	18.9

4.8.3 Instrumental analysis of CANF

The FE-SEM images confirmed the CANF synthesis. The FE-SEM image showed that CANF had a flower-like morphology (Figure 4.36A-B). To determine the elemental configuration of CANF, the elemental mapping was conducted, as shown in Figure 4.36(C-I). The resulting images revealed that CANF composed of N, C, P, O, and Cu, *etc*. The elemental Cu originated from Cu^{2+} of $Cu_3(PO_4)_2$ and nitrogen derived from amino acid residues of CA.

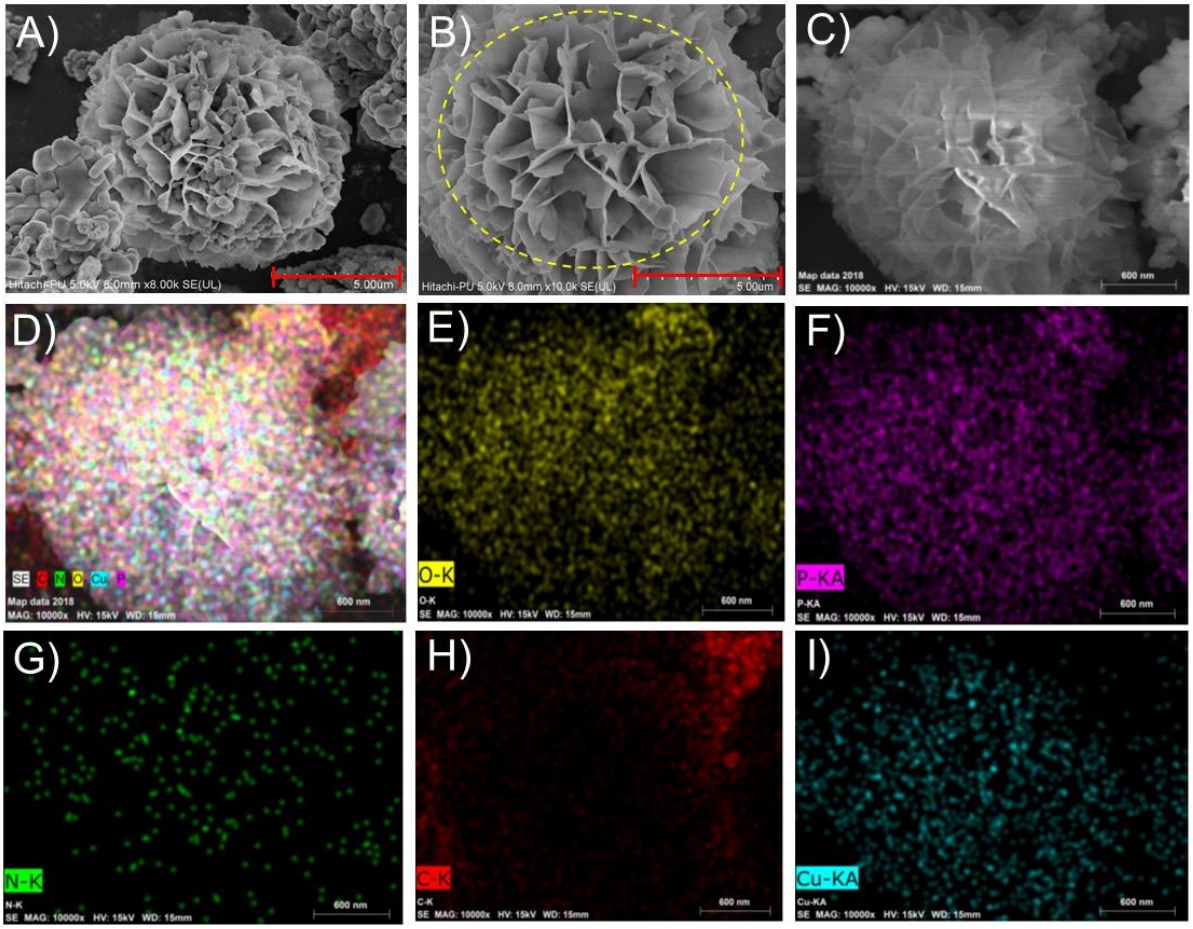

Figure 4.36: A, B) FE-SEM pictures of CANF C) area chosen for mapping D-I) Elemental mapping showing E) oxygen F) potassium G) nitrogen H) oxygen I) copper

In addition, FTIR analysis provided the chemical structure of CANF. As shown in Figure 4.37, the peaks at 1650-1680 cm^{-1} & 1020-1220 cm^{-1} are assigned to the protein stretches C=O, NH_2, and the peptide bond. The peak at 1037, 670, and 1300 cm^{-1} corresponds to P-O stretches, thus showing the presence of a phosphate group [37]. In a prior study, vibrational frequencies around 1300 cm^{-1} were due to the presence of phosphate groups [303].

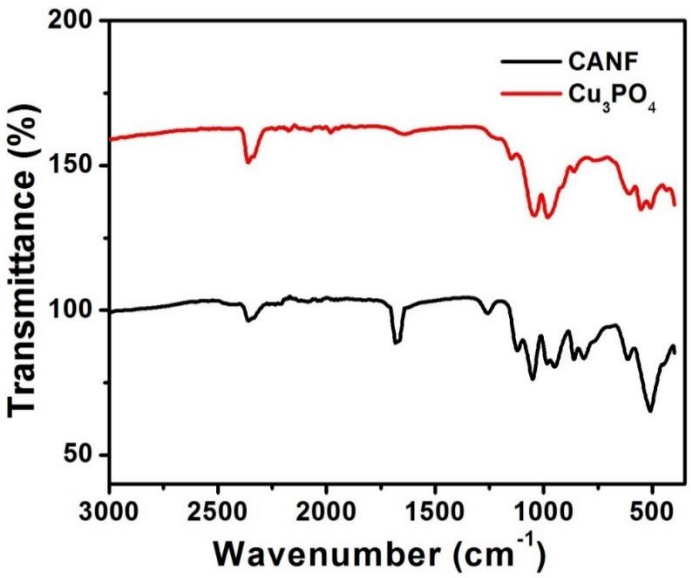

Figure 4.37: FTIR pattern of CANF, Cu_3PO_4 in the 500-3000 cm^{-1} region

4.9 Conversion of CO_2 into $CaCO_3$ using CANF and free CA

The ability of CANF and free CA to catalyze the conversion of CO_2 was determined. The results indicated that the $CaCO_3$ formation using CANF and free CA was 94.65 and 65.05 mg $CaCO_3$, respectively, under experimental conditions (Figure 4.38). CANF exhibited a 1.45-fold more yield than purified CA. The conversion of CO_2 to $CaCO_3$ was due to the involvement of CA, which catalyzes the HCO_3^- formation. The CO_2 experiment was carried out in alkaline circumstances. The CO_2 hydration enhanced the acidity, which inhibits the formation of $CaCO_3$ precipitates, if not buffered. Remarkably, the CANF showed higher CO_2 conversion efficacy than that of immobilized CA on the mesoporous aluminosilicate (10.73 mg) and CA nanoflower (76.27 mg) [175, 261].

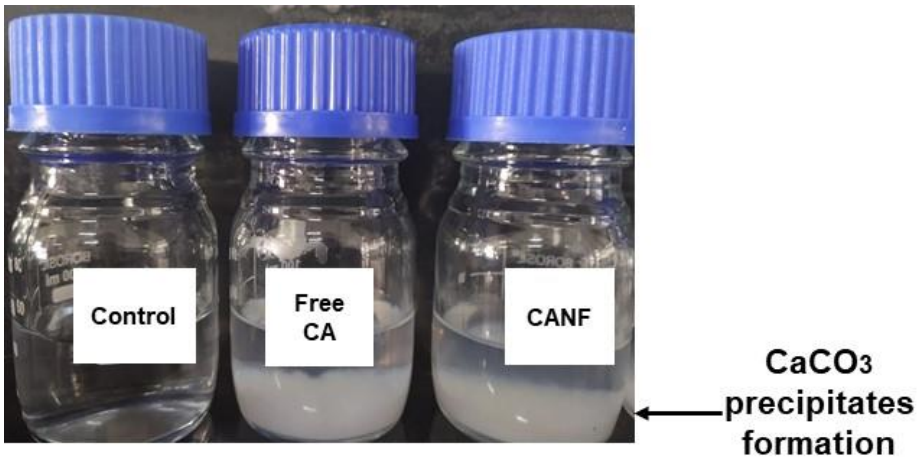

Figure 4.38: Conversion of CO_2 into $CaCO_3$ using free CA and CANF

These findings indicate that CANF has a higher CO_2 conversion capability than purified CA. $CaCO_3$ is also used in the building industry as a key element of marble and cement. And it can be also utilized as fertilizer for stabilizing the soil pH and providing calcium to plants [304].

Summary:

- The cost of the commercial CA purified from blood and bovine serum is approximately $3,000 g-1, thus to isolate CA from microbial flora of cow saliva is comparatively economic.
- The CA production was improved by the optimization of different production parameters.
- The optimum production parameters were media (nutrient broth), temperature (40°C), inoculum size (4% v/v), inoculum age (24 h), and agitation speed 120 rpm. The optimized reaction parameters were reaction pH (7.0), buffer molarity (50mM), reaction time (10 min), and temperature (35°C). All the tested organic solvents and denaturing agent inhibits the enzyme activity.
- Also, the keratin particles were used to immobilize the *C. flavescens* cells and the immobilized cells were utilized for the CO_2 conversion.
- Various parameters for cell immobilization were also optimized. The optimum glutaraldehyde concentration, optimum temperature, and incubation period were found to be 0.6 % (v/v), 25 h, and 4°C respectively.
- After 10 cycles, the production of $CaCO_3$ for immobilized cells was found to be 53.46 %.
- The FE-SEM analysis of synthesized $CaCO_3$ showed the vaterite form of the crystal. The FTIR analysis confirms the functional groups, while the XRD analysis revealed the crystalline structure of $CaCO_3$.
- The whole cells immobilization on to keratin particles proved to be effective for CO_2 conversion.
- Additionally, the CA was purified using column chromatography and exhibited a molecular mass of 29.00 kDa in SDS-PAGE. Furthermore, MALDI-TOF-MS analysis confirmed that the purified protein of *C. flavescens* was CA.
- The homology model of *C. flavescens* CA was made to predict the CA structure showing the active site region.

- Then, purified CA was used to synthesize the NFs with the self-assembly of CA and metal phosphate. The production of insoluble protein inorganic hybrid structures at the nanoscale is very beneficial for catalyzing catalytic biotransformation.
- The flower-like structure of CANF was confirmed by FE-SEM. The CANF showed 90% of immobilization yield and good catalytic activity.
- The optimal reaction temperature of free CA and CANF was 35 and 40°C, whereas the optimal pH and reaction time was 7.5 and 10 min.
- The CANF exhibited a lower K_m value (4.7 mM) as compared to free CA (5.1 mM), suggesting that CANF has higher accessibility for a substrate.
- CANF still retained 51% of activity at 50°C after 4 h, while free CA lost 66% of activity under similar conditions. The stability of CANF was improved remarkably. Furthermore, the CANF showed good reusability retained 80% of activity after 9 reuse cycle.
- The CANF exhibited 1.71-folds higher $CaCO_3$ production than free CA.
- This study proved that CANF has a promising future for converting CO_2 into $CaCO_3$.

Future prospective

- Advanced protein engineering techniques such as directed evolution can be utilized to construct the CA mutants with improved stability for industrial usage.
- In future studies, techniques for the utilization of NFs and new immobilized forms of enzymes at an industrial scale need to be explored for their effective use in CO_2 conversions.
- Overall, this work can be further explored to reduce the CO_2 level in the environment and mitigate climate change which is one of the major concerns of the 21st century.

REFERENCES

[1] Z. Zhang, S.Y. Pan, H. Li, J. Cai, A. G. Olabi, E. J. Anthony,and V. Manovic "Recent advances in carbon dioxide utilization," *Renewable Sustainable Energy Rev.,* vol. 125, pp. 109799, 2020, doi: https://doi.org/10.1016/j.rser.2020.109799.

[2] T. Sharma, S. Sharma, H. Kamyab, and A. Kumar, "Energizing the CO_2 utilization by chemo-enzymatic approaches and potentiality of carbonic anhydrases: A review," *J. Clean. Prod.*, vol. 247, pp. 119138, 2020, doi: https://doi.org/10.1016/j.jclepro.2019.119138.

[3] R. Calmanti, M. Selva, and A. Perosa, "Tungstate ionic liquids as catalysts for CO_2 fixation into epoxides," *Mol. Catal.*, vol. 486, pp. 110854, 2020, doi: https://doi.org/10.1016/j.mcat.2020.110854 .

[4] Z. Zhang, T. Wang, M. J. Blunt, E. J. Anthony, A.-H. A. Park, R. W. Hughes, *et al.*, "Advances in carbon capture, utilization and storage," *Appl. Energy.*, vol. 278, pp. 115627, 2020, doi: https://doi.org/10.1016/j.apenergy.2020.115627.

[5] M. Khalil, J. Gunlazuardi, T. A. Ivandini, and A. Umar, "Photocatalytic conversion of CO2 using earth-abundant catalysts: A review on mechanism and catalytic performance," *Renewable and Sustainable Energy Rev.*, vol. 113, pp. 109246, 2019, doi: https://doi.org/10.1016/j.rser.2019.109246.

[6] A. Kumar, T. Sharma, S. I. Mulla, H. Kamyab, D. Pant, and S. Sharma, "Let's Protect Our Earth: Environmental Challenges and Implications," in *Microbes and Enzymes in Soil Health and Bioremediation*, A. Kumar and S. Sharma, Eds., ed Singapore: Springer Singapore, 2019, pp. 1-10.

[7] C.H. Huang and C.S. Tan, "A Review: CO_2 Utilization," *Aerosol and Air Qual. Res.* vol. 14, pp. 480-499, 2014, doi: https://doi.org/10.4209/aaqr.2013.10.0326.

[8] L.J.R. Nunes, "The Rising Threat of Atmospheric CO_2: A Review on the Causes, Impacts, and Mitigation Strategies," *Environ*, vol. 10, pp. 66, 2023. doi: https://doi.org/10.3390/environments10040066.

[9] S. Jung, Y.K. Park, and E.E. Kwon, "Strategic use of biochar for CO_2 capture and sequestration," *J. CO_2 Util.*, vol. 32, pp. 128-139, 2019, doi: https://doi.org/10.1016/j.jcou.2019.04.012.

[10] L. Pastero, N. Curetti, M. A. Ortenzi, M. Schiavoni, E. Destefanis, and A. Pavese, "CO_2 capture and sequestration in stable Ca-oxalate, via Ca-ascorbate promoted green reaction," *Sci. Total Environ.*, vol. 666, pp. 1232-1244, 2019., doi:10.1016/j.scitotenv.2019.02.114.

[11] S. Talekar, B. Jo, J. Dordick, and J. Kim, "Carbonic anhydrase for CO_2 capture, conversion and utilization," *Curr. Opin. Biotechnol.*, vol. 74, pp. 230-240, 2022, doi: https://doi.org/10.1016/j.copbio.2021.12.003.

[12] J.M. Park, M. Kim, H. J. Lee, A. Jang, J. Min, and Y.H. Kim, "Enhancing the Production of Rhodobacter sphaeroides-Derived Physiologically Active Substances Using Carbonic Anhydrase-Immobilized Electrospun Nanofibers," *Biomacromolecules.*, vol. 13, pp. 3780-3786, 2012, doi: https://doi.org/10.1021/bm3012264.

[13] A. I. Osman, M. Hefny, M. I. A. Abdel Maksoud, A. M. Elgarahy, and D. W. Rooney, "Recent advances in carbon capture storage and utilisation technologies: a review," *Environ. Chem. Lett.*, vol. 19, pp. 797-849, 2021, doi: https://doi.org/10.1007/s10311-020-01133-3.

[14] S.-G. Hong, H. Jeon, H. S. Kim, S.-H. Jun, E. Jin, and J. Kim, "One-Pot Enzymatic Conversion of Carbon Dioxide and Utilization for Improved Microbial Growth," *Environ. Sci. Technol.*, vol. 49, pp. 4466-4472, 2015, doi: https://doi.org/10.1021/es505143f.

[15] J. K. Kim, C. Lee, S. W. Lim, A. Adhikari, J. T. Andring, R. McKenna, *et al.*, "Elucidating the role of metal ions in carbonic anhydrase catalysis," *Nat Commun.*, vol. 11, pp. 4557, 2020, doi: https://doi.org/10.1038/s41467-020-18425-5.

[16] T. Tekeli, S. Akocak, A. Petreni, N. Lolak, S. Çete, and C. T. Supuran, "Potent carbonic anhydrase I, II, IX and XII inhibition activity of novel primary benzenesulfonamides incorporating bis-ureido moieties," *J. Enzyme Inhib. Med. Chem.*, vol. 38, pp. 2185762, 2023, doi: 10.1080/14756366.2023.2185762.

[17] C. T. Supuran, "Anti-obesity carbonic anhydrase inhibitors: challenges and opportunities," *J. Enzyme Inhib. Med. Chem.*, vol. 37, pp. 2478-2488, 2022, doi:10.1080/14756366.2022.2121393.

[18] O. Amata, T. Marino, N. Russo, and M. Toscano, "Catalytic activity of class zinc and cadmium containing carbonic anhydrase. Compared work mechanisms," *Phys. Chem.* Chem. Phys., vol. 13 8, pp. 3468-77, 2011, doi:10.1039/c0cp01053g.

[19] N. Thakur, A. Kumar, A. Sharma, T. C. Bhalla, and D. Kumar, "Purification and characterization of alkaline, thermostable and organic solvent stable protease from a mutant of Bacillus sp," *Biocatal. Agric. Biotechnol.*, vol. 16, pp. 217-224, 2018, doi: doi: https://doi.org/10.1016/j.bcab.2018.08.005.

[20] H. Moon, S. Kim, B. H. Jo, and H. J. Cha, "Immobilization of genetically engineered whole-cell biocatalysts with periplasmic carbonic anhydrase in polyurethane foam for enzymatic CO2 capture and utilization," *J. CO_2 Util.*, vol. 39, pp. 101172, 2020, doi: doi: https://doi.org/10.1016/j.jcou.2020.101172.

[21] S. Ren, S. Jiang, X. Yan, R. Chen, and H. Cui, "Challenges and Opportunities: Porous Supports in Carbonic Anhydrase Immobilization," *J. CO_2 Util.*, vol. 42, pp. 101305, 2020, doi:https://doi.org/10.1016/j.jcou.2020.101305.

[22] J. Sun, C. Wang, Y. Wang, S. Ji, and W. Liu, "Immobilization of carbonic anhydrase on polyethylenimine/dopamine codeposited membranes," *J. Appl. Polym. Sci.*, vol. 136, pp. 47784, 2019, doi: https://doi.org/10.1002/app.47784.

[23] H. Chi, H. Chen, K. Gong, X. Wang, and Y. Zhang, "Protein-caged zinc porphyrin as a carbonic anhydrase mimic for carbon dioxide capture," *Sci. Rep.*, vol. 10, pp. 19581, 2020, doi: https://doi.org/10.1038/s41598-020-76482-8.

[24] Z. Wu, Y. Nan, Y. Zhao, X. Wang, S. Huang, and J. Shi, "Immobilization of carbonic anhydrase for facilitated CO2 capture and separation," *Chin. J. Chem. Eng.*, 2020, doi: https://doi.org/10.1016/j.cjche.2020.06.002.

[25] S. Kim, K. I. Joo, B. H. Jo, and H. J. Cha, "Stability-Controllable Self-Immobilization of Carbonic Anhydrase Fused with a Silica-Binding Tag onto Diatom Biosilica for

Enzymatic CO_2 Capture and Utilization," *ACS Appl. Mater. Interfaces.*, vol. 12, pp. 27055-27063, 2020, doi: https://doi.org/10.1021/acsami.0c03804

[26] R. R. Yadav, S. N. Mudliar, A. Y. Shekh, A. B. Fulke, S. S. Devi, K. Krishnamurthi, *et al.*, "Immobilization of carbonic anhydrase in alginate and its influence on transformation of CO_2 to calcite," *Process Biochem.*, vol. 47, pp. 585-590, 2012, doi: https://doi.org/10.1016/j.procbio.2011.12.017.

[27] Q. Liu, J. Chapman, A. Huang, K. C. Williams, A. Wagner, N. Garapati, *et al.*, "User-Tailored Metal–Organic Frameworks as Supports for Carbonic Anhydrase," *ACS Appl. Mater. Interfaces.*, vol. 10, pp. 41326-41337, 2018, doi: https://doi.org/10.1021/acsami.8b14125.

[28] C. Molina Fernandez and P. Luis Alconero, "Immobilization of carbonic anhydrase for CO_2 capture and its industrial implementation: A review," *J. CO_2 Util.*, vol. 47, pp. 101475, 2021, doi: https://doi.org/10.1016/j.jcou.2021.101475.

[29] N. Li, Q. Xia, M. Niu, Q. Ping, and H. Xiao, "Immobilizing Laccase on Different Species Wood Biochar to Remove the Chlorinated Biphenyl in Wastewater," *Sci. Rep.*, vol. 8, pp. 13947, 2018, doi: https://doi.org/10.1038/s41598-018-32013-0.

[30] R. A. Sheldon, "Enzyme Immobilization: The Quest for Optimum Performance,"*Adv. Synth. Catal.*, vol. 349, pp. 1289-1307, 2007, doi: https:/doi.org/10.1002/adsc.200700082.

[31] R. A. Sheldon and S. van Pelt, "Enzyme immobilisation in biocatalysis: why, what and how," *Chem Soc Rev*, vol. 42, pp. 6223-35, 2013, doi: 10.1039/c3cs60075k.

[32] M. Koenig, U. König, K.-J. Eichhorn, M. Müller, M. Stamm, and P. Uhlmann, "In-situ-Investigation of Enzyme Immobilization on Polymer Brushes," *Fron. chem.*, vol. 7, pp. 101-101, 2019, doi: 10.3389/fchem.2019.00101.

[33] A. Nadda, G. D. Park, S. Patel, S. kondaveeti, S. Otari, M. Anwar, *et al.*, "Unique structured SiO2 microparticles with carbon nanotube-derived mesopores as an efficient support for enzyme immobilization," *Chem. Eng. J.*, vol. 359, 2018, doi: https://doi.org/10.1016/j.cej.2018.11.052.

[34] C. Mateo, J. M. Palomo, G. Fernández-Lorente, J. Guisan, and R. Fernandez-Lafuente, "Improvement of enzyme activity, stability and selectivity via immobilization techniques," *Enzyme Microb. Technol.*, vol. 40, pp. 1451-1463, 2007, doi: https://doi.org/10.1016/j.enzmictec.2007.01.018.

[35] H. Wen, L. Zhang, Y. Du, Z. Wang, Y. Jiang, H. Bian, *et al.*, "Bimetal based inorganic-carbonic anhydrase hybrid hydrogel membrane for CO_2 capture," *J. CO_2 Util.*, vol. 39, p. 101171, 2020, doi: https://doi.org/10.1016/j.jcou.2020.101171.

[36] X. Zhang, W. Shao, B. Chen, and M. Wang, "Cross-linking of carbonic anhydrase and formate dehydrogenase based on amino acid specific recognition: Conversion of carbon dioxide to formic acid," *Enzyme Microb. Technol.*, vol. 146, p. 109763, 2021, doi: 10.1016/j.enzmictec.2021.109763.

[37] C. Ke, Y. Fan, Y. Chen, L. Xu, and Y. Yan, "A new lipase–inorganic hybrid nanoflower with enhanced enzyme activity," *RSC Advances.*, vol. 6, pp. 19413-19416, 2016, doi: https://doi.org/10.1039/C6RA01546F.

[38] S. J. Lee, H. Jang, and D. N. Lee, "Inorganic Nanoflowers-Synthetic Strategies and Physicochemical Properties for Biomedical Applications: A Review," *Pharmaceutics.*, vol. 14, 2022, doi: https://doi.org/10.3390/pharmaceutics14091887.

[39] J.M. Lalande and A. Tremblay, "Process and a plant for the production of Portland cement clinker," ed: Google Patents, 2005.

[40] A. Alonso, J. Moral-Vico, A. Abo Markeb, M. Busquets-Fité, D. Komilis, V. Puntes, *et al.*, "Critical review of existing nanomaterial adsorbents to capture carbon dioxide and methane," *Sci. Total Environ.*, vol. 595, pp. 51-62, 2017, doi: 10.1016/j.scitotenv.2017.03.229.

[41] G. Supran, S. Rahmstorf, and N. Oreskes, "Assessing ExxonMobil&2019;s global warming projections," *Science.*, vol. 379, pp. 0063, 2023, doi: 10.1126/science.abk0063.

[42] B. Goldstein, D. Gounaridis, and J. Newell, "The carbon footprint of household energy use in the United States," *Proc. Nat. Acad Sci.*, vol. 117, p. 201922205, 2020, doi: 10.1073/pnas.1922205117.

[43] M. D. Burkart, N. Hazari, C. L. Tway, and E. L. Zeitler, "Opportunities and Challenges for Catalysis in Carbon Dioxide Utilization," *ACS Catalysis.*, vol. 9, pp. 7937-7956, 2019, doi: https://doi.org/10.1021/acscatal.9b02113

[44] W. Lamb, T. Wiedmann, J. Pongratz, R. Andrew, M. Crippa, J. Olivier, *et al.*, "A review of trends and drivers of greenhouse gas emissions by sector from 1990 to 2018," *Environ. Res. Lett.*, vol. 16, 2021, doi: 10.1088/1748-9326/abee4e.

[45] H. Onyeaka, T. Miri, K. Obileke, A. Hart, C. Anumudu, and Z. T. Al-Sharify, "Minimizing carbon footprint via microalgae as a biological capture," *Carbon Capture Sci. Technol.*, vol. 1, pp. 100007, 2021, doi: https://doi.org/10.1016/j.ccst.2021.100007

[46] J. Tollefson, "COVID curbed carbon emissions in 2020 - but not by much," *Nature.*, vol. 589, pp. 343, 2021, doi: 10.1038/d41586-021-00090-3.

[47] V. Kumaravel, J. Bartlett, and S. C. Pillai, "Photoelectrochemical Conversion of Carbon Dioxide (CO_2) into Fuels and Value-Added Products," *ACS Energy Lett.*, vol. 5, pp. 486-519, 2020, doi: https://doi.org/10.1021/acsenergylett.9b02585.

[48] C. Huang, A. G. Barnett, Z. Xu, C. Chu, X. Wang, L. R. Turner, *et al.*, "Managing the health effects of temperature in response to climate change: challenges ahead," *Environ. Health Perspect.*, vol. 121, pp. 415-9, 2013, doi: 10.1289/ehp.1206025.

[49] O. C. Ekwebelem, E. S. Ofielu, O. V. N. Dike, J. C. Aleke, and G. A. Nwachukwu, "Towards Sustainable Energy: The Requisite Role of Microorganisms in the Production of Biogas and Bioethanol," *J. Energy Res.*, 2020, doi: 10.9734/jenrr/2020/v6i230164.

[50] R. Bhardwaj, T. Sharma, D. D. Nguyen, C. K. Cheng, S. S. Lam, C. Xia, *et al.*, "Integrated catalytic insights into methanol production: Sustainable framework for CO_2 conversion," *J. Environ. Manage.*, vol. 289, pp. 112468, 2021, doi: https://doi.org/10.1016/j.jenvman.2021.112468.

[51] F. Moura and J. de Abreu e Silva, "Smart Cities: Definitions, Evolution of the Concept and Examples of Initiatives," ed, pp. 1-9, 2019, doi:10.1007/978-3-319-71059-4_6-1.

[52] S. Galati, "Funding a Smart City: From Concept to Actuality," ed, 2018, pp. 17-39. doi: 10.1007/978-3-319-59381-4_2.

[53] E. Sanseverino, R. Sanseverino, V. Vaccaro, I. Macaione, and E. Anello, "Smart Cities: Case Studies," ed, 2017, pp. 47-140. doi: 10.1007/978-3-319-47361-1_3.

[54] C. Ma, "Smart city and cyber-security; technologies used, leading challenges and future recommendations," *Energy Rep.*, vol. 7, pp. 7999-8012, 2021, doi: https://doi.org/10.1016/j.egyr.2021.08.124.

[55] A. S. Syed, D. Sierra-Sosa, A. Kumar, and A. Elmaghraby, "IoT in Smart Cities: A Survey of Technologies, Practices and Challenges," *Smart Cities.*, vol. 4, pp. 429-475, 2021, doi:https://doi.org/10.3390/smartcities4020024.

[56] T. Sharma, A. Sharma, S. Sharma, A. Giri, A. Kumar, and D. Pant, "Recent developments in CO2-capture and conversion technologies," *Chemo-biological systems for CO_2 utilization*, pp. 1-14, 2020, doi: 10.1201/9780429317187-1.

[57] X. Zhou, G. Jing, B. Lv, F. Liu, and Z. Zhou, "Low-viscosity and efficient regeneration of carbon dioxide capture using a biphasic solvent regulated by 2-amino-2-methyl-1-propanol," *Appl. Energy.*, vol. 235, pp. 379-390, 2019, doi: https://doi.org/10.1016/j.apenergy.2018.10.118.

[58] P. Luis, "Use of monoethanolamine (MEA) for CO_2 capture in a global scenario: Consequences and alternatives," *Desalination.*, vol. 380, pp. 93-99, 2016, doi: https://doi.org/10.1016/j.desal.2015.08.004.

[59] L. B. Hamdy, C. Goel, J. A. Rudd, A. R. Barron, and E. Andreoli, "The application of amine-based materials for carbon capture and utilisation: an overarching view," *Materials Adv.*, vol. 2, pp. 5843-5880, 2021, doi: 10.1039/D1MA00360G.

[60] R. Wang, S. Liu, Q. Li, S. Zhang, L. Wang, and S. An, "CO_2 capture performance and mechanism of blended amine solvents regulated by N-methylcyclohexyamine," *Energy.*, vol. 215, pp. 119209, 2021, doi: https://doi.org/10.1016/j.energy.2020.119209.

[61] L. Wang, S. Yu, Q. Li, Y. Zhang, S. An, and S. Zhang, "Performance of sulfolane/DETA hybrids for CO2 absorption: Phase splitting behavior, kinetics and thermodynamics," *Appl. Energy.*, vol. 228, 2018, doi: https://doi.org/10.1016/j.apenergy.2018.06.077.

[62] R. Wang, Y. Yang, M. Wang, J. Lin, S. Zhang, S. An, *et al.*, "Energy efficient diethylenetriamine–1-propanol biphasic solvent for CO_2 capture: Experimental and theoretical study," *Appl. Energy.*, vol. 290, pp. 116768, 2021, doi: https://doi.org/10.1016/j.apenergy.2021.116768.

[63] F. Liu, Y. Shen, L. Shen, C. Sun, L. Chen, Q. Wang, *et al.*, "Novel Amino-Functionalized Ionic Liquid/Organic Solvent with Low Viscosity for CO_2 Capture," *Environ. Sci. Technol.*, vol. XXXX, 2020, doi: 10.1021/acs.est.9b06717.

[64] S. Zhang, Y. Shen, P. Shao, J. Chen, and L. Wang, "Kinetics, Thermodynamics, and Mechanism of a Novel Biphasic Solvent for CO_2 Capture from Flue Gas," *Environ. Sci. Technol.*, vol. 52, pp. 3660-3668, 2018, doi: https://doi.org/10.1021/acs.est.7b05936.

[65] W. Li, X. Zhang, B. Lu, C. Sun, S. Li, and S. Zhang, "Performance of a hybrid solvent of amino acid and ionic liquid for CO_2 capture," *Int. J. Greenh. Gas Con.*, vol. 42, pp. 400-404, 2015, doi: https://doi.org/10.1016/j.ijggc.2015.08.014,

[66] G. Jing, F. Liu, B. Lv, X. Zhou, and Z. Zhou, "Novel Ternary Absorbent: Dibutylamine Aqueous–Organic Solution for CO_2 Capture," *Energ Fuels.*, vol. 31, pp. 12530-12539, 2017, doi: 10.1021/acs.energyfuels.7b02382.

[67] X. Zhou, F. Liu, B. Lv, Z. Zhou, and G. Jing, "Evaluation of the novel biphasic solvents for CO 2 capture: Performance and mechanism," *Int. J. Greenh. Gas Con.*, vol. 60, pp. 120-128, 2017, doi: https://doi.org/10.1016/j.ijggc.2017.03.013.

[68] H. Shu and Y. Xu, "Tuning the strength of cation coordination interactions of dual functional ionic liquids for improving CO_2 capture performance," *Int. J. Greenh. Gas Con.*, vol. 94, pp. 102934, 2020, doi: https://doi.org/10.1016/j.ijggc.2019.102934.

[69] Y. E. Kim, J. H. Park, S. H. Yun, S. C. Nam, S. K. Jeong, and Y. I. Yoon, "Carbon dioxide absorption using a phase transitional alkanolamine–alcohol mixture," *J. Ind. Eng. Chem.*, vol. 20, pp. 1486-1492, 2014, doi: https://doi.org/10.1016/j.jiec.2013.07.036.

[70] H. Zhou, X. Xu, X. Chen, and G. Yu, "Novel ionic liquids phase change solvents for CO2 capture," *Int. J. Greenh. Gas Con.*, vol. 98, pp. 103068, 2020, doi: https://doi.org/10.1016/j.ijggc.2020.103068.

[71] S. Saravanamurugan, A. J. Kunov-Kruse, R. Fehrmann, and A. Riisager, "Amine-functionalized amino acid-based ionic liquids as efficient and high-capacity absorbents for CO(2)," *Chem Sus Chem.*, vol. 7, pp. 897-902, 2014, doi: 10.1002/cssc.201300691.

[72] F. Zhang, F. Cheng-Gang, Y. Wu, W. Yuan-Tao, L. Ai-Min, and Z. Zhi-Bing, "Absorption of CO2 in the aqueous solutions of functionalized ionic liquids and MDEA," *Chem. Eng. J.*, vol. 160, pp. 691-697, 2010, doi: https://doi.org/10.1016/j.cej.2010.04.013.

[73] Q. Huang, G. Jing, X. Zhou, B. Lv, and Z. Zhou, "A novel biphasic solvent of amino-functionalized ionic liquid for CO2 capture: High efficiency and regenerability," *J CO_2 Util.*, vol. 25, pp. 22-30, 2018. doi: https://doi.org/10.1016/j.jcou.2018.03.001.

[74] L. Shen, F. Liu, Y. Shen, C. Sun, Y. Zhang, Q. Wang, *et al.*, "Novel biphasic solvent of AEP/1-propanol/H2O for CO2 capture with efficient regeneration performance and low energy consumption," *Sep. Puri. Technol.*, vol. 270, pp. 118700, 2021. doi: https://doi.org/10.1016/j.seppur.2021.11870

[75] Z. Chen, G. Jing, B. Lv, and Z. Zhou, "An Efficient Solid–Liquid Biphasic Solvent for CO2 Capture: Crystalline Powder Product and Low Heat Duty," *ACS Sustainable Chem. Eng.*, vol. 8, pp. 14493-14503, 2020, doi: https://doi.org/10.1021/acssuschemeng.0c04616.

[76] C. Li, T. Zhao, A. Yang, and F. Liu, "Highly Efficient Absorption of CO_2 by Protic Ionic Liquids-Amine Blends at High Temperatures," *ACS Omega.*, vol. 6, pp. 34027-34034, 2021, doi: https://doi.org/10.1021/acsomega.1c05416.

[77] W.T. Zheng, F. Zhang, Y.T. Wu, and X.B. Hu, "Concentrated aqueous solutions of protic ionic liquids as effective CO_2 absorbents with high absorption capacities," *J. Mol. Liq.*, vol. 243, pp. 169-177, 2017, doi: https://doi.org/10.1016/j.molliq.2017.08.035.

[78] B. Dutcher, M. Fan, and A. G. Russell, "Amine-based CO_2 capture technology development from the beginning of 2013-a review," *ACS Appl. Mater. Interfaces.*, vol. 7, pp. 2137-48, 2015, doi: https://doi.org/10.1021/am507465f.

[79] L. Wang, S. Yu, Q. Li, Y. Zhang, S. An, and S. Zhang, "Performance of sulfolane/DETA hybrids for CO_2 absorption: Phase splitting behavior, kinetics and thermodynamics," *Appl. Energy.,* vol. 228, pp. 568-576, 2018, doi: https://doi.org/10.1016/j.apenergy.2018.06.077.

[80] W. Li, S. Wen, L. Shen, Y. Zhang, C. Sun, and S. Li, "Mechanism and Kinetic Study of Carbon Dioxide Absorption into a Methyldiethanolamine/1-Hydroxyethyl-3-methylimidazolium Lysine/Water System," *Energy Fuels.,* vol. 32, pp. 10813-10821, 2018, doi: https://doi.org/10.1021/acs.energyfuels.8b02612.

[81] S. Voskian, P. Brown, C. Halliday, K. Rajczykowski, and T. A. Hatton, "Amine-Based Ionic Liquid for CO_2 Capture and Electrochemical or Thermal Regeneration," *ACS Sustainable Chem. Eng.,* vol. 8, pp. 8356-8361, 2020, doi: https://doi.org/10.1021/acssuschemeng.0c02172.

[82] G. Singh, J. Lee, A. Karakoti, R. Bahadur, J. Yi, D. Zhao, *et al.*, "Emerging trends in porous materials for CO_2 capture and conversion," *Chem. Soc. Rev.,* vol. 49, pp. 4360-4404, 2020, doi: 10.1039/D0CS00075B.

[83] W. Zhang, Y. Bao, and A. Bao, "Preparation of nitrogen-doped hierarchical porous carbon materials by a template-free method and application to CO_2 capture," *J. Environ. Chem. Eng.,* vol. 8, pp. 103732, 2020, doi: https://doi.org/10.1016/j.jece.2020.103732.

[84] S. Gaikwad, S.-J. Kim, and S. Han, "Novel metal–organic framework of UTSA-16 (Zn) synthesized by a microwave method: Outstanding performance for CO_2 capture with improved stability to acid gases," *J. Ind. Eng. Chem.,* vol. 87, pp. 250-263, 2020. doi: https://doi.org/10.1016/j.jiec.2020.04.015.

[85] S. Kumar, K. Prasad, J. M. Gil, A. J. F. N. Sobral, and J. Koh, "Mesoporous zeolite-chitosan composite for enhanced capture and catalytic activity in chemical fixation of CO_2," *Carbohydr. Polym.,* vol. 198, pp. 401-406, 2018, doi: https://doi.org/10.1016/j.carbpol.2018.06.100.

[86] M. M. Zagho, M. K. Hassan, M. Khraisheh, M. A. A. Al-Maadeed, and S. Nazarenko, "A review on recent advances in CO_2 separation using zeolite and zeolite-like materials as adsorbents and fillers in mixed matrix membranes (MMMs)," *Chem. Eng. J. Adv.,* vol. 6, pp. 100091, 2021, doi: https://doi.org/10.1016/j.ceja.2021.100091.

[87] S. Kumar, M. Y. Wani, C. T. Arranja, J. d. A. e Silva, B. Avula, and A. J. F. N. Sobral, "Porphyrins as nanoreactors in the carbon dioxide capture and conversion: a review," *J. Mater. Chem.,* vol. 3, pp. 19615-19637, 2015, doi: 10.1039/C5TA05082K.

[88] D. Dedić, A. Dorniak, U. Rinner, and W. Schöfberger, "Recent Progress in (Photo-)-Electrochemical Conversion of CO_2 With Metal Porphyrinoid-Systems," *FronT Chem.,* vol. 9, 2021, doi: 10.3389/fchem.2021.685619.

[89] X. Jiang, Z. Liu, L. Ma, Y. Tao, and Y. Luo, "Facile synthesis of porous porphyrin-based polymers by solvent-crosslinking method," *New J. Chem.,* vol. 45, 2021, doi: 10.1039/D1NJ03480D.

[90] N. Vrtovec, M. Mazaj, G. Buscarino, A. Terracina, S. Agnello, I. Arčon, *et al.*, "Structural and CO2 Capture Properties of Ethylenediamine-Modified HKUST-1 Metal–Organic Framework," *Cryst. Growth Des.,* vol. 20, pp. 5455-5465, 2020, doi: https://doi.org/10.1021/acs.cgd.0c00667.

[91] L. Rao, L. Yue, L. Wang, Z. Wu, C. Ma, L. An, *et al.*, "Low-Temperature and Single-Step Synthesis of N-Doped Porous Carbons with a High CO_2 Adsorption Performance by Sodium Amide Activation," *Energy Fuels.*, vol. 32, pp. 10830-10837, 2018, doi: https://doi.org/10.1021/acs.energyfuels.8b02659.

[92] J. He, J. W. F. To, P. C. Psarras, H. Yan, T. Atkinson, R. T. Holmes, *et al.*, "Tunable Polyaniline-Based Porous Carbon with Ultrahigh Surface Area for CO2 Capture at Elevated Pressure," *Adv. Energy Mater.*, vol. 6, pp. 1502491, 2016, doi: 10.1002/aenm.201502491.

[93] L. Estevez, D. Barpaga, J. Zheng, S. Sabale, R. L. Patel, J.-G. Zhang, *et al.*, "Hierarchically Porous Carbon Materials for CO_2 Capture: The Role of Pore Structure," *Ind. Eng. Chem. Res.*, vol. 57, pp. 1262-1268, 2018, doi: https://doi.org/10.1021/acs.iecr.7b03879.

[94] H. Wei, H. Chen, N. Fu, J. Chen, G. Lan, W. Qian, *et al.*, "Excellent electrochemical properties and large CO_2 capture of nitrogen-doped activated porous carbon synthesised from waste longan shells," *Electrochimica Acta.*, vol. 231, pp. 403-411, 2017, doi: https://doi.org/10.1016/j.electacta.2017.01.194.

[95] G. Jiangfei, W. Lizhi, D. Zhang, and J. Huang, "Amino-Functionalized Porphyrin-Based Porous Organic Polymers for CO_2 Capture and Hg^{2+} Removal," *Energy Fuels.*, vol. 34, pp. 9771-9778, 2020, doi: https://doi.org/10.1021/acs.energyfuels.9b04206.

[96] F. Martinez, R. Sanz, G. Orcajo, D. Briones, and V. Yanguez, "Amino-impregnated MOF materials for CO_2 capture at post-combustion conditions," *Chem. Eng. Sci.*, vol. 142, pp. 55-61, 2016, doi: https://doi.org/10.1016/j.ces.2015.11.033.

[97] J. Park, J.-R. Li, Y.-P. Chen, J. Yu, A. A. Yakovenko, Z. U. Wang, *et al.*, "A versatile metal–organic framework for carbon dioxide capture and cooperative catalysis," *Chem. Comm.*, vol. 48, pp. 9995-9997, 2012, doi: 10.1039/c2cc34622b .

[98] P. Puthiaraj, S.-S. Kim, and W.-S. Ahn, "Covalent triazine polymers using a cyanuric chloride precursor via Friedel-Crafts reaction for CO_2 adsorption/separation," *Chem. Eng. J.*, vol. 283, pp. 184-192, 2016, doi: 10.1016/j.cej.2015.07.069.

[99] R. Kodasma, J. Fermoso, and A. Sanna, "Li-LSX-zeolite evaluation for post-combustion CO2 capture," *Chem. Eng. J.*, vol. 358, pp. 1351-1362, 2019, doi: https://doi.org/10.1016/j.cej.2018.10.063.

[100] S.-H. Hong, M.-S. Jang, S. J. Cho, and W.-S. Ahn, "Chabazite and zeolite 13X for CO2 capture under high pressure and moderate temperature conditions," *Chem. Comm.*, vol. 50, pp. 4927-4930, 2014, doi: 10.1039/c3cc46313c.

[101] J. Shi, Y. Jiang, Z. Jiang, X. Wang, X. Wang, S. Zhang, *et al.*, "Enzymatic conversion of carbon dioxide," *Chem. Soc. Rev.*, vol. 44, pp. 5981-6000, 2015, doi: 10.1039/c5cs00182j.

[102] C. Bathellier, L.-J. Yu, G. D. Farquhar, M. L. Coote, G. H. Lorimer, and G. Tcherkez, "Ribulose 1,5-bisphosphate carboxylase/oxygenase activates O2 by electron transfer," *Proc. Natl. Acad. Sci.*, vol. 117, pp. 24234-24242, 2020, doi: https://doi.org/10.1073/pnas.200882411.

[103] T. Wu, Y. Wang, C. Yu, R. Chiarawipa, X. Zhang, Z. Han, *et al.*, "Carbon sequestration by fruit trees--Chinese apple orchards as an example," *Plos one.*, vol. 7, pp. e38883-e38883, 2012, doi: https://doi.org/10.1371/journal.pone.0038883.

[104] A. N. Mistry, U. Ganta, J. Chakrabarty, and S. Dutta, "A review on biological systems for CO2 sequestration: Organisms and their pathways," *Environ. Prog. Sustain. Energy.*, vol. 38, pp. 127-136, 2019, doi: https://doi.org/10.1016/j.jksus.2020.101282.

[105] R. Ray and T. K. Jana, "Carbon sequestration by mangrove forest: One approach for managing carbon dioxide emission from coal-based power plant," *Atmos. Environ.* vol. 171, pp. 149-154, 2017, doi: http:// doi.org/10.1016/j.atmosenv.2017.10.019.

[106] S. Vizzini, E. T. Apostolaki, E. Ricevuto, P. Polymenakou, and A. Mazzola, "Plant and sediment properties in seagrass meadows from two Mediterranean CO_2 vents: Implications for carbon storage capacity of acidified oceans," *Mar. Environ. Res.,* vol. 146, pp. 101-108, 2019, doi: https://doi.org/10.1016/j.marenvres.2019.03.001.

[107] W. Evans and J. T. Mathis, "The Gulf of Alaska coastal ocean as an atmospheric CO_2 sink," *Cont. Shelf Res.,* vol. 65, pp. 52-63, 2013, doi: https://doi.org/10.1016/j.csr.2013.06.013.

[108] I. Y. López-Pacheco, L. I. Rodas-Zuluaga, S. Fuentes-Tristan, C. Castillo-Zacarías, J. E. Sosa-Hernández, D. Barceló, *et al.*, "Phycocapture of CO2 as an option to reduce greenhouse gases in cities: Carbon sinks in urban spaces," *J. CO_2 Util.*, vol. 53, pp. 101704, 2021, doi: https://doi.org/10.1016/j.jcou.2021.101704.

[109] P. Nogia, G. Sidhu, R. Mehrotra, and S. Mehrotra, "Capturing atmospheric carbon: Biological and nonbiological methods," *Int. J. Low Carbon Technol.,* vol. 11, 2013, doi: https://doi.org/10.1093/ijlct/ctt077.

[110] J. Gao and L. Wang, "Embedding spatiotemporal changes in carbon storage into urban agglomeration ecosystem management A case study of the Yangtze River Delta, China," *J. CO_2 Util.*, vol. 237, pp. 117764, 2019, doi: https://doi.org/10.1016/j.jclepro.2019.117764.

[111] C. Gerotto, A. Norici, and M. Giordano, "Toward Enhanced Fixation of CO_2 in Aquatic Biomass: Focus on Microalgae," *Front. Energy Res.,* vol. 8, 2020, doi: 10.3389/fenrg.2020.00213.

[112] D. Pavlik, Y. Zhong, C. Daiek, W. Liao, R. Morgan, W. Clary, *et al.*, "Microalgae cultivation for carbon dioxide sequestration and protein production using a high-efficiency photobioreactor system," *Algal Res.*, vol. 25, pp. 413-420, 2017, doi: https://doi.org/10.1002/jctb.6902.

[113] M. A. Kassim and T. K. Meng, "Carbon dioxide (CO2) biofixation by microalgae and its potential for biorefinery and biofuel production," *Sci. Total Environ.*, vol. 584-585, pp. 1121-1129, 2017, doi: 10.1016/j.scitotenv.2017.01.172.

[114] Z. Wang, X. Wen, Y. Xu, Y. Ding, Y. Geng, and Y. Li, "Maximizing CO_2 biofixation and lipid productivity of oleaginous microalga Graesiella sp. WBG-1 via CO_2-regulated pH in indoor and outdoor open reactors," *Sci. Total Environ.,* vol. 619-620, pp. 827-833, 2018, doi: https://doi.org/10.1016/j.scitotenv.2017.10.127.

[115] R. Sayre, "Microalgae: The Potential for Carbon Capture," *BioScience.*, vol. 60, pp. 722-727, 2010, doi: 10.1525/bio.2010.60.9.9.

[116] A. Talec, M. Philistin, F. Ferey, G. Walenta, J.-O. Irisson, O. Bernard, *et al.*, "Effect of gaseous cement industry effluents on four species of microalgae," *Bioresour. Technol.,* vol. 143, pp. 353-359, 2013, doi: 10.1016/j.biortech.2013.05.

[117] R. Obert and B. C. Dave, "Enzymatic Conversion of Carbon Dioxide to Methanol: Enhanced Methanol Production in Silica Sol−Gel Matrices," *J. Am. Chem. Soc.,* vol. 121, pp. 12192-12193, 1999, doi: https://doi.org/10.1021/ja991899r.

[118] M. Zezzi do Valle Gomes, G. Masdeu, P. Eiring, A. Kuhlemann, M. Sauer, B. Åkerman, *et al.*, "Improved biocatalytic cascade conversion of CO_2 to methanol by enzymes Co-immobilized in tailored siliceous mesostructured cellular foams," *Catal. Sci. Technol.,* vol. 11, pp. 6952-6959, 2021, doi: 10.1039/D1CY01354H.

[119] Y. Jiang, Q. Sun, L. Zhang, and Z. Jiang, "Capsules-in-bead scaffold: a rational architecture for spatially separated multienzyme cascade system," *J. Mater. Chem.,* vol. 19, pp. 9068-9074, 2009, doi: :10.1039/b914268a.

[120] L. Xu, Y. Xiu, F. Liu, Y. Liang, and S. Wang, "Research Progress in Conversion of $CO(_2)$ to Valuable Fuels," *Molecules.,* vol. 25, pp. 3653, 2020, doi: 10.3390/molecules25163653.

[121] M. A. Razzak, D. W. Lee, J. Lee, and I. Hwang, "Overexpression and Purification of Gracilariopsis chorda Carbonic Anhydrase (GcCAα3) in Nicotiana benthamiana, and Its Immobilization and Use in $CO(_2)$ Hydration Reactions," *Front Plant Sci.,* vol. 11, p. 563721, 2020, doi: 10.3389/fpls.2020.563721.

[122] S. Sundaram and I. S. Thakur, "Induction of calcite precipitation through heightened production of extracellular carbonic anhydrase by $CO(_2)$ sequestering bacteria," *Bioresour. Technol.,* vol. 253, pp. 368-371, 2018, doi: https://doi.org/10.1016/j.biortech.2018.01.081.

[123] C.-X. Li, X.-C. Jiang, Y.-J. Qiu, and J.-H. Xu, "Identification of a new thermostable and alkali-tolerant α-carbonic anhydrase from Lactobacillus delbrueckii as a biocatalyst for CO_2 biomineralization," *Bioresour. Bioprocess.,* vol. 2, p. 44, 2015, doi: https://doi.org/10.1186/s40643-015-0074-4.

[124] A. Angeli, F. Carta, and C. T. Supuran, "Carbonic Anhydrases: Versatile and Useful Biocatalysts in Chemistry and Biochemistry," *Catalysts.,* vol. 10, p. 1008, 2020, doi: https://doi.org/10.3390/catal10091008.

[125] M. Vinoba, M. Bhagiyalakshmi, S. K. Jeong, S. C. Nam, and Y. Yoon, "Carbonic Anhydrase Immobilized on Encapsulated Magnetic Nanoparticles for CO_2 Sequestration," *Chem. Eur. J.,* vol. 18, pp. 12028-12034, 2012. doi:10.1002/chem.201201112.

[126] K. S. Smith and J. G. Ferry, "Prokaryotic carbonic anhydrases," *FEMS Microbiol. Rev.,* vol. 24, pp. 335-66, 2000, doi: 10.1002/chem.201201112.

[127] C. Campestre, V. De Luca, S. Carradori, R. Grande, V. Carginale, A. Scaloni, *et al.*, "Carbonic Anhydrases: New Perspectives on Protein Functional Role and Inhibition in Helicobacter pylori," *Front. Microbiol.,* vol. 12, 2021, doi: 10.3389/fmicb.2021.629163.

[128] F. Steger, J. Reich, W. Fuchs, S. K.-M. R. Rittmann, G. M. Gübitz, D. Ribitsch, *et al.*, "Comparison of Carbonic Anhydrases for CO2 Sequestration," *Int J. Mol. Sci.,* vol. 23, p. 957, 2022, doi: 10.3390/ijms23020957.

[129] R. J. DiMario, M. C. Machingura, G. L. Waldrop, and J. V. Moroney, "The many types of carbonic anhydrases in photosynthetic organisms," *Plant Sci.,* vol. 268, pp. 11-17, 2018, doi: 10.1016/j.plantsci.2017.12.002.

[130] J. C. R. Cardoso, V. Ferreira, X. Zhang, L. Anjos, R. C. Félix, F. M. Batista, *et al.*, "Evolution and diversity of alpha-carbonic anhydrases in the mantle of the Mediterranean mussel (Mytilus galloprovincialis)," *Sci. Rep.*, vol. 9, pp. 10400, 2019, doi: 10.1038/s41598-019-46913-2.

[131] C. Campestre, V. De Luca, S. Carradori, R. Grande, V. Carginale, A. Scaloni, *et al.*, "Carbonic Anhydrases: New Perspectives on Protein Functional Role and Inhibition in Helicobacter pylori," *Front. Microbiol.*, vol. 12, 2021, doi: 10.3389/fmicb.2021.629163.

[132] A. Di Fiore, V. De Luca, E. Langella, A. Nocentini, M. Buonanno, S. Maria Monti, *et al.*, "Biochemical, structural, and computational studies of a γ-carbonic anhydrase from the pathogenic bacterium Burkholderia pseudomallei," *Comput. Struct. Biotechnol. J.*, vol. 20, pp. 4185-4194, 2022, doi: 10.1016/j.csbj.2022.07.033.

[133] E. L. Jensen, R. Clement, A. Kosta, S. C. Maberly, and B. Gontero, "A new widespread subclass of carbonic anhydrase in marine phytoplankton," *The ISME J.*, vol. 13, pp. 2094-2106, 2019, doi: 10.1038/s41396-019-0426-8.

[134] C. T. Supuran and C. Capasso, "An Overview of the Bacterial Carbonic Anhydrases," *Metabolites.*, vol. 7, pp. 56, 2017, doi: 10.3390/metabo7040056.

[135] S. Del Prete, A. Nocentini, C. T. Supuran, and C. Capasso, "Bacterial ι-carbonic anhydrase: a new active class of carbonic anhydrase identified in the genome of the Gram-negative bacterium Burkholderia territorii," *J Enzyme Inhib. Med. Chem.*, vol. 35, pp. 1060-1068, 2020, doi: 10.1080/14756366.2020.1755852.

[136] J. F. Domsic and R. McKenna, "Sequestration of carbon dioxide by the hydrophobic pocket of the carbonic anhydrases," *Biochim. Biophys. Acta.*, vol. 1804, pp. 326-31, 2010, doi: 10.1016/j.bbapap.2009.07.025.

[137] P. C. Sahoo, M. Kumar, S. K. Puri, and S. S. V. Ramakumar, "Enzyme inspired complexes for industrial CO_2 capture: Opportunities and challenges," *J. CO_2 Utiliz.*, vol. 24, pp. 419-429, 2018, doi: https://doi.org/10.1016/j.jcou.2018.02.003.

[138] S. Kondaveeti, I. M. Abu-Reesh, G. Mohanakrishna, M. Bulut, and D. Pant, "Advanced Routes of Biological and Bio-electrocatalytic Carbon Dioxide (CO_2) Mitigation Toward Carbon Neutrality," *Front. Energy Res.*, vol. 8, 2020, doi: 10.3389/fenrg.2020.00094.

[139] A. Chafik, K. el Hassani, A. Essamadi, S. Çelik, and A. Mavi, "Efficient sequestration of carbon dioxide into calcium carbonate using a novel carbonic anhydrase purified from liver of camel (Camelus dromedarius)," *J. CO_2 Utiliz.*, vol. 42, pp. 101310, 2020, doi: https://doi.org/10.1016/j.jcou.2020.101310.

[140] L. Xu, Y. Xiu, F. Liu, Y. Liang, and S. Wang, "Research Progress in Conversion of $CO(_2)$ to Valuable Fuels," *Molecules.*, vol. 25, 2020, doi: 10.3390/molecules25163653.

[141] P. Jaya, V. K. Nathan, and P. Ammini, "Characterization of marine bacterial carbonic anhydrase and their CO(2) sequestration abilities based on a soil microcosm," *Prep. Biochem. Biotechnol.*, vol. 49, pp. 891-899, 2019, doi: 10.1080/10826068.2019.1633669.

[142] H. Bose and T. Satyanarayana, "Utility of thermo-alkali-stable γ-CA from polyextremophilic bacterium Aeribacillus pallidus TSHB1 in biomimetic sequestration

of CO_2 and as a virtual peroxidase," *Environ. Sci. Pollut. Res.*, vol. 24, pp. 10869-10884, 2017, doi: 10.1007/s11356-017-8739-5.

[143] N. Maheshwari, M. Kumar, I. S. Thakur, and S. Srivastava, "Cloning, expression and characterization of β- and γ-carbonic anhydrase from Bacillus sp. SS105 for biomimetic sequestration of $CO_{(2)}$," *Int. J. Biol. Macromol.*, vol. 131, pp. 445-452, 2019, doi: 10.1016/j.ijbiomac.2019.03.082..

[144] B. Jo, J. Seo, and H. J. Cha, "Bacterial extremo-α-carbonic anhydrases from deep-sea hydrothermal vents as potential biocatalysts for CO_2 sequestration," *J. Mol. Catal. B Enz.*, vol. 109, 2014. doi: https://doi.org/10.1016/j.molcatb.2014.08.002.

[145] A. Giri, U. C. Banerjee, M. Kumar, and D. Pant, "Intracellular carbonic anhydrase from Citrobacter freundii and its role in bio-sequestration," *Bioresour. Technol.*, vol. 267, pp. 789-792, 2018, doi: 10.1016/j.biortech.2018.07.089.

[146] S. S. W. Effendi, S. I. Tan, W. W. Ting, and I. S. Ng, "Genetic design of co-expressed Mesorhizobium loti carbonic anhydrase and chaperone GroELS to enhancing carbon dioxide sequestration," *Int. J. Biol. Macromol.*, vol. 167, pp. 326-334, 2021, doi: 10.1016/j.ijbiomac.2020.11.189

[147] S. Srivastava, R. K. Bharti, P. K. Verma, and I. S. Thakur, "Cloning and expression of gamma carbonic anhydrase from Serratia sp. ISTD04 for sequestration of carbon dioxide and formation of calcite," *Bioresour. Technol.*, vol. 188, pp. 209-13, 2015, doi: 10.1016/j.biortech.2015.01.108.

[148] R. Ramanan, K. Kannan, N. Vinayagamoorthy, K. M. Ramkumar, S. D. Sivanesan, and T. Chakrabarti, "Purification and characterization of a novel plant-type carbonic anhydrase from Bacillus subtilis," *Biotechnol. Bioproc. Eng.*, vol. 14, pp. 32-37, 2009, doi: https://doi.org/10.1007/s12257-008-0099-z.

[149] S. Y. Jun, S. H. Kim, B. K. Kanth, J. Lee, and S. P. Pack, "Expression and characterization of a codon-optimized alkaline-stable carbonic anhydrase from Aliivibrio salmonicida for $CO_{(2)}$ sequestration applications," *Bioprocess Biosyst. Eng.*, vol. 40, pp. 413-421, 2017, doi: 10.1007/s00449-016-1709-3.

[150] D. Alagöz, N. E. Varan, A. Toprak, D. Yildirim, S. S. Tukel, and R. Fernandez-Lafuente, "Immobilization of xylanase on differently functionalized silica gel supports for orange juice clarification," *Process Biochem.*, vol. 113, pp. 270-280, 2022, doi: https://doi.org/10.1016/j.procbio.2021.12.027.

[151] R. Sheldon, A. Basso, and D. Brady, "New frontiers in enzyme immobilisation: robust biocatalysts for a circular bio-based economy," *Chem. Soc. Rev.*, vol. 50, 2021, doi: 10.1039/DICS00015B.

[152] E. L. Bell, W. Finnigan, S. P. France, A. P. Green, M. A. Hayes, L. J. Hepworth, *et al.*, "Biocatalysis," *Nat. Rev. Methods Primers.*, vol. 1, pp. 46, 2021, doi: https://doi.org/10.1038/s43586-021-00044-z.

[153] A. Kumar, G. Wu, Z. Wu, N. Kumar, and Z. Liu, "Improved catalytic properties of a serine hydroxymethyl transferase from Idiomarina loihiensis by site directed mutagenesis," *Int. J. Biol. Macromol.*, vol. 117, pp. 1216-1223, 2018, doi: 10.1016/j.ijbiomac.2018.05.003.

[154] V. G. Tacias-Pascacio, R. Morellon-Sterling, D. Castañeda-Valbuena, Á. Berenguer-Murcia, M. R. Kamli, O. Tavano, *et al.*, "Immobilization of papain: A review," *Int. J. Biol. Macromol.*, vol. 188, pp. 94-113, 2021, doi: 10.1016/j.ijbiomac.2021.08.016.

[155] B. H. Jo, T. Y. Park, H. J. Park, Y. J. Yeon, Y. J. Yoo, and H. J. Cha, "Engineering de novo disulfide bond in bacterial α-type carbonic anhydrase for thermostable carbon sequestration," *Sci. Rep.*, vol. 6, pp. 29322, 2016, doi: 10.1038/srep29322.

[156] R. Parra-Cruz, C. M. Jäger, P. L. Lau, R. L. Gomes, and A. Pordea, "Rational Design of Thermostable Carbonic Anhydrase Mutants Using Molecular Dynamics Simulations," *J. Phys. Chem. B.*, vol. 122, pp. 8526-8536, 2018, doi: https://doi.org/10.1021/acs.jpcb.8b05926.

[157] R. Parra-Cruz, P. L. Lau, H.-S. Loh, and A. Pordea, "Engineering of Thermovibrio ammonificans carbonic anhydrase mutants with increased thermostability," *J. CO_2 Util.*, vol. 37, pp. 1-8, 2020, doi: https://doi.org/10.1016/j.jcou.2019.11.015.

[158] B. H. Jo and I. S. Hwang, "Characterization and High-Level Periplasmic Expression of Thermostable α-Carbonic Anhydrase from Thermosulfurimonas Dismutans in Escherichia Coli for $CO_{(2)}$ Capture and Utilization," *Int. J. mol. sci.*, vol. 21, pp. 103, 2019, doi: 10.3390/ijms21010103.

[159] B. Jo, S.-K. Im, and H. J. Cha, "Halotolerant carbonic anhydrase with unusual N-terminal extension from marine Hydrogenovibrio marinus as novel biocatalyst for carbon sequestration under high-salt environments," *J. CO_2 Util.*, vol. 26, pp. 415-424, 2018, doi: https://doi.org/10.1016/j.jcou.2018.05.030.

[160] O. Alvizo, L. J. Nguyen, C. K. Savile, J. A. Bresson, S. L. Lakhapatri, E. O. Solis, *et al.*, "Directed evolution of an ultrastable carbonic anhydrase for highly efficient carbon capture from flue gas," *Proc. Natl. Acad. Sci. U S A.*, vol. 111, pp. 16436-41, 2014, doi: 10.1073/pnas.1411461111.

[161] Y. Zhang, J. Ge, and Z. Liu, "Enhanced Activity of Immobilized or Chemically Modified Enzymes," *ACS Catal.*, vol. 5, pp. 4503-4513, 2015, doi: https://doi.org/10.1021/acscatal.5b00996.

[162] J. Huang, L. Jiao, W. Xu, Q. Fang, H. Wang, X. Cai, *et al.*, "Immobilizing Enzymes on Noble Metal Hydrogel Nanozymes with Synergistically Enhanced Peroxidase Activity for Ultrasensitive Immunoassays by Cascade Signal Amplification," *ACS Appl. Mater. Interfaces.*, vol. 13, pp. 33383-33391, 2021, doi: https://doi.org/10.1021/acsami.1c09100.

[163] M.G. Sánchez-Otero, R. Quintana-Castro, A.S. Rojas-Vázquez, G.L. Badillo-Zeferino, K. Mondragón-Vázquez, G. Espinosa-Luna, *et al.*, "Polypropylene as a selective support for the immobilization of lipolytic enzymes: hyper-activation, purification and biotechnological applications," *J. Chem. Technol. Biotechnol.*, vol. 97, pp. 436-445, 2022, doi: https://doi.org/10.1002/jctb.6876.

[164] Y. R. Maghraby, R. M. El-Shabasy, A. H. Ibrahim, and H. M. E.-S. Azzazy, "Enzyme Immobilization Technologies and Industrial Applications," *ACS Omega.*, vol. 8, pp. 5184-5196, 2023, doi: https://doi.org/10.1021/acsomega.2c07560.

[165] J. Bié, B. Sepodes, P. C. B. Fernandes, and M. H. L. Ribeiro, "Enzyme Immobilization and Co-Immobilization: Main Framework, Advances and Some Applications," *Processes.*, vol. 10, pp. 494, 2022, doi: https://doi.org/10.3390/pr10030494

[166] C. Molina-Fernández and P. Luis, "Immobilization of carbonic anhydrase for CO_2 capture and its industrial implementation: A review," *J. CO_2 Util.*, vol. 47, pp. 101475, 2021, doi: https://doi.org/10.1016/j.jcou.2021.101475.

[167] T. Sharma, C. Xia, A. Sharma, P. Raizada, P. Singh, S. Sharma, *et al.*, "Mechano-chemical and biological energetics of immobilized enzymes onto functionalized polymers and their applications," *Bioengineered.*, vol. 13, pp. 10518-10539, 2022, doi: 10.1080/21655979.2022.2062526.

[168] S. Ren, C. Li, Z. Tan, Y. Hou, S. Jia, and J. Cui, "Carbonic Anhydrase@ZIF-8 Hydrogel Composite Membrane with Improved Recycling and Stability for Efficient $CO(_2)$ Capture," *J. Agric. Food Chem.*, vol. 67, pp. 3372-3379, 2019, https://doi.org/10.1021/acs.jafc.8b06182.

[169] S. S. W. Effendi, C.-Y. Chiu, Y.-K. Chang, and I. S. Ng, "Crosslinked on novel nanofibers with thermophilic carbonic anhydrase for carbon dioxide sequestration," *Int. J. Biol. Macromol.*, vol. 152, pp. 930-938, 2020, doi: 10.1016/j.ijbiomac.2019.11.234.

[170] S. I, S. Jeong, and M. Bhagiyalakshmi, "Covalent Immobilization of Carbonic Anhydrase on Amine Functionalized Alumino-Siloxane Aerogel Beads for Biomimetic Sequestration of CO_2," *J. Ind. Eng. Chem.*, vol. 100, pp. 285-295, 2021, doi: https://doi.org/10.1016/j.jiec.2021.05.010.

[171] J. Sun, C. Wang, Y. Wang, S. Ji, and W. Liu, "Immobilization of carbonic anhydrase on polyethylenimine/dopamine codeposited membranes," *J. Appl. Polym. Sci.*, vol. 2019, doi: https://doi.org/10.1002/app.47784.

[172] S. Peirce, M. E. Russo, R. Isticato, R. F. Lafuente, P. Salatino, and A. Marzocchella, "Structure and activity of magnetic cross-linked enzyme aggregates of bovine carbonic anhydrase as promoters of enzymatic CO_2 capture," *Biochem. Eng. J.*, vol. 127, pp. 188-195, 2017, doi: https://doi.org/10.1016/j.bej.2017.08.014.

[173] A. Sharma, T. Sharma, K. R. Meena, A. Kumar, and S. S. Kanwar, "High throughput synthesis of ethyl pyruvate by employing superparamagnetic iron nanoparticles-bound esterase," *Process Biochem.*, vol. 71, pp. 109-117, 2018, doi: https://doi.org/10.1016/j.procbio.2018.05.004.

[174] J. Ge, J. Lei, and R. N. Zare, "Protein–inorganic hybrid nanoflowers," *Nat. Nanotechnol.*, vol. 7, pp. 428-432, 2012, doi: 10.1038/nnano.2012.80.

[175] L. Duan, H. Li, and Y. Zhang, "Synthesis of Hybrid Nanoflower-Based Carbonic Anhydrase for Enhanced Biocatalytic Activity and Stability," *ACS Omega.*, vol. 3, pp. 18234-18241, 2018, doi: https://doi.org/10.1021/acsomega.8b02247.

[176] G. Cao, J. Gao, L. Zhou, Y. He, J. Li, and Y. Jiang, "Enrichment and Coimmobilization of Cofactors and His-Tagged ω-Transaminase into Nanoflowers: A Facile Approach to Constructing Self-Sufficient Biocatalysts," *ACS Appl. Nano Mater.*, vol. 1, pp. 3417-3425, 2018, doi: https://doi.org/10.1021/acsanm.8b00626.

[177] Z. Lin, Y. Xiao, Y. Yin, W. Hu, W. Liu, and H. Yang, "Facile Synthesis of Enzyme-Inorganic Hybrid Nanoflowers and Its Application as a Colorimetric Platform for Visual Detection of Hydrogen Peroxide and Phenol," *ACS Appl. Mater. Interfaces.*, vol. 6, pp. 10775-10782, 2014, doi: 10.1021/am502757e.

[178] B. Sun, Z. Wang, X. Wang, M. Qiu, Z. Zhang, Z. Wang, *et al.*, "Paper-based biosensor based on phenylalnine ammonia lyase hybrid nanoflowers for urinary phenylalanine

measurement," *Int. J. Biol. Macromol.*, vol. 166, pp. 601-610, 2021, doi: https://doi.org/10.1016/j.ijbiomac.2020.10.218.

[179] V. Asadi, R. Kardanpour, S. Tangestaninejad, M. Moghadam, V. Mirkhani, and I. Mohammadpoor-Baltork, "Novel bovine carbonic anhydrase encapsulated in a metal–organic framework: a new platform for biomimetic sequestration of CO_2," *RSC Advances.*, vol. 9, pp. 28460-28469, 2019, doi: 10.1039/C9RA04603H.

[180] J. Hou, G. Dong, B. Xiao, C. Malassigne, and V. Chen, "Preparation of titania based biocatalytic nanoparticles and membranes for CO_2 conversion," *J. Mater. Chem. A.*, vol. 3, pp. 3332-3342, 2015, doi: 10.1039/C4TA05760K.

[181] R. Yadav, S. T, S. Kotwal, and S. Rayalu, "Enhanced carbonation reaction using chitosan-based carbonic anhydrase nanoparticles," *Curr. Sci.*, vol. 100, pp. 520-524, 2011.

[182] M. Oviya, S. S. Giri, V. Sukumaran, and P. Natarajan, "Immobilization of carbonic anhydrase enzyme purified from Bacillus subtilis VSG-4 and its application as $CO_{(2)}$ sequesterer," *Prep. Biochem. Biotechnol.*, vol. 42, pp. 462-75, 2012, doi: 10.1080/10826068.2012.654571.

[183] S. Chang, Y. He, Y. Li, and X. Cui, "Study on the immobilization of carbonic anhydrases on geopolymer microspheres for CO_2 capture," *J. Clean. Prod.*, vol. 316, pp. 128163, 2021, doi: https://doi.org/10.1016/j.jclepro.2021.128163

[184] S. Ren, Y. Feng, H. Wen, C. Li, B. Sun, J. Cui, *et al.*, "Immobilized carbonic anhydrase on mesoporous cruciate flower-like metal organic framework for promoting $CO_{(2)}$ sequestration," *Int. J. Biol. Macromol.*, vol. 117, pp. 189-198, 2018, doi: 10.1016/j.ijbiomac.2018.05.173.

[185] C. S. Kim, Y. J. Yang, S. Y. Bahn, and H. J. Cha, "A bioinspired dual-crosslinked tough silk protein hydrogel as a protective biocatalytic matrix for carbon sequestration," *NPG Asia Mater.*, vol. 9, pp. e391-e391, 2017, doi: https://doi.org/10.1038/am.2017.71.

[186] K. M. Woo, I. Lee, S.-G. Hong, S. An, J. Lee, E. Oh, *et al.*, "Crosslinked chitosan coating on magnetic mesoporous silica with pre-adsorbed carbonic anhydrase for carbon dioxide conversion," *Chem. Eng. J.*, vol. 276, pp. 232-239, 2015, doi: https://doi.org/10.1016/j.cej.2015.04.057.

[187] S. Faridi, H. Bose, and T. Satyanarayana, "Utility of Immobilized Recombinant Carbonic Anhydrase of Bacillus halodurans TSLV1 on the Surface of Modified Iron Magnetic Nanoparticles in Carbon Sequestration," *Energy Fuels.*, vol. 31, pp. 3002-3009, 2017, doi: https://doi.org/10.1021/acs.energyfuels.6b02777.

[188] K. Maeshima and M. Yoshimoto, "Preparation and characterization of carbonic anhydrase-conjugated liposomes for catalytic synthesis of calcium carbonate particles," *Enzyme Microb. Technol.*, vol. 105, pp. 9-17, 2017, doi: 10.1016/j.enzmictec.2017.06.002.

[189] M. Vinoba, M. Bhagiyalakshmi, S. K. Jeong, Y. Yoon, II, and S. C. Nam, "Capture and Sequestration of CO2 by Human Carbonic Anhydrase Covalently Immobilized onto Amine-Functionalized SBA-15," *J. Phys. Chem.*, vol. 115, pp. 20209-20216, 2011, doi: https://doi.org/10.1021/jp204661v.

[190] M. Iijima and T. Endo, "CO2 capture technology for mitigating global warming and climate change," *Mitsubishi Heavy Industries, Ltd. Technical Review.*, vol. 47, pp. 37-45, 2010.

[191] E. Ping, M. Sakwa-Novak, and P. Eisenberger, "Global thermostat low cost direct air capture technology," in *International Conference on Negative CO_2 Emissions., Gothenburg*, pp. 22-24, 2018.

[192] M. Fasihi, O. Efimova, and C. Breyer, "Techno-economic assessment of CO_2 direct air capture plants," *J. Clean. Prod.*, vol. 224, pp. 957-980, 2019, doi:.https://doi.org/10.1016/j.jclepro.2019.03.086

[193] A. Agrawal, "Carbon Capture and Storage," *Int. J. Res. Appl. Sci. Eng. Technology.*, vol. 9, pp. 1891-1894, 2021.

[194] P. Viebahn, A. Scholz, and O. Zelt, "The Potential Role of Direct Air Capture in the German Energy Research Program-Results of a Multi-Dimensional Analysis," *Energies.*, vol. 12, pp. 3443, 2019, doi: https://doi.org/10.3390/en12183443.

[195] M. J. Regufe, A. Pereira, A. F. P. Ferreira, A. M. Ribeiro, and A. E. Rodrigues, "Current Developments of Carbon Capture Storage and/or Utilization–Looking for Net-Zero Emissions Defined in the Paris Agreement," *Energies.*, vol. 14, pp. 2406, 2021, doi: https://doi.org/10.3390/en14092406.

[196] L. Fradette, S. Lefebvre, and J. Carley, "Demonstration Results of Enzyme-Accelerated CO_2 Capture," *Energy Procedia.*, vol. 114, pp. 1100-1109, 2017, doi: https://doi.org/10.1016/j.egypro.2017.03.1263.

[197] O. Alvizo, L. J. Nguyen, C. K. Savile, J. A. Bresson, S. L. Lakhapatri, E. O. P. Solis, *et al.*, "Directed evolution of an ultrastable carbonic anhydrase for highly efficient carbon capture from flue gas," *Proc. Nat. Acad. Sci.*, vol. 111, pp. 16436-16441, 2014, doi: https://doi.org/10.1073/pnas.1411461111.

[198] J. Reardon, T. Bucholz, M. Hulvey, J. Tuttle, A. Shaffer, D. Pulvirenti, *et al.*, "Low Energy CO_2 Capture Enabled by Biocatalyst Delivery System," *Energy Procedia.*, vol. 63, 2014, doi: https://doi.org/10.1016/j.egypro.2014.11.033.

[199] S. Saito, M. Udatsu, H. Kitamura, S. Murai, Y. Kato, Y. Maezawa, *et al.*, "Development and Evaluation of a New Amine Solvent at the Mikawa CO_2 Capture Pilot Plant," *Energy Procedia.*, vol. 51, pp. 176-183, 2014, doi: https://doi.org/10.1016/j.egypro.2014.07.020.

[200] P. Madahar and J. R. Beitler. Emerging concepts in ventilation-induced lung injury. *F1000Research*., vol. 9, 2020, doi: 10.12688/f1000research.20576.1.

[201] B. T. Duy Nguyen, H. Y. Nguyen Thi, B. P. Nguyen Thi, D.-K. Kang, and J. F. Kim, "The Roles of Membrane Technology in Artificial Organs: Current Challenges and Perspectives," *Membranes.*, vol. 11, pp. 239, 2021, doi: 10.3390/membranes11040239.

[202] J. Kaar, H.-I. Oh, A. Russell, and W. Federspiel, "Towards Improved Artificial Lungs Through Biocatalysis," *Biomaterials.*, vol. 28, pp. 3131-9, 2007, doi: 10.1016/j.biomaterials.2007.03.021.

[203] J. D. Kimmel, D. T. Arazawa, S. H. Ye, V. Shankarraman, W. R. Wagner, and W. J. Federspiel, "Carbonic anhydrase immobilized on hollow fiber membranes using glutaraldehyde activated chitosan for artificial lung applications," *J. Mater. Sci. Mater. Med.*, vol. 24, pp. 2611-2621, 2013, doi:10.1007/s10856-013-5006-2.

[204] D. T. Arazawa, J. D. Kimmel, and W. J. Federspiel, "Kinetics of CO2 exchange with carbonic anhydrase immobilized on fiber membranes in artificial lungs," *J. Mater Sci Mater Med.,* vol. 26, pp. 193, 2015, doi: 10.1007/s10856-015-5525-0.

[205] C. Boone, A. Habibzadegan, S. Gill, and R. McKenna, "Carbonic Anhydrases and Their Biotechnological Applications," *Biomolecules.,* vol. 3, pp. 553-62, 2013, doi: 10.3390/biom3030553.

[206] M. Gheorghiu, "Carbonic anhydrases: hematologic relevance and a biosensing perspective," *Blood Genomics.,* vol. 4, pp. 19-30, 2020, doi: 10.46701/BG.2020012019132.

[207] S. Iraninasab, S. Sharifian, A. Homaei, M. B. Homaee, T. Sharma, A. K. Nadda, *et al.*, "Emerging trends in environmental and industrial applications of marine carbonic anhydrase: a review," *Bioprocess Biosyst. Eng.,* 2021, doi: 10.1007/s00449-021-02667-8.

[208] V. Alterio, E. Langella, G. De Simone, and S. M. Monti, "Cadmium-containing carbonic anhydrase CDCA1 in marine diatom Thalassiosira weissflogii," *Mar. drugs.,* vol. 13, pp. 1688-1697, 2015, doi: 10.3390/md13041688.

[209] R. Caricato, M. E. Giordano, T. Schettino, M. Maisano, A. Mauceri, A. Giannetto, *et al.*, "Carbonic anhydrase integrated into a multimarker approach for the detection of the stress status induced by pollution exposure in Mytilus galloprovincialis: A field case study," *Sci. Total Environ.,* vol. 690, pp. 140-150, 2019, https://doi.org/10.1016/j.scitotenv.2019.06.446.

[210] S. Bagchi, S. Sengupta, and S. Mandal, "Development and Characterization of Carbonic Anhydrase-Based CO2 Biosensor for Primary Diagnosis of Respiratory Health," *IEEE Sensors Journal.,* vol.9, pp. 1-1, 2017, doi: 10.1109/JSEN.2017.2649686.

[211] A. Angeli, F. Carta, A. Nocentini, J. Y. Winum, R. Zalubovskis, A. Akdemir, *et al.*, "Carbonic Anhydrase Inhibitors Targeting Metabolism and Tumor Microenvironment," *Metabolites.,* vol. 10, 2020, doi: https://doi.org/10.3390/metabo10100412.

[212] C. T. Supuran, "Carbonic anhydrases: novel therapeutic applications for inhibitors and activators," *Nat. Rev. Drug Discov.,* vol. 7, pp. 168-181, 2008, doi: 10.1038/nrd2467.

[213] C. T. Supuran, "Multitargeting approaches involving carbonic anhydrase inhibitors: hybrid drugs against a variety of disorders," *J. Enzyme Inhib. Med. Chem.,* vol. 36, pp. 1702-1714, 2021, doi:10.1080/14756366.2021.1945049.

[214] B.-H. Jonsson and A. Liljas, "Perspectives on the Classical Enzyme Carbonic Anhydrase and the Search for Inhibitors," *Biophys. J.,* vol. 119, pp. 1275-1280, 2020, doi: 10.1016/j.bpj.2020.08.020.

[215] C. T. Supuran and C. Capasso, "Antibacterial carbonic anhydrase inhibitors: an update on the recent literature," *Expert Opin. Ther. Pat.,* vol. 30, pp. 963-982, 2020, doi: 10.1080/13543776.2020.1811853

[216] T. Nishita, J. Yatsu, M. Murakami, S. Kamoshida, K. Orito, N. Ichihara, *et al.*, "Isolation and sequencing of swine carbonic anhydrase VI, an enzyme expressed in the swine kidney," *BMC Res. Notes.,* vol. 7, pp. 116, 2014, doi: https://doi.org/10.1186/1756-0500-7-116.

[217] R. Ramanan, K. Kannan, S. D. Sivanesan, S. Mudliar, S. Kaur, A. K. Tripathi, *et al.*, "Bio-sequestration of carbon dioxide using carbonic anhydrase enzyme purified from Citrobacter freundii," *World J. Microbiol. Biotechnol.*, vol. 25, pp. 981-987, 2009, doi: 10.1007/s11274-009-9975-8.

[218] J. Li, X. Zhou, L. Zhang, H. Di, H. Wu, and L. Yang, "Investigation on the Immobilization of Carbonic Anhydrase and the Catalytic Absorption of Carbon Dioxide," *Energ. Fuels.*, vol. 31, pp. 778-784, 2017, doi: https://doi.org/10.1021/acs.energyfuels.6b02652 .

[219] M. M. Bradford, "A rapid and sensitive method for the quantitation of microgram quantities of protein utilizing the principle of protein-dye binding," *Anal. Biochem,*, vol. 72, pp. 248-54, 1976, doi: 10.1006/abio.1976.9999.

[220] K. Meena, A. Sharma, R. Kumar, and S. Kanwar, "Two factor at a time approach by response surface methodology to aggrandize the Bacillus subtilis KLP2015 surfactin lipopeptide to use as antifungal agent," *J. King Saud Univ. Sci.*, vol. 32, 2018, doi: .https://doi.org/10.1016/j.jksus.2018.05.025.

[221] D. K. Verma, G. Vasudeva, C. Sidhu, A. K. Pinnaka, S. E. Prasad, and K. G. Thakur, "Biochemical and Taxonomic Characterization of Novel Haloarchaeal Strains and Purification of the Recombinant Halotolerant α-Amylase Discovered in the Isolate," *Front Microbiol.,* vol. 11, pp. 2082, 2020, doi: 10.3389/fmicb.2020.02082.

[222] A. Sharma, K. R. Meena, and S. S. Kanwar, "Molecular characterization and bioinformatics studies of a lipase from Bacillus thermoamylovorans BHK67," *Int. J. Biol. Macromol.*, vol. 107, pp. 2131-2140, 2018, doi:10.1016/j.ijbiomac.2017.10.092.

[223] M. Gupta, S. Aggarwal, N. K. Navani, and B. Choudhury, "Isolation and characterization of a protease-producing novel haloalkaliphilic bacterium Halobiforma sp. strain BNMIITR from Sambhar lake in Rajasthan, India," *Ann. Microbiol.*, vol. 65, pp. 677-686, 2015, doi: https://doi.org/10.1007/s13213-014-0906-z.

[224] N. Srivastava, S. Kumari, S. Kurmi, A. K. Pinnaka, and A. R. Choudhury, "Isolation, purification, and characterization of a novel exopolysaccharide isolated from marine bacteria Brevibacillus borstelensis M42," *Arch. Microbiol.*, vol. 204, p. 399, 2022, doi: 10.1007/s00203-022-02993-9.

[225] A. Sharma, A. Bhattacharya, and S. Singh, "Purification and characterization of an extracellular carbonic anhydrase from Pseudomonas fragi," *Process Biochem.*, vol. 44, pp. 1293-1297, 2009, doi: https://doi.org/10.1016/j.procbio.2009.07.022.

[226] Y. Zhu, "Immobilized Cell Fermentation for Production of Chemicals and Fuels," *Bioprocessing for Value-Added Products from Renewable Resources,* pp. 373-396, 2007, doi: 10.1016/B978-044452114-9/50015-3.

[227] S. K. S. Patel, R. K. Singh, A. Kumar, J. H. Jeong, S. H. Jeong, V. C. Kalia, *et al.*, "Biological methanol production by immobilized Methylocella tundrae using simulated biohythane as a feed," *Bioresour. Technol.*, vol. 241, pp. 922-927, 2017, doi: https://doi.org/10.1016/j.biortech.2017.05.160.

[228] S. Sharma, A. Gupta, S. M. S. T. Chik, C. G. Kee, B. M. Mistry, D. H. Kim, *et al.*, "Characterization of keratin microparticles from feather biomass with potent antioxidant and anticancer activities," *Int. J. Biol. Macromol.*, vol. 104, pp. 189-196, 2017, doi: 10.1016/j.ijbiomac.2017.06.015.

[229] S. K. S. Patel, M. S. Jeon, R. K. Gupta, Y. Jeon, V. C. Kalia, S. C. Kim, *et al.*, "Hierarchical Macroporous Particles for Efficient Whole-Cell Immobilization: Application in Bioconversion of Greenhouse Gases to Methanol," *ACS Appl. Mater. Interfaces.*, vol. 11, pp. 18968-18977, 2019, doi: 10.1021/acsami.9b03420.

[230] S. Dutt, A. Balasubrahmanyam, and M. L. Lodha, "Purification and Partial Characterization of Antiviral Proteins from Chenopodium album L. Leaves," *J. Plant Physiol.*, vol. 156, pp. 808-810, 2000, doi: https://doi.org/10.1016/S0176-1617(00)80253-9.

[231] U. K. Laemmli, "Cleavage of Structural Proteins during the Assembly of the Head of Bacteriophage T4," *Nature.*, vol. 227, pp. 680-685, 1970, doi:10.1038/227680a0.

[232] P. S. Juvale, R. L. Wagner, and M. H. Spalding, "Opportunistic proteolytic processing of carbonic anhydrase 1 from Chlamydomonas in Arabidopsis reveals a novel route for protein maturation," *J. Exp. Bot.*, vol. 67, pp. 2339-2351, 2016, doi:10.1093/jxb/erw044.

[233] D. Eramian, N. Eswar, M.-Y. Shen, and A. Sali, "How well can the accuracy of comparative protein structure models be predicted?," *Protein science : a publication of the Protein Society.*, vol. 17, pp. 1881-1893, 2008, doi: 10.1110/ps.036061.108.

[234] M. Wiederstein and M. J. Sippl, "ProSA-web: interactive web service for the recognition of errors in three-dimensional structures of proteins," *Nucleic Acids Res.*, vol. 35, pp. W407-10, 2007, doi: https://doi.org/10.1093/nar/gkm290.

[235] S. Kumar, S. Darnal, V. Patial, V. Kumar, V. Kumar, S. Kumar, *et al.*, "Molecular cloning, characterization, and in-silico analysis of l-asparaginase from Himalayan Pseudomonas sp. PCH44," *3 Biotech.*, vol. 12, pp. 162, 2022, doi: 10.1007/s13205-022-03224-0. Epub 2022 Jul 9.

[236] J. Cui, Y. Zhao, R. Liu, C. Zhong, and S. Jia, "Surfactant-activated lipase hybrid nanoflowers with enhanced enzymatic performance," *Sci. Rep.*, vol. 6, pp. 27928, 2016, doi: 10.1038/srep27928.

[237] A. Singh and S. Yadav, "Immobilization of L-ribose isomerase on the surface of activated mesoporous MCM41 and SBA15 for the synthesis of L-ribose," *J. Biotechnol.*, vol. 362, 2022, doi: 10.1016/j.jbiotec.2022.12.010. Epub 2022 Dec 30.

[238] E. Kupriyanova, A. Villarejo, A. Markelova, L. Gerasimenko, G. Zavarzin, G. Samuelsson, *et al.*, "Extracellular carbonic anhydrases of the stromatolite-forming cyanobacterium Microcoleus chthonoplastes," *Microbiology.*, vol. 153, pp. 1149-1156, 2007, doi:10.1099/mic.0.2006/003905-0.

[239] M. Li, X. Zhu, S. Wilkinson, M. Huang, and V. Achal, "Complete Genome Sequence of Carbonic Anhydrase Producing Psychrobacter sp. SHUES1," *Front Microbiol.*, vol. 7, pp. 1442, 2016, doi:10.3389/fmicb.2016.01442.

[240] R. Ramanan, K. Kannan, S. d. Sivanesan, S. Mudliar, S. Kaur, A. Tripathi, *et al.*, "Bio-sequestration of carbon dioxide using carbonic anhydrase enzyme purified from Citrobacter freundii," *World J. Microbiol. Biotechnol.*, vol. 25, pp. 981-987, 2009, doi: 10.1007/s11274-009-9975-8.

[241] D. Deka, S. P. Das, N. Sahoo, D. Das, M. Jawed, D. Goyal, *et al.*, "Enhanced Cellulase Production from Bacillus subtilis by Optimizing Physical Parameters for Bioethanol Production," *ISRN Biotechnol.*, vol. 2013, pp. 965310, 2013, doi: https://doi.org/10.5402/2013/965310.

[242] K. S. Smith and J. G. Ferry, "A plant-type (beta-class) carbonic anhydrase in the thermophilic methanoarchaeon Methanobacterium thermoautotrophicum," *J. Bacteriol.*, vol. 181, pp. 6247-6253, 1999, doi: 10.1128/jb.181.20.6247-6253.1999.

[243] Z. Zhang, B. Lian, W. Hou, M. Chen, X. Li, W. Shen, *et al.*, "Optimization of nutritional constituents for carbonic anhydrase production by Bacillus mucilaginosus K02," *Afr. J. Biotechnol.*, vol. 10, pp. 8403-8413, 2011, doi: 10.5897/AJB10.1508.

[244] A. L. Kamble, V. S. Meena, and U. C. Banerjee, "Effect of agitation and aeration on the production of nitrile hydratase by Rhodococcus erythropolis MTCC 1526 in a stirred tank reactor," *Lett. Appl. Microbiol.*, vol. 51, pp. 413-420, 2010, doi: 10.1111/j.1472-765X.2010.02909.x.

[245] H. Bose and T. Satyanarayana, "Suitability of the alkalistable carbonic anhydrase from a polyextremophilic bacterium Aeribacillus pallidus TSHB1 in biomimetic carbon sequestration," *Bioprocess. Biosyst. Eng.*, vol. 39, pp. 1515-25, 2016, doi: 10.1007/s00449-016-1627-4.

[246] A. Srivastava, L. K. Dangi, S. Kumar, and R. Rani, "Microbial decolorization of Reactive Black 5 dye by Bacillus albus DD1 isolated from textile water effluent: kinetic, thermodynamics & decolorization mechanism," *Heliyon.*, vol. 8, pp. e08834, 2022, doi: 10.1016/j.heliyon.2022.e08834.

[247] L. Banoth, K. Devarapalli, I. Paul, K. N. Thete, S. V. Pawar, and U. Chand Banerjee, "Screening, isolation and selection of a potent lipase producing microorganism and its use in the kinetic resolution of drug intermediates," *J. Indian Chem. Soc.*, vol. 98, pp. 100143, 2021, doi:10.1016/j.jics.2021.100143.

[248] P. K. Robinson, "Enzymes: principles and biotechnological applications," *Essays Biochem.*, vol. 59, pp. 1-41, 2015, doi:10.1042/bse0590001.

[249] L. C. Chirica, B. Elleby, and S. Lindskog, "Cloning, expression and some properties of alpha-carbonic anhydrase from Helicobacter pylori," *Biochim. Biophys. Acta.*, vol. 1544, pp. 55-63, 2001, doi:10.1016/s0167-4838(00)00204-1.

[250] R. Perfetto, S. Del Prete, D. Vullo, G. Sansone, C. Barone, M. Rossi, *et al.*, "Biochemical characterization of the native α-carbonic anhydrase purified from the mantle of the Mediterranean mussel, Mytilus galloprovincialis," *J. Enzyme Inhib. Med. Chem.*, vol. 32, pp. 632-639, 2017, doi:10.1080/14756366.2017.1284069.

[251] R. Bhatia, K. R, R. Rathour, K. V, S. V, R. N, *et al.*, "Enhancement of Cellulose Degradation Potential of Bacillus sp. Hcb-21 through Mutagenesis," *J. Microb. Biochem. Technol.*, vol. 09, 2017, doi:10.4172/1948-5948.1000374.

[252] U. M. Kocyigit, P. Taslimi, and I. Gulcin, "Characterization and inhibition effects of some metal ions on carbonic anhydrase enzyme from Kangal Akkaraman sheep," *J. Biochem. Mol. Toxicol.*, vol. 32, pp. e22172, 2018, doi:10.1002/jbt.22172.

[253] C. Caglayan, P. Taslimi, C. Türk, F. M. Kandemir, Y. Demir, and İ. Gulcin, "Purification and characterization of the carbonic anhydrase enzyme from horse mackerel (Trachurus trachurus) muscle and the impact of some metal ions and pesticides on enzyme activity," *Comp. Biochem. Physiol. C Toxicol. Pharmacol.*, vol. 226, pp. 108605, 2019, doi: 10.1016/j.cbpc.2019.108605.

[254] S. Kumar and P. A. Deshpande, "Structural and thermodynamic analysis of factors governing the stability and thermal folding/unfolding of SazCA," *PLoS One*, vol. 16, pp. e0249866, 2021.doi: https://doi.org/10.1371/journal.pone.0249866.

[255] M. J. Tamás, S. K. Sharma, S. Ibstedt, T. Jacobson, and P. Christen, "Heavy metals and metalloids as a cause for protein misfolding and aggregation," *Biomolecules.*, vol. 4, pp. 252-67, 2014, doi:10.3390/biom4010252.

[256] S. B. Ceyhun, M. Sentürk, E. Yerlikaya, O. Erdoğan, O. Küfrevioğlu, and D. Ekinci, "Purification and characterization of carbonic anhydrase from the teleost fish Dicentrarchus labrax (European seabass) liver and toxicological effects of metals on enzyme activity," *Environ. Toxicol. Pharmacol.*, vol. 32, pp. 69-74, 2011, doi:10.1016/j.etap.2011.03.013.

[257] T. Abdulkadir Coban, S. Beydemir, I. Gulcin, and D. Ekinci, "The effect of ethanol on erythrocyte carbonic anhydrase isoenzymes activity: An in vitro and in vivo study, "*J. Enzyme Inhib. Med. Chem.*, vol. 23, pp. 266-270, 2008, doi: 10.1080/14756360701474780.

[258] A. Kumar, K. Dhar, S. S. Kanwar, and P. K. Arora, "Lipase catalysis in organic solvents: advantages and applications," *Biol. Proced Online.*, vol. 18, pp. 2, 2016, doi: 10.1186/s12575-016-0033-2.

[259] R. Sinha and S. K. Khare, "Protective role of salt in catalysis and maintaining structure of halophilic proteins against denaturation," *Front Microbiol.*, vol. 5, pp. 165-165, 2014, doi: 10.3389/fmicb.2014.00165.

[260] H. Hou, H. He, and Y. Wang, "Effects of SDS on the activity and conformation of protein tyrosine phosphatase from thermus thermophilus HB27," *Sci. Rep.*, vol. 10, pp. 3195, 2020, doi: 10.1038/s41598-020-60263-4.

[261] S. Wanjari, D. C. Prabhu, R. Yadav, T. Satyanarayana, N. Labhsetwar, and S. Rayalu, "Immobilization of carbonic anhydrase on chitosan beads for enhanced carbonation reaction," *Process Biochem.*, vol. 46, pp. 1010-1018, 2011, doi: 10.1016/j.procbio.2011.01.023.

[262] E. Ono and J. L. Cuello, "Carbon Dioxide Mitigation using Thermophilic Cyanobacteria," *Biosyst. Eng.*, vol. 96, pp. 129-134, 2007, doi:10.1016/j.biosystemseng.2006.09.010.

[263] N. Yoshida, E. Higashimura, and Y. Saeki, "Catalytic biomineralization of fluorescent calcite by the thermophilic bacterium Geobacillus thermoglucosidasius," *Appl Environ. Microbiol.*, vol. 76, pp. 7322-7, 2010, doi:10.1128/AEM.01767-10.

[264] L. Dal Magro, J. F. Kornecki, M. P. Klein, R. C. Rodrigues, and R. Fernandez-Lafuente, "Pectin lyase immobilization using the glutaraldehyde chemistry increases the enzyme operation range," *Enzyme Microb. Technol.*, vol. 132, pp. 109397, 2020, doi: https://doi.org/10.1016/j.enzmictec.2019.109397.

[265] M. R. Bagherinejad, H. Korbekandi, N. Tavakoli, and D. Abedi, "Immobilization of penicillin G acylase using permeabilized Escherichia coli whole cells within chitosan beads," *Res. Pharm. Sci.*, vol. 7, pp. 79-85. 2012.

[266] Y. W. Zhang, P. Prabhu, J. K. Lee, and I. W. Kim, "Enhanced stability of Bacillus licheniformis L-arabinose isomerase by immobilization with alginate," *Prep. Biochem. Biotechnol.*, vol. 40, pp. 65-75, 2010, doi: 10.1080/10826060903400567.

[267] S. K. S. Patel, V. C. Kalia, J. B. Joo, Y. C. Kang, and J.-K. Lee, "Biotransformation of methane into methanol by methanotrophs immobilized on coconut coir," *Bioresour. Technol.*, vol. 297, pp. 122433, 2020, doi:10.1016/j.biortech.2019.122433.

[268] J. Wang, Y. Hu, C. Qiu, H. Fan, Y. Yue, A. Jiao, *et al.*, "Immobilized Cells of Bacillus circulans ATCC 21783 on Palm Curtain for Fermentation in 5 L Fermentation Tanks," *Molecules.*, vol. 23, 2018, doi:10.3390/molecules23112888.

[269] K. Adinarayana, B. Jyothi, and P. Ellaiah, "Production of alkaline protease with immobilized cells of Bacillus subtilis PE-11 in various matrices by entrapment technique," *AAPS Pharm. Sci. Tech.*, vol. 6, pp. E391-7, 2005, doi:10.1208/pt060348.

[270] G. S. Kocher and S. Mishra, "Immobilization of Bacillus circulans MTCC 7906 for enhanced production of alkaline protease under batch and packed bed fermentation conditions," *Int. J. microbiol.*, vol. 7, 2008, doi:10.5580/2599.

[271] H. Bose and T. Satyanarayana, "Microbial Carbonic Anhydrases in Biomimetic Carbon Sequestration for Mitigating Global Warming: Prospects and Perspectives," *Front. Microbiol.*, vol. 8, 2017, doi: https://doi.org/10.3389/fmicb.2017.01615.

[272] J. Heuer, Y. Kraus, M. Vučak, and A.-P. Zeng, "Enhanced sequestration of carbon dioxide into calcium carbonate using pressure and a carbonic anhydrase from alkaliphilic Coleofasciculus chthonoplastes," *Eng. Life Sci.*, vol. 22, pp. 178-191, 2022, doi: https://doi.org/10.1002/elsc.202100033.

[273] Y. Demir, N. Demir, H. Nadaroglu, and E. Bakan, "Purification and characterization of carbonic anhydrase from bovine erythrocyte plasma membrane," *Prep. Biochem. Biotechnol.*, vol. 30, pp. 49-59, 2000, doi: 10.1080/10826060008544944.

[274] R. Bharti, S. Srivastava, and I. Thakur, "Isolation, purification, characterization and mass spectroscopic analysis of carbonic anhydrase from Serratia sp. for sequestration of carbon dioxide and formation of calcite," *J. Environ. Chem. Eng.*, vol. 2, pp. 31-39, 2014, doi: https://doi.org/10.1016/j.jece.2013.11.018.

[275] J. Cui and S. Jia, "Organic–inorganic hybrid nanoflowers: A novel host platform for immobilizing biomolecules," *Coord. Chem. Rev.*, vol. 352, pp. 249-263, 2017, doi: https://doi.org/10.1016/j.ccr.2017.09.008.

[276] K. A. Al-Maqdi, M. Bilal, A. Alzamly, H. M. N. Iqbal, I. Shah, and S. S. Ashraf, "Enzyme-Loaded Flower-Shaped Nanomaterials: A Versatile Platform with Biosensing, Biocatalytic, and Environmental Promise," *Nanomaterials.*, vol. 11, pp. 1460, 2021, doi: https://doi.org/10.3390/nano11061460.

[277] A. Kumar, S. K. S. Patel, B. Mardan, R. Pagolu, R. Lestari, S. H. Jeong, *et al.*, "Immobilization of Xylanase Using a Protein-Inorganic Hybrid System," *J. Microbiol. Biotechnol.*, vol. 28, pp. 638-644, 2018, doi: 10.4014/jmb.1710.10037.

[278] D. S. Chormey, S. Erarpat, B. T. Zaman, N. Ozdogan, O. Yagmuroglu, and S. Bakırdere, "Nanoflower synthesis, characterization and analytical applications: a review," *Environ. Chem. Lett.*, vol. 21, pp. 1863-1880, 2023, doi: https://doi.org/10.1007/s10311-023-01572-8.

[279] B. Somturk, I. Yilmaz, C. Altinkaynak, A. Karatepe, N. Ozdemir, and I. Ocsoy, "Synthesis of urease hybrid nanoflowers and their enhanced catalytic properties," *Enzyme Microb. Technol.*, vol. 86, pp. 134-142, 2016, doi:https://doi.org/10.1016/j.enzmictec.2015.09.005.

[280] H. Yang, P. He, Y. Yin, Z. Mao, J. Zhang, C. Zhong, *et al.*, "Succinic anhydride-based chemical modification making laccase@Cu3(PO4)2 hybrid nanoflowers robust in removing bisphenol A in wastewater," *Bioprocess Biosyst. Eng.*, vol. 44, pp. 2061-2073, 2021, doi:10.1007/s00449-021-02583-x.

[281] A. A. Homaei, R. Sariri, F. Vianello, and R. Stevanato, "Enzyme immobilization: an update," *J. Chem. Biol.*, vol. 6, pp. 185-205, 2013, doi:10.1007/s12154-013-0102-9.

[282] M. E. Peterson, R. M. Daniel, M. J. Danson, and R. Eisenthal, "The dependence of enzyme activity on temperature: determination and validation of parameters," *Biochem. J.*, vol. 402, pp. 331-7, 2007, doi: 10.1042/BJ20061143.

[283] C. Altinkaynak, C. Gulmez, O. Atakisi, and N. Ozdemir, "Evaluation of organic-inorganic hybrid nanoflower's enzymatic activity in the presence of different metal ions and organic solvents," *Int. J. Biol. Macromol.*, vol. 164, pp. 162-171, 2020, doi: https://doi.org/10.1016/j.ijbiomac.2020.07.118.

[284] S. Ren, R. Chen, Z. Wu, S. Su, J. Hou, and Y. Yuan, "Enzymatic characteristics of immobilized carbonic anhydrase and its applications in CO_2 conversion," *Colloids Surf. Biointerfaces.*, vol. 204, pp. 111779, 2021, doi: phttps://doi.org/10.1016/j.colsurfb.2021.111779.

[285] R. C. Kuhad, R. Gupta, and A. Singh, "Microbial cellulases and their industrial applications," *Enzyme Res.*, vol. 2011, pp. 280696, 2011, doi: https://doi.org/10.4061/2011/280696.

[286] I. Shamna, S. Kwan Jeong, and B. Margandan, "Covalent immobilization of carbonic anhydrase on amine functionalized alumino-Siloxane aerogel beads for biomimetic sequestration of CO_2," *J. Ind. Eng. Chem.*, vol. 100, pp. 288-295, 2021, doi: https://doi.org/10.1016/j.jiec.2021.05.010.

[287] B. Zhang, P. Li, H. Zhang, H. Wang, X. Li, L. Tian, *et al.*, "Preparation of lipase/Zn3(PO4)2 hybrid nanoflower and its catalytic performance as an immobilized enzyme," *Chem. Eng. J.*, vol. 291, pp. 287-297, 2016, doi: https://doi.org/10.1016/j.cej.2016.01.104.

[288] A. Hazarika, C. Bhuyan, and M. Yadav, "Isolation, purification, and characterization of carbonic anhydrase from *Azadirachta indica* (neem) leaves and its CO_2 sequestration efficiency," *Biocatal. Agric. Biotechnol.*, vol. 53, p. 102855, 2023. doi: https://doi.org/10.1016/j.bcab.2023.102855.

[289] B. Lv, Z. Yang, F. Pan, Z. Zhou, and G. Jing, "Immobilization of carbonic anhydrase on carboxyl-functionalized ferroferric oxide for CO_2 capture," *Int. J. Biol. Macromol.*, vol. 79, pp. 719-725, 2015, doi: https://doi.org/10.1016/j.ijbiomac.2015.05.051.

[290] R. Sareen and P. Mishra, "Purification and characterization of organic solvent stable protease from Bacillus licheniformis RSP-09-37," *Appl. Microbiol. Biotechnol.*, vol. 79, pp. 399-405, 2008, doi:10.1007/s00253-008-1429-y.

[291] M. A. Salameh and J. Wiegel, "Effects of Detergents on Activity, Thermostability and Aggregation of Two Alkalithermophilic Lipases from Thermosyntropha lipolytica," *Open Biochem J.*, vol. 4, pp. 22-8, 2010, doi: 10.2174/1874091X01004010022 .

[292] A. Singh, M. Bhattacharyya, and U. Banerjee, "Purification and characterization of carbonyl reductase from Geotrichum candidum," *Process Biochem.*, vol. 44, pp. 986-991, 2009, doi: https://doi.org/10.1016/j.procbio.2009.04.020.

[293] H. Rasouli, I. Iliuta, F. Bougie, A. Garnier, and M. C. Iliuta, "Enhanced CO_2 capture in packed-bed column bioreactors with immobilized carbonic anhydrase," *Chem. Eng. J.*, vol. 432, pp. 134029, 2022, doi: https://doi.org/10.1016/j.cej.2021.134029.

[294] S. K. S. Patel, S. V. Otari, Y. Chan Kang, and J.-K. Lee, "Protein–inorganic hybrid system for efficient his-tagged enzymes immobilization and its application in l-xylulose production," *RSC Adv.*, vol. 7, pp. 3488-3494, 2017, doi: https://doi.org/10.1039/C6RA24404A.

[295] H. Rasouli, I. Iliuta, F. Bougie, A. Garnier, and M. C. Iliuta, "Enzyme-immobilized flat-sheet membrane contactor for green carbon capture," *Chem. Eng. J.*, vol. 421, pp. 129587, 2021, doi: https://doi.org/10.1016/j.cej.2021.129587.

[296] C. Altinkaynak, I. Yilmaz, Z. Koksal, H. Ozdemir, I. Ocsoy, and N. Özdemir, "Preparation of lactoperoxidase incorporated hybrid nanoflower and its excellent activity and stability," *Int. J. Biol. Macromol.*, vol. 84, pp. 402-419, 2016, doi: 10.1016/j.ijbiomac.2015.12.018.

[297] B. H. Jo, J. H. Seo, Y. J. Yang, K. Baek, Y. S. Choi, S. P. Pack, *et al.*, "Bioinspired Silica Nanocomposite with Autoencapsulated Carbonic Anhydrase as a Robust Biocatalyst for CO_2 Sequestration," *ACS Catal.*, vol. 4, pp. 4332-4340, 2014, doi: https://doi.org/10.1021/cs5008409.

[298] N. Sharma, M. Parhizkar, W. Cong, S. Mateti, M. A. Kirkland, M. Puri, *et al.*, "Metal ion type significantly affects the morphology but not the activity of lipase–metal–phosphate nanoflowers," *RSC Adv.*, vol. 7, pp. 25437-25443, 2017, doi: https://doi.org/10.1039/C7RA00302A.

[299] S. Singh, P. K. Dikshit, V. S. Moholkar, and A. Goyal, "Purification and characterization of acidic cellulase from Bacillus amyloliquefaciens SS35 for hydrolyzing Parthenium hysterophorus biomass," *Environ. Prog. Sustain. Energy*, vol. 34, pp. 810-818, 2015, doi:10.1002/ep.12046.

[300] W. Ren, Y. Li, J. Wang, L. Li, L. Xu, Y. Wu, *et al.*, "Synthesis of magnetic nanoflower immobilized lipase and its continuous catalytic application," *New J. Chem.*, vol. 43, pp. 11082-11090, 2019, doi: https://doi.org/10.1039/C8NJ06429F.

[301] A. H. A. Al-Dhrub, S. Sahin, I. Ozmen, E. Tunca, and M. Bulbul, "Immobilization and characterization of human carbonic anhydrase I on amine functionalized magnetic nanoparticles," *Process Biochem.*, vol. 57, pp. 95-104, 2017, doi: https://doi.org/10.1016/j.procbio.2017.03.025.

[302] M. T. Reetz and J. D. Carballeira, "Iterative saturation mutagenesis (ISM) for rapid directed evolution of functional enzymes," *Nat. Protoc.*, vol. 2, pp. 891-903, 2007, doi: https://doi.org/10.1038/nprot.2007.72.

[303] K. Vojdanitalab, H. Jafari-Nodoushan, S. Mojtabavi, M. Shokri, H. Jahandar, and M. A. Faramarzi, "Instantaneous synthesis and full characterization of organic–inorg laccase-cobalt phosphate hybrid nanoflowers," *Sci. Rep.*, vol. 12, pp. 9297, 2022, doi: https://doi.org/10.1038/s41598-022-13490-w.

[304] R. Chang, S. Kim, S. Lee, S. Choi, M. Kim, and Y. Park, "Calcium Carbonate Precipitation for CO_2 Storage and Utilization: A Review of the Carbonate Crystallization and Polymorphism," *Front. Energy Res.*, vol. 5, 2017, doi: https://doi.org/10.3389/fenrg.2017.00017.

JOURNAL PAPERS

1) **T. Sharma** and A. Kumar, "Efficient reduction of CO_2 using novel carbonic anhydrase producing *Corynebacterium flavescens*," Environmental Engineering Research, vol. 12, p. 45-55, 2020. **(IF-3.8, Sci, Unpaid)**

2) **T. Sharma** and A. Kumar, "Bioprocess development for efficient conversion of CO_2 into calcium carbonate using keratin microparticles immobilized *Corynebacterium flavescens*," Process Biochemistry, vol. 100, p. 171-177, 2021. **(IF-4.8, Sci, Unpaid)**

3) **T. Sharma** and A. Kumar, "Protein inorganic hybrid nanoflowers of a microbial carbonic anhydrase as efficient tool for the conversion of CO_2 into value added product," Journal of Chemical Technology and Biotechnology, vol. 98, p. 1303-1311, 2023. **(IF-3.7, Sci, Unpaid)**

CONFERENCES ATTENDED

1) Tanvi Sharma and Ashok Kumar. "Screening and isolation of carbonic anhydrase producing bacteria from cow saliva" *Poster presentation in 3rd Himachal Pradesh science congress*, IIT Mandi, India, October 22-23, 2018.

2) Tanvi Sharma and Ashok Kumar. "Potential of bacterial carbonic anhydrase in carbon dioxide sequestration to mitigate the climatic change" *Poster presentation in 13th India- Japan bilateral conference*, Biyani group of collage Jaipur, India, November 25-28, 2018.

3) Tanvi Sharma and Ashok Kumar. "Enhanced production of carbonic anhydrase from bacterial isolate T5" *Oral presentation in International Conference on Recent Trends in Biotechnology and Bioinformatics*, Jaypee University of Information Technology, Waknaghat, India, August 1-3, 2019.

4) Tanvi Sharma and Ashok Kumar. "Conversion of atmospheric CO_2 into calcium carbonates using bacterial carbonic anhydrase" *Poster presentation in Association of Microbiologist of India*, Central University, Haryana, India, November 15-18, 2019.